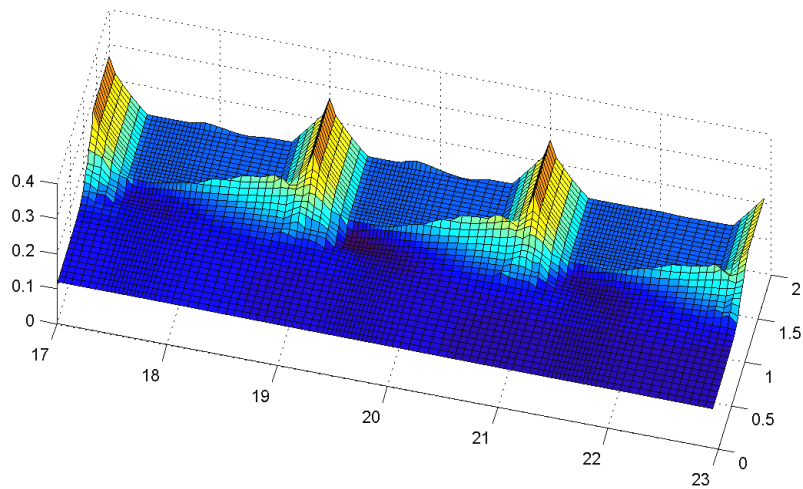


**MODELLING OF THE MORPHOLOGICAL INTERACTION
BETWEEN A RIVER AND ITS GROUYNE FIELDS
(USING DELFT3D-FLOW WITH ONLINE-SEDIMENT AND HLES)**



DIPLOMA THESIS / DIPLOMARBEIT

Rebekka Rupprecht
April 2004



Delft University of Technology
Faculty of Civil Engineering and Geosciences
Section of Hydraulic Engineering

Universität Karlsruhe (TH)
Fakultät für Bauingenieur-, Geo- und Umweltwissenschaften
Institut für Hydromechanik

**MODELLING OF THE MORPHOLOGICAL INTERACTION
BETWEEN A RIVER AND ITS GROUYNE FIELDS
(USING DELFT3D-FLOW WITH ONLINE-SEDIMENT AND HLES)**

DIPLOMA THESIS / DIPLOMARBEIT

Rebekka Rupprecht
April 2004

Graduation Committee:

TU Delft:	Prof. dr.ir. H.J. de Vriend Dr.ir. W.S.J. Uijtewaal M.F.M. Yossef, M.Sc.
Universität Karlsruhe (TH):	Prof. G.H. Jirka, Ph.D. Dr.-Ing. V. Weitbrecht



Diplomarbeit / Diploma thesis

for

cand. ing. Rebekka Rupprecht
Matriculation No.: 0963455

MODELLING OF THE MORPHOLOGICAL INTERACTION BETWEEN A RIVER AND ITS GROUYNE FIELDS

At the section of hydraulic engineering at the TU Delft a research project is momentarily performed, which deals with the effects of groynes on rivers. This research has the general objective to gain more knowledge about the morphological interaction between a river and its groyne fields. The sediment exchange between the river's main channel and its groyne fields as well as the turbulent eddies are here of special interest. Furthermore the capability of numerical models in simulating the hydraulic and morphological interaction between the main channel and the groyne fields of a river is to be investigated.

Within the framework of this study a diploma thesis is included, whose principal topic is the numerical simulation of the interaction between the main channel and the groyne fields. The specific objective of the studies in the context of this thesis is to evaluate the model capabilities in simulating these interactions.

Recently, experiments have been conducted in a mobile-bed flume for a straight river with groynes on one side to study the morphological interaction between the groyne fields and the main channel. The flume had a geometrical scale of 1:100 based on typical dimensions of the River Waal. The bed material has been scaled to have bed load (ripples) as well as suspended sediment transport. The flow conditions covered one situation, where the groynes were emerged, and three different situations with submerged groynes. Measurements covered bed changes, suspended sediment concentration, and flow velocity. The experiments provide benchmark data for model calibration.

In order to achieve the goal of this study the above-mentioned flume experiment is modelled numerically. This diploma thesis will also include a survey of literature on this topic. Then, an analysis of the experimental data will be necessary in order to set-up benchmark data for the model verification. The computational grid, its initial conditions and boundary conditions have to be implemented in accordance with the actual situation in the flume experiment. The system to be applied for modelling the flume experiment is the Delft3D system. In this system, the flow model is based on the depth averaged shallow water equations. To resolve the large horizontal eddies, the effect of the turbulent motions is modelled on a sub-grid scale using a recently developed sub grid scale (SGS) model. This SGS model computes spatially and temporally varying

horizontal eddy viscosity. The modelling of turbulence in this way is called Horizontal Large Eddy Simulation (HLES), where the hydrodynamics and the sediment transport are solved on time- and length-scales much smaller than the dominant 2D turbulent motions. The hydrodynamic and morphological simulation will be done for some examples of the emerged and the submerged situations of the experiment. The parameters of main interest are the bed level changes, velocity and direction of the flow, and the suspended sediment concentration. A sensitivity simulation for some parameters concerning the flow and the morphology of the modelled flume is also part of this thesis.

Finally, the results of the numerical simulation will be compared to the results, which have been drawn from the model experiments. This comparison will show the model capabilities in simulating the interaction between the main channel and the groyne fields of the river, which is going to be discussed in the conclusion.

The following details are to be made for the diploma thesis:

- Literature survey
- Analysis of the experimental data to set-up benchmarks for the model verification.
- Setting-up the model's grid and boundary conditions in accordance with the experiments.
- Hydrodynamic and morphodynamic modelling
- (Sensitivity simulations for the model.)

Working period:

Emission: 17. November 2003
Return: 19. April 2004
Duration: 22 weeks

Supervision:

Mohamed F.M. Yossef, M.Sc.	Delft University of Technology
Dr.ir. Wim S.J. Uijttewaai	Delft University of Technology
Prof. dr.ir. Huib J. de Vriend	Delft University of Technology
Dr.-Ing. Volker Weitbrecht	University of Karlsruhe

Prof. Gerhard H. Jirka, Ph.D.

STATEMENT

Herewith I assure that I composed the present Diploma Thesis single-handed and that did not use any further additives and references as sources than the one's specified.

I agree, that my Diploma Thesis is placed in a library or duplicated.

ERKLÄRUNG

Hiermit versichere ich, die vorliegende Diplomarbeit selbständig verfasst und keine weiteren als die angegebenen Hilfsmittel und Quellen benutzt zu haben.

Ich erkläre mich damit einverstanden, dass meine Diplomarbeit in eine Bibliothek eingestellt oder kopiert wird.

Rebekka Rupprecht

ABSTRACT

Groynes are dam-like structures in a river, which are constructed at an angle to the direction of the flow. Their purpose is to maintain the navigable depth during low water conditions and to divert the flow from critical zones during high water conditions. The spaces between the groynes, the groyne fields, are areas of shallow flow. Groynes have an impact of the hydrodynamic and morphologic conditions of the river. They cause specific turbulent structures in the groyne field. The morphological impact of groynes are bed level changes, such as scour holes near the groyne tips and deposition ridges in the groyne field.

In flume experiments, which have been carried out at the Laboratory of Fluid Mechanics at the TU Delft, these flow conditions and bed level changes were studied for various test cases. In this thesis a numerical simulation of an emerged case of the laboratory experiment is performed. Here, the exchange processes between the main channel and the groyne field are of special interest. The simulation was done using the Delft3D-FLOW system. The add-on Horizontal Large Eddy Simulation (HLES) models the small-scale turbulences on a sub-grid scale. For the morphological computations the module 'Online-sediment' was used, which calculates the sediment concentration, the sediment transport, and the bed level changes simultaneously with the flow. The model was calibrated against data from the experiment.

The results of the hydrodynamic computations show the typical turbulent structures in emerged groyne fields, that have also been observed in previous experiments and described by several authors. However, a comparison with the experimental results could only be made at the locations, where the velocity was measured. With a sensitivity analysis, the influence of some input parameters on the computed flow field was studied. For this analysis some physical parameters were modified and the influence of the use of a high-pass filter for the velocity signals was investigated. The results of the morphological computation showed a qualitative accordance with the measured bed levels. Yet, the suspended sand settles too quickly at the entrance of the groyne field instead of entering it. Furthermore, the scour holes are less pronounced than in the experiment, while the erosion of the main channel is computed to be stronger than in the experiment. Another sensitivity analysis was carried out for the morphological computations.

In conclusion, it can be stated, that Delft3D-FLOW computes the morphological pattern qualitatively well. When analysing the details, though, some major differences with the observations occur. Especially the sediment transport into the groyne field is not reproduced realistically at the moment.

ZUSAMMENFASSUNG

Buhnen sind dammähnliche Bauwerke, welche in einem Fluss in einem Winkel zur Fließrichtung errichtet werden. Sie gewährleisten bei Niedrigwasser eine ausreichende Fahrwassertiefe, bei Hochwasser dagegen lenken Buhnen das Wasser von kritischen Zonen weg, wie z.B. den Uferbereichen. Die Bereiche zwischen den Buhnen, die Buhnenfelder, sind Flachwasserzonen. Buhnen haben Auswirkungen auf die Hydrodynamik und Morphodynamik des Flusses. Sie bewirken charakteristische turbulente Strukturen im Buhnenfeld. Der Einfluss der Buhnen auf die Morphodynamik beinhaltet Veränderungen der Sohle, wie z. B. die Ausbildung von Kolken am Buhnenkopf und Sedimentanlagerungen im Buhnenfeld.

Diese turbulenten Strömungen und die daraus resultierenden Sohlveränderungen wurden in einer Testreihe eines Modellversuchs im Laboratorium für Fluidmechanik an der TU Delft untersucht. Das Thema der vorliegenden Diplomarbeit ist die numerische Simulation eines Tests mit nicht überströmten Buhnen. Die Mischvorgänge zwischen Hauptkanal und Buhnenfeld waren hierbei von besonderem Interesse. Für die numerische Simulation wurde das Delft3D-System benutzt. Das Add-on Horizontal Lange Eddy Simulation (HLES) modelliert die kleinskaligen Turbulenzen mit Hilfe eines Sub-grid-scale-Modells. Für die morphologischen Berechnungen wurde das Modul ‚Online-sediment‘ verwendet, welches die Sedimentkonzentration, den Sedimenttransport und die Sohlveränderungen simultan zu den hydrodynamischen Berechnungen ermittelt. Zur Kalibrierung des Modells wurden Daten des Modellversuchs herangezogen.

Die Ergebnisse der hydrodynamischen Berechnungen zeigen die typischen turbulenten Strukturen in nicht überströmten Buhnenfeldern, welche in früheren Experimenten beobachtet und von mehreren Autoren beschrieben wurden. Ein quantitativer Vergleich mit den Resultaten des Modellversuchs konnte jedoch nur an den Messpunkten gemacht werden. Mittels einer Sensitivitätsanalyse wurde der Einfluss mehrerer physischer Parameter auf das Ergebnis der Simulation untersucht. Der Einfluss des high-pass-Filters, welcher für die Analyse der Geschwindigkeitsserien angewendet wurde, wurde ebenso betrachtet. Die Ergebnisse der morphologischen Berechnungen stimmten qualitativ mit den gemessenen Sohlveränderungen überein. Die Schwebstoffe wurden jedoch nicht in das Buhnenfeld transportiert, sondern sanken jedoch noch vor Eintritt in das Buhnenfeld ab und lagerten sich an. Die Kolke waren deutlich weniger ausgeprägt als die im Experiment gemessenen, während die berechnete Erosion des Hauptkanals stärker war als die gemessene Sohlerosion. Eine Sensitivitätsanalyse wurde auch für die morphologischen Berechnungen durchgeführt.

Zusammenfassend kann festgehalten werden, dass die von Delft3D-FLOW berechneten Sohlveränderungen qualitativ mit den im Modellversuch gemessenen übereinstimmt. Bei detaillierter Betrachtung werden jedoch Abweichungen deutlich. Besonders der Transport von Schwebstoffen aus dem Hauptkanal in das Buhnenfeld wird nicht realitätsnah reproduziert.

ACKNOWLEDGEMENTS

The thesis on hand was written during an exchange of six month between the TU Delft and the University of Karlsruhe (TH). I would like to thank all members from the TU Delft and the University of Karlsruhe (TH), who made this stay possible; many thanks to Prof. G.H. Jirka, Ph.D., dr. ir. W.S.J. Uijttewaal, and Dipl.-Ing. T. Bleninger, for the initialization of this exchange.

I would like to thank a lot my committee at the TU Delft, Prof. dr.ir. H.J. de Vriend, dr.ir. W.S.J. Uijttewaal, and M.F.M. Yossef, M.Sc., for their support and their constructive criticism on my thesis. Furthermore, I'd like to thank my counsellors at the University of Karlsruhe, Prof. G.H. Jirka, Ph.D., and Dr.-Ing. V. Weitbrecht for their advice and help.

For the professional support I would like to express my gratitude to M.F.M. Yossef, M.Sc. and dr.ir. W.S.J. Uijttewaal, who always took their time to answer questions, and give explanations and advice during these months. Furthermore they provided literature to me. I highly appreciate their valuable help and support.

Additionally I would like to thank dr.ir J.A. Roelvink and dr.ir. C.J. Sloff for their explanations and their support with Delft3D-FLOW, and to Prof. dr.ir. G.S. Stelling and ir. J.Th. van Kester for their helpful advice and discussion, when I had problems with instabilities in the numerical model. I also thank Delft Hydraulics for making available the Delft3D system and the user manuals.

The laboratory experiments were performed by K.E. Thiemann, M.Sc., whom I would also like to thank for the provision of the experimental data. These experiments could not have been performed without the help of the crew in the Laboratory of Fluid Mechanics and of M. van der Mer, who was in charge of the measuring devices, to whom I'm also very grateful.

I was partly financed by the German Academic Exchange Service (DAAD) and supported by my parents. I really would like to thank all of them very much. Furthermore, I would like to thank the International Office at the University of Karlsruhe for the support with the application for the scholarship from the DAAD.

TABLE OF CONTENTS

ASSIGNMENT	I
STATEMENT	III
ABSTRACT	IV
ZUSAMMENFASSUNG	V
ACKNOWLEDGEMENTS	VI
TABLE OF CONTENTS	VII
FIGURES AND TABLES	X
LIST OF SYMBOLS	XIII
1 INTRODUCTION	1
1.1 BACKGROUND	1
1.2 DEFINITION OF THE PROBLEM	1
1.3 OBJECTIVES	2
1.4 APPROACH	2
2 THEORETICAL BACKGROUND	3
2.1 TURBULENT FLOW	3
2.1.1 Characteristics of turbulent flow	3
2.1.2 Basic equations for turbulent fluid motion	4
2.1.3 Flow conditions in groyne fields	6
2.2 SEDIMENT TRANSPORT	7
2.2.1 General	7
2.2.2 Basic equations	7
2.2.3 Morphological impact of groynes	9
2.3 NUMERICAL MODELLING	10
2.3.1 Model description (Delft3D-FLOW with add-ons HLES and Online-Sediment)	10
2.3.2 Morphological Computation	13
3 EXPERIMENTAL STUDIES	18
3.1 DESCRIPTION OF THE EXPERIMENT	18
3.2 GEOMETRY OF THE FLUME	18
3.3 CONDITIONS FOR THE TEST CASES	19
3.4 MEASUREMENTS	20

3.4.1	Water level measurements.....	20
3.4.2	Velocity measurements.....	20
3.4.3	Bed level measurements.....	21
3.5	RESULTS.....	22
3.5.1	Flow field.....	22
3.5.2	Bed levels.....	24
4	HYDRODYNAMIC SIMULATION.....	26
4.1	MODEL SET-UP.....	26
4.1.1	Computational Grid.....	26
4.1.2	Bathymetry.....	27
4.1.3	Time step.....	27
4.1.4	Initial and boundary conditions.....	27
4.2	CALIBRATION.....	28
4.2.1	Comparison points.....	28
4.2.2	Calibration parameters.....	29
4.3	RESULTS.....	31
4.3.1	Adaptation of the flow.....	31
4.3.2	Instabilities.....	32
4.3.3	Flow field.....	33
4.3.4	Turbulence intensity.....	34
4.3.5	Horizontal eddy viscosity.....	35
4.3.6	Spectral analysis.....	36
4.4	SENSITIVITY ANALYSIS.....	38
4.4.1	Influence of the physical parameters.....	39
4.4.2	Influence of the relaxation time.....	43
4.4.3	Influence of a constant eddy viscosity.....	44
5	MORPHODYNAMIC SIMULATION.....	47
5.1	MODEL SET-UP.....	47
5.1.1	Sediment.....	47
5.1.2	Time management.....	48
5.1.3	Initial and boundary conditions.....	49
5.2	RESULTS AND COMPARISON WITH THE EXPERIMENT.....	51
5.2.1	Bed levels.....	51
5.2.2	Sediment transport rate.....	53
5.2.3	Suspended sediment concentration.....	55
5.3	SENSITIVITY ANALYSIS FOR THE MORPHODYNAMIC COMPUTATIONS.....	56

5.3.1	Influence of the sediment gradation	57
5.3.2	Influence of spatially varying enhancement of the actual bed shear stress	59
5.3.3	Influence of the relaxation time τ	61
5.3.4	Influence of the transport boundary conditions	62
5.3.5	Influence of the slip condition.....	63
6	DISCUSSION, REMARKS, AND CONCLUSIONS	67
6.1	DISCUSSION.....	67
6.2	RESTRICTIONS	68
6.3	RECOMMENDATIONS.....	69
6.4	CONCLUSIONS	70
7	REFERENCES	71
APPENDICES		
A	DELFT3D-FLOW - MODEL DESCRIPTION.....	A-1
B	NUMERICAL SIMULATIONS.....	B-1
C	RESULTS OF THE EXPERIMENTS	C-1
D	CONTENTS OF THE DATA MEDIUM	D-1

FIGURES AND TABLES

Figure 2-1	Turbulence generation	4
Figure 2-2	a) Simulated flow pattern in a groyne field during emerged situation b) Shape of the mixing layer in an emerged groyne field	6
Figure 2-3	Definition sketch suspended load transport	9
Figure 2-4:	Morphological modelling procedure when using Delft3D-FLOW with the add- ons HLES and Online-sediment	11
Figure 3-1	Set-up of the flume experiment (Yossef & de Vriend, 2004)	19
Table 3-1	Hydraulic conditions for the different test cases (Yossef, 2003).....	19
Figure 3-2	Locations of measurements	21
Figure 3-3	Measuring devices for the lab experiment	21
Figure 3-4	Photograph from the dye test with indication of the fluctuations at the groyne tip and the circular movement of the primary gyre.....	22
Figure 3-5	Velocity measurements along the width of the flume across S2 and S1	23
Figure 3-6	Morphological features for emerged groynes.....	24
Figure 3-7	Perspective view of the results of the bed level readings after 40 hours	25
Figure 3-8	left: indication of the dimension of ripples right: observed dimension of ripples in the test section.....	25
Figure 4-1	Excerpt from the grid with indication of the groynes.....	26
Figure 4-2	Perspective view of the initial bathymetry in QUICKIN (test section).....	27
Table 4-1	Co-ordinates of the location of measurements in the flume experiment and their respective grid co-ordinates	29
Table 4-2	Input parameters for the hydrodynamic simulation	31
Figure 4-3	Adaptation of the flow: a) temporal development of the discharge (US and DS boundary) b) temporal development of the water level (US and DS boundary)	32
Figure 4-4	Instantaneous view of the water level progression in the main channel	32
Figure 4-5	Mean velocity components in the test section: magnitude, u -component, and v -component	33
Figure 4-6:	Instantaneous picture of the velocity vectors in a groyne field with indication of the primary gyre and dynamic eddy.....	34
Figure 4-7	Standard deviation of the magnitude and the velocity components in the test section.....	35
Figure 4-8	Mean horizontal eddy viscosity ν_H in the test section with indication of the primary gyre and the location of the finer grid.....	36
Figure 4-9	Location of the cross-sections and observation points in the middle groyne field of the test section	36

Figure 4-10	Energy density spectra for both velocity components at four monitoring points....	37
Figure 4-11	Comparison between the spectra at point 1-2 (simulation and experiment)	38
Table 4-3	Overview of the runs of the sensitivity analysis	39
Figure 4-12:	Variation of H along x for the reference run and runs with a modified bed roughness.....	40
Figure 4-13	Distribution of u along S1 and S2 for the reference run and runs with a modified bed roughness.....	40
Figure 4-14:	Distribution of H across x for the reference and runs with a modified slip condition/wall roughness.....	41
Figure 4-15	Distribution of u across S1 and S2 for the reference run and runs with a modified slip condition/wall roughness	41
Figure 4-16	Influence of the slip condition and the wall roughness on the flow field	42
Figure 4-17	Computed turbulence intensities for the components u and v for the reference run (no filtering) and the run with $\tau = 0.1828$	43
Figure 4-18	Computed horizontal eddy viscosity for the reference run (no filtering) and for run H18 (lower plot)	44
Figure 4-19	Distribution of u across S1 and S2 for the reference run (with HLES) and some runs with various constant horizontal eddy viscosities	45
Figure 4-20	Influence of the eddy viscosity on the flow field when not using HLES.....	46
Figure 5-1	Distribution curve of the sediment with indication of the grain size.....	48
Figure 5-2	Time line for the morphological computation.....	49
Table 5-1	Input parameters for the morphological simulation.....	50
Figure 5-3	Comparison of simulation and experiment: bed levels after 40 hours.....	52
Figure 5-4:	Comparison of simulation and experiment: temporal development of the erosion at the deepest point of the scour hole and the middle of the main channel	52
Figure 5-5	Comparison of simulation and experiment: bed levels in the main channel.....	52
Figure 5-6	Deposition volumes inside the groyne fields (upper plots are the summations over the length of one groyne field, lower plots are the summations over the width of one groyne field).....	53
Figure 5-7	Components of the mean depth averaged suspended sediment and bed-load transport in one groyne field	54
Figure 5-8:	upper plot: mean velocity (y-component) along the normal line middle plot: mean susp. sed. transport (y-component) along the normal line lower plot: mean concentration along the normal line and for the experiment	54
Figure 5-9	Equilibrium concentration upstream and downstream left: c_e as a function of time right: c_e at the last time step ($t=38\text{min}$) across y (wetted distance).....	55
Figure 5-10	Transverse sediment concentration profile across S1 and S2.....	56
Table 5-2	Overview over the sensitivity analysis for the morphological runs	57

Figure 5-11	Distribution curve of the sediment used in the flume experiment with indication of the grain sizes used in the simulation (run M2).....	57
Table 5-3	Modifications for the input when using three grain size fractions (run M2)	58
Figure 5-12	Comparison of simulations: bed levels after 40 hours for the reference run and for run M2 (3 grain sizes).....	58
Figure 5-13	Comparison of simulations: bed level at $y=1\text{m}$ in the reference run (M1) and in run M2 (3 grain fractions)	59
Figure 5-14	Example of an instability for one run with several grain size fractions.....	59
Figure 5-15	Comparison of the erosion/deposition pattern after 2.5 hours for the reference run and for run M4.....	61
Figure 5-16	Comparison of simulations: bed level after 2.5 hours (upper plots) and after 40 hours (lower plots) for the reference run and for run M4 (enhanced bed shear stress) with indication of the scour holes	61
Figure 5-17	Comparison of simulations: bed level after 40 hours for the reference run and for run M5 (modified relaxation time) with indication of the erosion/deposition pattern near the side wall	62
Table 5-4	Modifications of the transport boundary conditions for the run M6	63
Figure 5-18	Comparison of simulations: bed level after 40 hours for the reference run and for run M7 (free slip condition).....	64
Figure 5-19	Comparison of simulations: bed level in the main channel across S2 for the reference run and for run M7 (free slip condition)	64
Figure 5-20	Comparison of simulations: concentration across S1 and S2 for the reference run (left plots) and the run M7 (free slip condition, right plots)	65

APPENDICES

Table A-1	Used attribute files for the simulation.....	A-1
Table A-2	Used output files for the simulation.....	A-1
Figure B-1:	Grid with contour lines of the bathymetry	B-1
Figure B-2:	Velocity vectors for run H10 with indication of the dynamic eddy.....	B-2
Figure C-1	Results of the bed level measurements: bed levels	C-1
Figure C-2	Photographs from the dye test with indication of the fluctuations at the groyne tip and the circular movement of the primary gyre.	C-2

LIST OF SYMBOLS

Roman symbols

A	flow area	[m]
a	reference height according to Van Rijn	[m]
BED	user-specified multiplication factor	[-]
B	effect of bottom friction	[m/s ³]
C	Chézy coefficient	[m ^{1/2} /s]
C_U	CFL-criterion for advection	[-]
C_{BT}	barotropic Courant number	[-]
c	concentration	[kg/m ³]
c_a	reference concentration according to Van Rijn	[kg/m ³]
c_e	equilibrium concentration	[kg/m ³]
D	deposition flux due to sediment settling	[kg/m ² s]
D^*	dimensionless particle parameter	[-]
D_{10}	grain parameter (10% passage)	[m]
D_{50}	median grain parameter	[m]
D_{90}	grain parameter (90% passage)	[m]
D_H, D_V	horizontal and vertical sediment mixing coefficients	[m ² /s]
d	water depth	[m]
E	erosion flux due to upward diffusion	[kg/m ² s]
E	spectral energy	[(m/s) ² /Hz]
F_x, F_y	horizontal Reynolds stress gradient terms	[m/s ²]
Fr	Froude number	[-]
f	frequency	[Hz]
g	gravitational acceleration	[m/s ²]
H	local water depth	[m]
i	water surface slope	[-]
k_s	truncation wave number	[1/m]
k_s	roughness height according to Nikuradse	[m]
k'_s	grain-related part of the bed roughness according to Van Rijn	[m]
$k''_{s,r}$	form-related (ripples) part of the bed roughness according to Van Rijn	[m]
L	length	[m]
M_x, M_y	contributions due to external sources or sinks of momentum	[m/s ²]
m, n	grid co-ordinates	[-]
P	wetted perimeter of the cross section	[m]
p	pressure	[N/m ²]
Q	discharge	[m ³ /s]
R	hydraulic radius	[m]
Re	Reynolds number	[-]

S	total sediment transport	[kg/ms]
S_b	bed load transport	[kg/ms]
S_s	suspended sediment transport	[kg/ms]
S^*	sum of the horizontal strain rates	[-]
SUS	user-specified multiplication factor	[-]
s	relative density of the sediment fraction	[-]
T	bed shear stress parameter	[-]
T_d	erosion or deposition rate of suspended sediment	[kg/m ² s]
T_s	adaptation time for the vertical sediment concentration profile	[-]
T_{start}	start date of morphological computation	[s]
T_{stop}	stop date of morphological computation	[s]
t_{mor}	morphological scale factor	[-]
t_{real}	real period of time (morphological time)	[s]
Δt	computational time step	[s]
U	characteristic velocity	[m/s]
u_*	bed shear velocity	[m/s]
u, v	velocity component in x - and y -direction	[m/s]
u', v'	fluctuating velocity component in x - and y -direction	[m/s]
\bar{u}, \bar{v}	mean velocity component in x - and y -direction	[m/s]
x, y	Cartesian co-ordinates in horizontal directions	[m]
$\Delta x, \Delta y$	mesh size in x -direction and y -direction	[m]
w_s	sediment settling velocity of the non-cohesive sediment	[m/s]
z	Cartesian co-ordinate in vertical direction	[m]
z_b	bed level	[m]

Greek symbols

α	multiplication factor for the enhancement of the bed shear stress	[-]
α	reflection parameter for the water level boundary	[s ²]
α	reflection parameter for the discharge boundary	[s]
β	'beta' factor according to Van Rijn	[-]
β_{eff}	effective 'beta' factor according to Van Rijn	[-]
γ	coefficient for the calculation of $v_H^{(SGS)}$ depending on the dimensionality of the turbulence and of the slope in the log-log spectrum of the energy-density spectra	[-]
γ_r	ripples presence factor	[-]
Δ	relative sediment density	[-]
Δ_r	ripples' height	[m]
ε_{por}	bed porosity	[-]
η	relative availability of the sediment in the mixing layer	[-]

λ_r	ripples' length	[m]
ν	kinematic viscosity	[m ² /s]
ν_t	turbulence viscosity	[m ² /s]
ν_H	horizontal eddy viscosity	[m ² /s]
$\nu_H^{(SGS)}$	sub-grid horizontal eddy viscosity computed by HLES	[m ² /s]
ρ	density of water	[kg/m ³]
ρ_s	sediment density	[kg/m ³]
σ	velocity in the σ -direction in the σ -co-ordinate system	[m/s]
σ_c, σ_T	Prandtl-Schmidt number	[-]
σ_u, σ_v	turbulence intensities in x - and y -direction	[m/s]
τ	relaxation time	[min]
τ_b	bed-shear stress	[N/m ²]
$\tau_{b,cr}$	critical bed-shear stress according to Shields	[N/m ²]
θ	dimensionless particle mobility parameter	[-]
θ_{cr}	critical Shields parameter	[-]

1 INTRODUCTION

1.1 BACKGROUND

Groynes are dam-like structures, which are constructed in a river at an angle with respect to the direction of the flow. Their purpose is to maintain the navigable depth during low water and to improve the conditions for navigation. During high water groynes divert the flow from critical zones such as the riverbanks. The spaces between the groynes are called groyne fields and are areas of shallow water, while the water depth in the main channel in a river is noticeably larger.

The research project “Ruimte voor Rijntakken” (in English: “Space for the Rhine Branches”), which is momentarily performed at the TU Delft, deals with the hydrodynamic and morphological effects of groynes on rivers. Sediment exchange and turbulent mixing processes between the groyne field and the main channel are points special of interest. This research project comprehends both laboratory experiments and numerical simulations.

To learn more about the exchange processes between the groyne field and the main channel, experiments have been carried out in the Laboratory of Fluid Mechanics at the TU Delft between July 2003 and October 2003. A flume was used, with a geometry based on the river Waal (scale: 1:100) and representing a straight river with groynes on one side. The bed material was chosen such that it was transported both as bed load (ripples) and as suspended sediment. As for the flow conditions, both emerged and submerged situations were investigated.

These experiments will be modelled numerically using the Delft3D system. This numerical simulation is the task of the thesis on hand. A comparison of the measured and the computed results is will be made and the capabilities of the numerical model to simulate the laboratory experiment will be evaluated.

1.2 DEFINITION OF THE PROBLEM

As already mentioned, there is a gap in the knowledge concerning the exchange processes between the groyne field and the main channel. The hydrodynamic as well as the morphodynamic exchanges in the mixing zones between the groyne field and the main channel need to be analysed and described. Some previous numerical models were unable to produce acceptable results in simulating these processes, but with the implementation of HLES (Horizontal Large Eddy Simulation) in Delft3-DFLOW it is now possible to simulate the turbulent flow near groynes and inside the groyne fields. So far, the model's capability to reproduce the morphology in the groyne field and the main channel have not yet been verified. A comparison between the model experiment and a simulation could give more information about how realistically the model represents reality.

1.3 OBJECTIVES

The aim of the project, in which the above-mentioned flume experiment and this thesis are included, is to acquire a better understanding of the hydrodynamic and morphodynamic effect of groynes on rivers.

The laboratory experiments have been conducted with the intention to gain insight into the sediment exchange processes between the groyne field and the main channel and furthermore to establish a relation between the submergence levels and the erosion/deposition patterns in the groyne field.

The objective of the thesis on hand is to judge whether the current sediment transport model is capable of simulating the morphological interaction between the main channel and the groyne fields. The results of the morphological computations will be compared to the observations which have been made in the experiment. The results of the hydrodynamic computations need to be compared with the observed flow field as well. Furthermore, a sensitivity analysis will be made for both hydrodynamic and morphodynamic computations. The objective of the sensitivity analysis is to study the influence of certain parameters on the result of the computation.

1.4 APPROACH

In order to achieve this objective, a numerical simulation will be made. The task is to model exactly the same situation, as investigated in the experiments. Due to the limited time, only one emerged case was modelled.

The numerical simulation will be carried out using the Delft3D software package. In this system, the flow model is based on the depth averaged shallow water equations. Horizontal eddies are solved with the add-on "Horizontal Large Eddy Simulation" (HLES), which uses a sub-grid-scale model to calculate the spatially and temporally varying horizontal eddy viscosity. With HLES it is possible to simulate the flow near groynes and in the groyne fields. The morphological simulation will be performed, using the "Online-sediment" add-on, which computes the sediment concentration, transport, and the bed level changes simultaneously with the flow and which has an immediate feedback to the hydrodynamics.

The numerical simulation will be done in two parts. First, only a hydrodynamic simulation will be made. The results of the hydrodynamic simulation will be discussed and a sensitivity analysis will be performed. When the hydrodynamic simulation represents the flow field of the laboratory experiment satisfactorily, the sediment transport can be added in the computations. The results of the morphological computations will then be compared with the results of the experiment. The changes of the bed level, such as scour holes near the groyne tips and deposition in the groyne field, are of special interest here. The conclusion will contain an evaluation of the model's capabilities to represent the hydrodynamic and morphodynamic situation in the laboratory experiment. Furthermore the model's applicability to other situations will be discussed.

2 THEORETICAL BACKGROUND

2.1 TURBULENT FLOW

2.1.1 Characteristics of turbulent flow

The majority of flows in nature are turbulent. Turbulent flows can be observed e.g. in rivers or channels, in seas or oceans, at the boundary layer of airplanes, cars or ships, and at the boundary layer of the earth's atmosphere.

An indication for the occurrence of turbulence is the dimensionless Reynolds number.

$$Re = \frac{UL}{\nu} \quad (2.1)$$

in which

- U characteristic velocity [m/s]
- L characteristic length [m]
- ν kinematic viscosity [m²/s]

The flow is considered to be laminar if viscosity dominates the flow (Reynolds number smaller than 1000). If the Reynolds number is large, the flow is turbulent, viscous forces no longer suppress instabilities, and inertial forces dominate instead.

Turbulence is a complex phenomenon, which is difficult to define precisely. It can be described though by listing some of its essential attributes (according to Tennekes and Lumely, 1972, taken from Uijtewaal 2003):

- irregularity or randomness, which requires a description using a statistical rather than a deterministic approach
- diffusivity, which means that turbulence causes an exchange of mass, momentum and heat at much higher rates than molecular motions
- large Reynolds numbers
- three-dimensional vorticity fluctuations
- dissipation of energy, which has to be continuously supplied from the mean flow while most of the energy is lost in viscous dissipation in the eddies in the smallest scales.
- Continuum: turbulent flow can be considered as the flow of a continuum and can therefore be described by the equations of fluid mechanics.
- the fact that turbulence is not a property of a fluid, but of a flow and that almost every fluid can flow in a laminar or turbulent manner.

Turbulence is generated at walls or boundaries of a channel (wall turbulence), at mixing layers and at locations where the flow is disturbed, e.g. wake flows (free turbulence), see Figure 2-1.

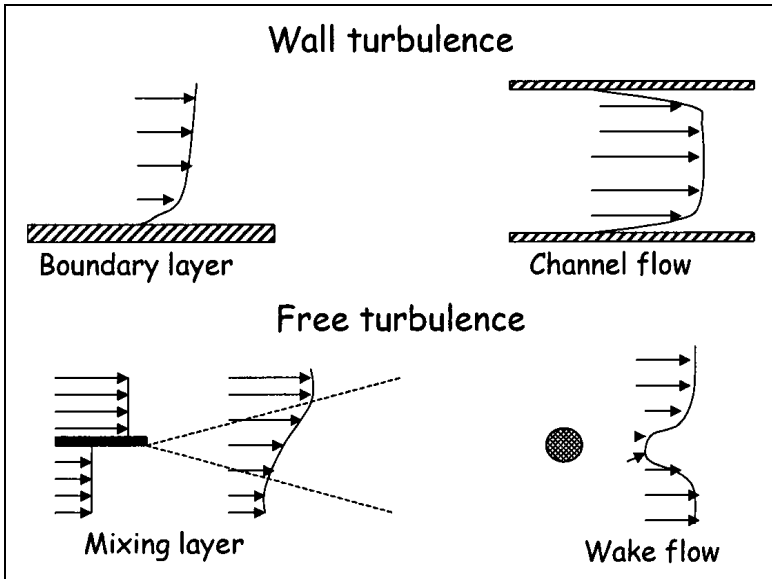


Figure 2-1 Turbulence generation (Uijtewaal, 2003)

In order to describe the properties of turbulence it is important to distinguish between the mean motion \bar{u} and the fluctuating component u' . The fluctuating component of a property is characterized by its variance σ_u^2 , which is a measure of the kinetic energy present in the fluctuating component. For the velocity component v in y -direction it is analogue.

$$\sigma_u^2 = \overline{u'^2} = \overline{(u - \bar{u})^2} \quad (2.2a)$$

$$\sigma_v^2 = \overline{v'^2} = \overline{(v - \bar{v})^2} \quad (2.2b)$$

Its square root and therefore the standard deviation of the velocity is also called the turbulence intensity σ_u and stands for the mean amplitude of the fluctuations.

$$\sigma_u = \sqrt{\overline{u'^2}} \quad (2.3a)$$

$$\sigma_v = \sqrt{\overline{v'^2}} \quad (2.3b)$$

2.1.2 Basic equations for turbulent fluid motion

The governing equations in hydrodynamics are the Continuity equation and the Momentum-equations, which are describing the balances of momentum and mass. In the depth-averaged case the momentum equations reduce to two equations while the vertical momentum equation is reduced to the hydrostatic pressure relation since vertical accelerations are assumed to be small in comparison to the gravitational acceleration, and can therefore be neglected (\rightarrow shallow water assumption).

Depth averaged momentum equations in horizontal directions:

$$\frac{\partial u}{\partial t} + u \frac{\partial u}{\partial x} + v \frac{\partial u}{\partial y} = -g \frac{\partial H}{\partial x} + F_x + M_x \quad (2.4a)$$

$$\frac{\partial v}{\partial t} + u \frac{\partial v}{\partial x} + v \frac{\partial v}{\partial y} = -g \frac{\partial H}{\partial y} + F_y + M_y \quad (2.4b)$$

The terms F_x and F_y are the horizontal Reynolds stress gradient terms which are modelled as:

$$F_x = \nu_H \left(\frac{\partial^2 u}{\partial x^2} + \frac{\partial^2 u}{\partial y^2} \right) \quad (2.5a)$$

$$F_y = \nu_H \left(\frac{\partial^2 v}{\partial x^2} + \frac{\partial^2 v}{\partial y^2} \right) \quad (2.5b)$$

M_x and M_y represent the contributions due to external sources and sinks of momentum (external forces by hydraulic structures, discharge or withdrawal of water, etc.)

Hydrostatic pressure assumption:

$$\frac{\partial p}{\partial z} = -\rho g \quad (2.6)$$

Continuity equation

$$\frac{\partial H}{\partial t} + \frac{\partial [uH]}{\partial x} + \frac{\partial [vH]}{\partial y} = 0 \quad (2.7)$$

where

g gravitational acceleration [m^2/s]

H local water depth [m]

p pressure [N/m^2]

u, v components of velocity [m/s]

x, y, z Cartesian co-ordinates [m]

ρ density of water [kg/m^3]

ν_H horizontal eddy viscosity [m^2/s]

As mentioned previously an important quality of turbulence is the ability of mixing mass, momentum and energy. An important property is the viscosity, which together with the velocity gradient the determines the shear stresses, which are measures of the turbulent transport of momentum. The viscosity is composed of

- the molecular viscosity ν_{mol} , a property of the fluid (for water at 20 C: $\nu_{mol} = 1.0 \cdot 10^{-6} \text{ m}^2/\text{s}$)
- and the turbulence viscosity ν_t , which is of a much higher order of magnitude. It is a property of the flow, that is a function of space and time and depends, among others, on the velocity. In the case of shallow flow, ν_t can be computed with a sub-grid model, as will be explained in Section 2.3.1 (Eq. 2.11).

A flow with a high turbulence viscosity has the capacity to transfer more momentum than a flow with a low turbulence viscosity. The higher the turbulence viscosity, the more exchange can take place and the larger therefore the influence of a disturbance on the flow and the mixing processes. The width of the mixing layer is then larger.

This is also the case in a channel with groynes, where the characteristic flow field in the groyne field differs much from straight flow in the main channel. In the region between groyne field and main channel a mixing layer develops in which the exchange of mass, momentum and energy takes place. The width of this mixing layer can be determined by regarding the characteristic length of the change in the magnitude of the velocity.

2.1.3 Flow conditions in groyne fields

When the groynes are emerged the flow inside a groyne field can be described as a system consisting of two or three horizontal gyres. This has been observed in model experiments and described by several authors, e.g. Uijttewaal et al. (2001). Since the water in the groyne field is shallow, these turbulent eddies have mainly 2D characteristics. Turbulences with 3D characteristics exist for example at locations where sudden bed level changes can be found. Horizontal quasi-2D turbulence, however, contributes most to the exchange processes.

The eddy-system in the groyne field (see Figure 2-2) consists of

- a primary large gyre, located in the downstream part of the groyne field, covering nearly two thirds of the groyne field, with a velocity of about 30% of the mean velocity of the main channel
- a secondary gyre of smaller size, located in the upstream corner of the groyne field, which is turning in the opposite direction and whose velocity is much smaller than that of the primary gyre
- a dynamic eddy, which is regularly shed from the tip of the upstream groyne, moving downstream towards the large gyre and ultimately merging with it.

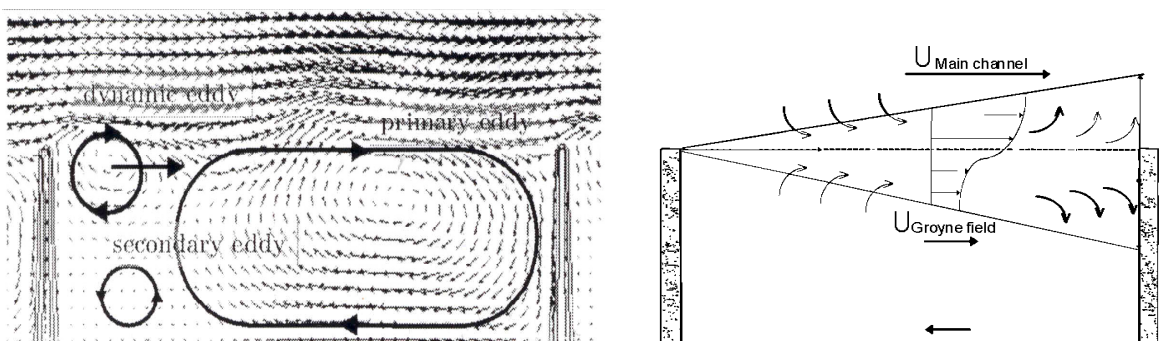


Figure 2-2 a) Simulated flow pattern in a groyne field during emerged situation (Yossef & de Vriend, 2004)
b) Shape of the mixing layer in an emerged groyne field (after Uijttewaal et al. 1999)

A mixing layer is located along the normal line, which is the line connecting the groyne tips of two adjacent groynes. The exchange between the main channel and the groyne fields takes place in this region. The mixing layer transfers momentum from the main stream to the primary gyre, which transfers it to the secondary gyre. The processes contributing to this exchange are the movements of the primary gyre and the dynamic eddy.

In the case of submerged groynes the flow in the groyne field differs much from the emerged situation. The gyre-system described above is not observed. The water flowing over the groynes flows in the same direction as the water in the main channel, but at a much lower velocity. The mixing layer formed between the two areas is weaker, has a constant width, and extends further into the main channel than in the emerged situation.

As in this thesis only the emerged case shall be simulated numerically, the case of submerged groynes is not further addressed. Reference is made to the appropriate literature, e.g. Yossef & Uijttewaal (2003).

2.2 SEDIMENT TRANSPORT

2.2.1 General

Sediment transport in rivers causes erosion and deposition and is responsible for changes of the course of the river as well as its bed forms. Sediment transport in rivers can be subdivided into bed-load transport and suspended load transport. Bed load predominantly slides, rolls, or saltates over the riverbed with a velocity, that is considerably lower than the flow velocity, whereas suspended sediment moves with flow velocity. Bed load transport leads to bed forms such as ripples, dunes, or antidunes. Several approaches exist to describe the initiation of motion. In the approach of Shields, bed material begins to move if the bed shear velocity exceeds a critical value, determined by the Shields curve. If the bed shear velocity increases further and exceeds the fall velocity of the particle, the particle can be lifted up and go into suspension. In this case the uplifting forces are higher than the submerged weight of the particle. Both bed-load and suspended sediment transport can be described using different approaches. Einstein (1950), Bagnold (1966), Bijker (1971) and Van Rijn distinguish in their approaches between bed load transport and suspended sediment transport, while Engelund-Hansen (1967), Ackers-White (1973,1990), and Yang (1973) directly give the total load transport rate. Since the Online-Sediment in Delft3D-FLOW module uses the approach of Van Rijn (1993), this will be referred to in this thesis.

2.2.2 Basic equations

Sediment balance equation

The sediment balance equation (Eq. 2.8) describes the relation between the bed load transport, the erosion/deposition rate of suspended sediment, and the bed level change:

$$(1 - \varepsilon_{por}) \frac{\partial z_b}{\partial t} + \frac{\partial S_{b,x}}{\partial x} + \frac{\partial S_{b,y}}{\partial y} = \frac{(c_e - c)H}{T_s} \quad (2.8)$$

where

c sediment concentration [kg/m^3]

c_e equilibrium concentration of suspended sediment [kg/m^3], which is computed, as explained in Appendix A.

H local water depth [m]

$S_{b,x}$, $S_{b,y}$ components of the bed load transport [kg/ms]. For the computation of the bed load transport, see eq (2.26 and 2.27).

$$T_s = \frac{H}{w_s} T_{sd} \quad (2.9)$$

where

T_{sd} is the dimensionless adaptation time for the vertical sediment concentration profile, which depends on the ratio (bed shear stress velocity/depth averaged velocity), the effective Van Rijn's 'beta' factor β_{eff} , (see Appendix A, Eq. A.12), and the sediment settling velocity w_s .

w_s sediment settling velocity of the non-cohesive sediment fraction [m/s], (for the calculation of w_s , see Appendix A)

z_b bed level [m]

ε_{por} bed porosity [-], generally equal to 0.4

Sediment transport

Concerning the sediment transport, Van Rijn distinguishes between bed-load and suspended load transport. The total transport of sediment is the sum of the bed-load transport S_b and the suspended load transport S_s [kg/ms]:

$$S = S_s + S_b \quad (2.10)$$

The depth-integrated suspended load transport rate S_s is calculated by integration of the product of the velocity u and the concentration c from the reference height $z=a$ (see Eq. 2.12) to the water surface $z=H$.

$$S_s = \int_a^H uc \, dz \quad (2.11)$$

where

c sediment concentration [kg/m^3]

Many analytical models exist which describe the sediment concentration. They can be divided into diffusion models, energy models, and stochastic models. In the Online-sediment add-on to Delft3D the concentration is calculated by solving the advection-diffusion equation, as will be

explained later on in the description of the formulae used in the morphological computation (Chapter 2.3.2, Equation 2.19).

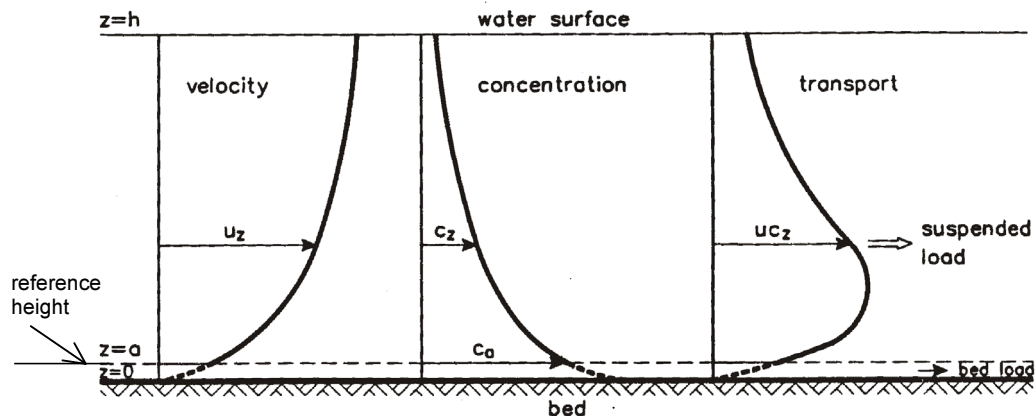


Figure 2-3 Definition sketch suspended load transport (Van Rijn, 1993)

The bed load transport rate S_b depends on the grain size D_{50} , the effective bed shear velocity u'_* , the sediment density ρ_s , the actual and the critical bed shear stresses τ_b and $\tau_{b,cr}$.

The reference height a is defined as the edge of the bed load layer and can be calculated according to the formula of Smith and McLean (1977), taken from Van Rijn (1993):

$$a = k'_s + 26.3(\theta - \theta_s)D_{50} \quad (2.12)$$

where

a reference height [m]

D_{50} mean grain diameter [m]

k'_s equivalent sand roughness [m]

θ dimensionless particle mobility parameter [-]

θ_{cr} critical dimensionless particle mobility parameter according to Shields.

The formula for the bed load transport, as well as the equations, which will be used for the computation of the concentration and bed level changes, will be given in Chapter 2.3.2, where the Online-sediment module will be described.

2.2.3 Morphological impact of groynes

Constructing a series of groynes on one or both sides of a river reduces the effective width of the channel. This decrease of the channel width leads to an increase of the velocity in the main channel, which results in an increase of the bed shear stress τ_b . This may cause erosion of the river bed and consequently an increased water depth in the main channel, especially in rivers of not too coarse sediment. This effect of groynes is advantageous for the navigation during low water. Due to the erosion the bed slope increases, which results in an increased downhill bed-load transport.

In contrast to the main channel, the groyne field is shallow and the velocities in the groyne field are much smaller. As has been explained in Section 2.1.3, the primary gyre dominates the flow field in the emerged case. Sediment is carried into the groyne field following the circular movement of the primary gyre. Inside the groyne field the velocity is smaller, which leads to sedimentation. On the downstream side of the groyne tip, which is the location where the dynamic eddy forms, scour holes have been observed in laboratory experiments as well as in nature.

2.3 NUMERICAL MODELLING

2.3.1 Model description

(Delft3D-FLOW with add-ons HLES and Online-Sediment)

Delft3D-FLOW solves the momentum equations in two horizontal dimensions on a curvilinear grid. For three-dimensional computations it is possible to introduce horizontal layers or σ -coordinates. The equations, which have been adapted to the use of a curvilinear grid are given in Appendix A.

With the implementation of Horizontal large eddy simulation (HLES) in Delft3D-FLOW it is now possible to resolve the large eddies and to parameterise the small eddies on a sub-grid-scale. In this way the time-varying flow field is computed, which constitutes the basis for the time-varying sediment transport. The advantage of using HLES is described by Yossef & Uijttewaal (2003). The technique of morphological modelling without using HLES can be described as follows:

The standard numerical model computes a flow field until it reaches a steady state, which means that the velocity difference between two time steps is less than a preset value. Then the sediment transport is calculated and the results are used to update the bed topography. On this new topography the flow field can be recomputed, etc. When using such a model for the simulation of a river with groynes, however, the morphological development in the groyne fields is poorly reproduced. The reason for this is the presence of the time-varying turbulent eddies, which are not resolved by this modelling technique. It is therefore recommended to use an eddy resolving approach, such as Horizontal Large Eddy Simulation (HLES). In the presence of horizontal eddies, as can be observed in emerged groyne fields, the flow conditions will not reach a steady state. The eddy resolving modelling technique computes the time varying flow field and averages it over a time period T_d . The representative time period T_d has to be determined by analysing the time scales of the velocity fluctuations in the groyne field as described by Yossef & Uijttewaal (2003).

Van Schijndel & Jagers (2003) compared observations of model experiments of a channel with groynes with the results of two-dimensional numerical simulations at lab-scale using Delft3D-FLOW with HLES. They found good agreement for the flow field as well as the sediment pattern in the case of emerged groynes. In their work they also emphasize the necessity to use HLES for the reproduction of the turbulent eddies.

The innovation of the Online-sediment add-on in Delft3D-FLOW is that the bed level is updated every half time step, that is to say simultaneously with the flow computations (in contrast with e.g. Delft3D-MOR, where the time-varying sediment transport is averaged over a time period before the bathymetry is updated). The advantage of Online-sediment is that any changes in the bathymetry immediately have a feedback onto the hydrodynamics. This makes the Online-sediment approach especially useful for the investigation of complex hydrodynamic situations, such as in the case of a series of groyne fields.

The modelling procedure of Delft3D-FLOW with the use of HLES and Online-sediment is shown in the flowchart in Figure 2-4.

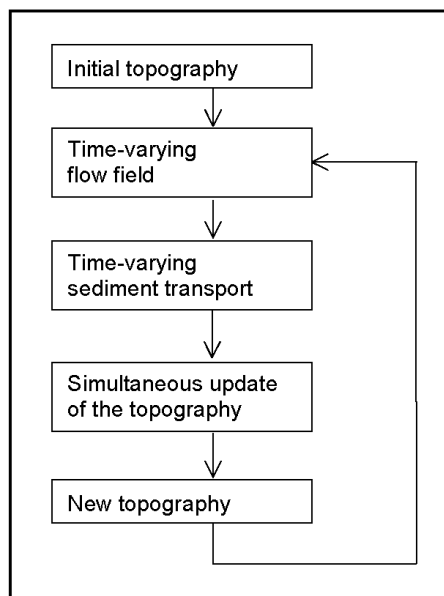


Figure 2-4:

Morphological modelling procedure when using Delft3D-FLOW with the add-ons HLES and Online-sediment

Horizontal large eddy simulation (HLES)

When using HLES, the turbulent velocity field is decomposed into turbulence at large scales (large eddies) and at small scales. The large-scale turbulent structures interact with the main flow, whereas the small-scale turbulent structures interact with the large-scale ones. With a coarse grid the model is able to resolve only the larger-scale turbulent structures, whereas the smaller-scale fluctuations cannot be resolved. Since the interaction between motions at all scales has to be taken into account, a sub-grid-scale (SGS) model is required to model the effects of the unresolved small-scale turbulence.

Horizontal large eddy simulation is appropriate in the case of quasi-2D turbulence. This means that the turbulent structures are of a 2D nature, the horizontal scale of the large eddies is thus larger than the water depth. This also applies in the case of an emerged groyne field, where the scale of the primary gyre is significantly larger than the water depth.

In 1999 the add-on HLES with the SGS model (Uittenbogaard & Van Vossen 1999) was implemented in the Delft3D-FLOW system. It computes the horizontal eddy viscosity as a function of time and position in the model domain, using the formula below. As the flow is shallow and

quasi-2D, this computed horizontal eddy viscosity $\nu_H^{(SGS)}$ can then be used in the depth averaged momentum equations (Eq. 2.4a and b).

$$\nu_H^{(SGS)} = \frac{1}{k_s^2} \left(\sqrt{(\gamma \sigma_T S)^2 + B^2} - B \right) \quad (2.13)$$

where

B effect of bottom friction [m/s³]

$$B = \frac{3}{4} \frac{g |\underline{U}|}{H C^2} \quad (2.14)$$

where C is the Chézy coefficient [-], H is the water depth [m], and \underline{U} is the depth averaged horizontal velocity [m/s]

k_s truncation wave number [1/m]

depending on the mesh size and the spatial filtering properties of the advection scheme and determines, which part of the length scales of turbulence is modelled in the SGS-model

S^{*2} sum of the horizontal strain rates squared

$$S^{*2} = 2 \left(\frac{\partial u^*}{\partial x} \right)^2 + 2 \left(\frac{\partial v^*}{\partial y} \right)^2 + \left(\frac{\partial u^*}{\partial y} \right)^2 + \left(\frac{\partial v^*}{\partial x} \right)^2 + 2 \frac{\partial u^*}{\partial y} \frac{\partial v^*}{\partial x} \quad (2.15)$$

where u^* and v^* are the fluctuating flow velocities which are defined through a high-pass-filter operator. This filter calculates the fluctuating component by subtracting a mean velocity, which has been averaged over the period τ (relaxation time), from the actual value.

γ coefficient [-] depending on the dimensionality of the turbulence (2D or 3D) and of the slope in the log-log spectrum of energy-density spectra

$\nu_H^{(SGS)}$ sub-grid horizontal eddy viscosity computed by HLES [m²/s]

σ_T Prandtl-Schmidt number (for the SGS-model: $\sigma_T = 0.7$)

According to Uittenbogaard & Van Vossen (2003) the proper use of HLES requires compliance with three criteria:

- The horizontal grid has to be sufficiently fine (at least in the order of the water depth) for being able to resolve the most energetic eddies as well as their interactions.
- In order to follow the temporal evolution of the vortex-vortex-interactions, the time step should be sufficiently small. This requirement is also called space-time consistency and the criterion to be met is the CFL-criterion for advection:

$$C_u = \frac{U \Delta t}{\Delta x} \leq 1 \quad (2.16)$$

where U is the mean velocity in the main channel [m/s], Δt is the computational time step [s], and Δx is the grid cell width in m -direction (flow direction) [m].

- The second criterion for the time step is the limitation of the barotropic Courant number C_{CB} , which is imposed to make sure that the conservation of energy and enstrophy (=square of vorticity) is approximated well:

$$C_{BT} = 2\sqrt{2} \frac{\Delta t \sqrt{gH}}{\Delta x} \leq 4\sqrt{2} \quad (2.17)$$

where g is the gravitational acceleration [m/s^2] and H is the water depth [m].

Furthermore the Delft3D-FLOW manual prescribes another time step criterion which has to be checked as well when using HLES:

- Stability criterion for the explicit integration of turbulent diffusion by the SGS-stress terms:

$$\Delta t \leq \frac{(\Delta x)^2}{2 \nu_H^{(SGS)}} \quad (2.18)$$

where $\nu_H^{(SGS)}$ is the horizontal eddy viscosity [m^2/s].

The most restrictive criterion is usually the barotropic Courant condition. For more detailed information about HLES and the sub-grid model, reference is made the Delft3D-FLOW user manual and to Uittenbogaard & Van Vossen (1999).

2.3.2 Morphological Computation

The sediment transport and morphology add-on in Delft3D-FLOW calculates sediment concentration, sediment transport and bed level changes, resulting in a change of the bathymetry, which in turn affects the flow conditions.

The user defines the characteristic sediment properties in a sediment input file and any further information which is necessary for the calculation of the morphodynamic changes in the morphological input file. A maximum of five sediment fractions (cohesive or non-cohesive) can be indicated in the input-file, each of them requires initial and boundary conditions.

The following equations are applicable in case of non-cohesive sediment and in situations without waves.

Suspended sediment concentration and transport rate

In the 3D-case the suspended sediment concentration is calculated by solving the three-dimensional advection-diffusion equation for the suspended sediment.

$$\begin{aligned} \frac{\partial c}{\partial t} + \frac{\partial uc}{\partial x} + \frac{\partial vc}{\partial y} + \frac{\partial (w - w_s)c}{\partial z} + \\ - \frac{\partial c}{\partial x} \left(D_H \frac{\partial c}{\partial x} \right) - \frac{\partial c}{\partial y} \left(D_H \frac{\partial c}{\partial y} \right) - \frac{\partial c}{\partial z} \left(D_V \frac{\partial c}{\partial z} \right) = \begin{cases} 0 & \text{for } z = kmx - \text{layer} \\ \text{source} - \text{sink} & \text{for } z = kmx - \text{layer} \end{cases} \end{aligned} \quad (2.19)$$

where

c mass concentration of sediment fraction [kg/m³]

$$T_s = \frac{H}{w_s} T_{sd} \quad (2.20)$$

where

H is the local water depth [m]

T_{sd} is the dimensionless adaptation time for the vertical sediment concentration profile, which depends on the ratio (bed shear stress velocity/depth averaged velocity), the effective Van Rijn's 'beta' factor β_{eff} , (see Appendix A, Eq. A.12), and the sediment settling velocity w_s .

w_s sediment settling velocity of the non-cohesive sediment fraction [m/s], (for the calculation of w_s , see Appendix A)

u , v , and w flow velocities resulting from the hydrodynamic computation [m/s]

D_H , D_V horizontal and vertical sediment mixing coefficients (=diffusivities) in [m²/s]

The local flow velocities are based on the results of the hydrodynamic calculations. The diffusivities needed for solving this equation are computed by the turbulence closure model (see Eq. 2.23) and Appendix A.

The suspended sediment transport rate S_s is then calculated by integration of the product of the local concentration with the local velocity from the bed to the surface.

Sediment exchange with the bed - sink- and source- terms

The exchange of sediment with the bed is implemented by way of sediment sink- and source-terms, which are located in the computational cell just above the reference level a , which marks the transition of bed load transport and suspended sediment transport. The relevant vertical flux is defined by Van Rijn (for the definition and calculation of a , see Equation 2.12). This cell is called the reference cell (or kmx-layer) and the sediment concentration in this cell equals the reference concentration c_a , which is calculated by the approach of Van Rijn (1993), see Appendix A. Cells located below the level a are assumed to respond instantaneously to changes in the bed shear stress. Furthermore it is assumed that the concentration in these cells is always equal to c_a . The derivation of the sink-and source-terms is shown below:

Erosive flux:

$$E = D_v \frac{\partial c}{\partial z} \approx \frac{D_v (c_a - c_{kmx})}{\Delta z} = \underbrace{\frac{D_v c_a}{\Delta z}}_{\text{= source-term due to erosion}} - \underbrace{\frac{D_v c_{kmx}}{\Delta z}}_{\text{= sink-term due to erosion}} \quad (2.21)$$

Deposition flux:

$$D = \underbrace{w_s c_{kmx}}_{\text{= sink-term due to deposition}} \quad (2.22)$$

where

- c_a reference concentration according to Van Rijn [kg/m^3]
 c_{kmx} sediment concentration in the reference cell [kg/m^3]
 D_V vertical sediment mixing coefficient at the reference cell [m^2/s]

$$D_V = \beta \frac{\nu_V}{\sigma_c} \quad (2.23)$$

where β is a dimensionless factor computed by the approach of Van Rijn, σ_c the Prandtl-Schmidt number [-] ($\sigma_c = 1$, if the k - ε turbulence closure model is used), and ν_V the vertical eddy viscosity, which is computed by the turbulence closure model. For a more detailed description of the calculation of ν_V and β , see Appendix A.

- Δz vertical distance from a to the centre of the reference cell [m]

The total sink- and source terms are therefore:

$$source = c_a \left(\frac{D_V}{\Delta z} \right) \quad (2.24)$$

$$sink = c_{kmx} \left(\frac{D_V}{\Delta z} + w_s \right) \quad (2.25)$$

These two terms are needed for the calculation of the net sediment change due to suspended sediment transport (see equation 2.31), which in turn is used for the computation of the bed level updating

Bed load transport

The bed load vectors $S_{b,u}$ and $S_{b,v}$, and the bed load transport rate $|S_b|$ in [kg/ms] are computed by the approach of Van Rijn (1993):

$$S_{b,u} = \frac{u_{b,u}}{|u_b|} |S_b| \quad (2.26a)$$

$$S_{b,v} = \frac{u_{b,v}}{|u_b|} |S_b| \quad (2.26b)$$

$$|S_b| = BED 0.5 \eta^{(l)} \rho_s D_{50} u_*' D_*^{-0.3} T \quad (2.27)$$

where

BED user-specified multiplication factor [-]

D_{50} median grain parameter [m]

D_* dimensionless particle parameter [-]

g gravitational acceleration [m/s^2]

$u_{b,u}$ $u_{b,v}$ components of the local bottom layer flow velocity [m/s]

$|u_b|$ magnitude of the local bottom layer flow velocity [m/s]

u_*' effective bed shear velocity [m/s], which in the case of a plane bed is equal to the bed

$$shear velocity $u_* = \frac{\sqrt{g}}{C} \bar{u}$ \quad (2.28)$$

T dimensionless bed shear stress [-]

$$T = \frac{\tau'_b - \tau_{b,cr}}{\tau_{b,cr}} \quad (2.29)$$

where τ_b is the bed-shear stress [N/m^2] and $\tau_{b,cr}$ the critical bed-shear stress according to Shields [N/m^2]

η relative availability of sediment in the mixing layer [-]

$$\eta = \frac{\text{mass of sediment in mixing layer}}{\text{total mass of sediment in mixing layer}} \quad (2.30)$$

ρ_s sediment density [kg/m^3].

The adjustment of the bed-load transport for bed-slope effects is included by multiplication of the magnitude of the bed-load transport vector with a factor, which is dependant on the bed slope. This adjustment is only made if a bed slope exists in direction of the bed-load transport vector. The bed-load vectors are then used for the calculation of $\Delta s_{bed}^{(m,n)}$, (Eq. 2.33), which in turn is needed to compute the bed level changes.

Available sediment at bed and bed level updating

The net sediment change of sediment mass at the bed due to suspended sediment transport is computed for each grid cell in dependence of the sink- and source-terms:

$$\Delta s_{sus}^{(m,n)} = f_{mor} (\text{sink} - \text{source}) \Delta t \quad (2.31)$$

where

Δt computational half-time step [s]

f_{mor} morphological scale factor used for temporal upscaling of the morphological changes [-].

$$\Delta t_{morphology} = f_{mor} \Delta t_{hydrodynamic} \quad (2.32)$$

The change in bottom sediment due to bed-load transport is calculated for each grid cell using the components of the computed bed-load vector:

$$\Delta s_{bed}^{(m,n)} = f_{mor} \left(S_{b,x}^{(m-1,n)} \Delta y^{(m-1,n)} - S_{b,x}^{(m,n)} \Delta y^{(m,n)} + S_{b,y}^{(m,n-1)} \Delta x^{(m,n-1)} - S_{b,y}^{(m,n)} \Delta x^{(m,n)} \right) \frac{\Delta t}{A^{(m,n)}} \quad (2.33)$$

where $A^{(m,n)}$ is the area of the computational cell (m,n) .

Delft3D computes the suspended sediment transport is over the entire water-column. In order to prevent the double-counting of the sediment transport below the reference height a , a suspended transport correction vector S_{cor} is used, which will not be further explained in this thesis. For further information it is referred to Lesser et al (2004), where the transport module is explained in detail. Analogue to the sediment change due to bed-load transport, the sediment change due to the suspended transport correction vector is $\Delta s_{cor}^{(m,n)}$.

Now the total change of sediment mass at the bed can be computed for each grid cell, which is simply the sum of $\Delta s_{sus}^{(m,n)}$, $\Delta s_{cor}^{(m,n)}$, and $\Delta s_{bed}^{(m,n)}$. This change in mass is then translated into a

change in thickness of the bottom sediment layer, which is equivalent to the change in bed elevation. The depth values can now be updated and used for the flow computation for the next time step.

3 EXPERIMENTAL STUDIES

3.1 DESCRIPTION OF THE EXPERIMENT

The hydraulic experiments were carried out between June 2003 and November 2003 in the Laboratory for Fluid Mechanics at the TU Delft. A flume with altogether 12 groynes was used to study the characteristics of bed formation, velocities and suspended sediment concentrations at different groyne heights. A total of 12 tests with varying water depths and varying ratios H/h_g (=water depth/groyne height) were carried out (see Table 3-1). Both emerged and submerged cases were investigated. The measurements concerned

- bed level heights in the entire test section
- velocities in x - and y -direction across the width of the flume (cross-sections S1 and S2)
- suspended sediment concentrations across the width of the flume (cross-sections S1 and S2)
- each water level, water depth, bed level, bed depth at two points (US and DS).

(The locations of the cross-sections and measuring points are shown in Figure 3-2.)

3.2 GEOMETRY OF THE FLUME

The flume was set up as a schematised model of the Dutch river Waal with a 1:100 geometrical scaling. The experiments were carried out in a flume of 26.85m length and 2m width, with 12 groynes on one side (of which 3 are wooden flow-adjusting groynes and 9 are made of concrete), the dimensions of which are shown in Figure 3-1. Sand and water were mixed in the desired proportion just before the inflow. Three wooden pseudo-groynes were placed in the upstream section in order to adjust the flow. The nine concrete groynes had a slope of 1:3 and their crest had a length of 65 cm. The groyne height was adjusted by varying the depth of the sand layer for the different test cases. The section in which the measurements were carried out (further referred to as the test section) was situated in the three groyne fields between the concrete groynes nr. 5 and nr.8. Behind the last groyne a settling basin for the sediment was located, after which a moveable weir was mounted. This adjustable weir used to regulate the water level.

In order to precisely describe the positions of measuring devices in the flume a Cartesian coordinate system is introduced. The origin is located at the inflow at the side of the flume without groynes. The z -axe has its origin at the concrete bottom of the flume and is positive upwards, see Fig 3-1.

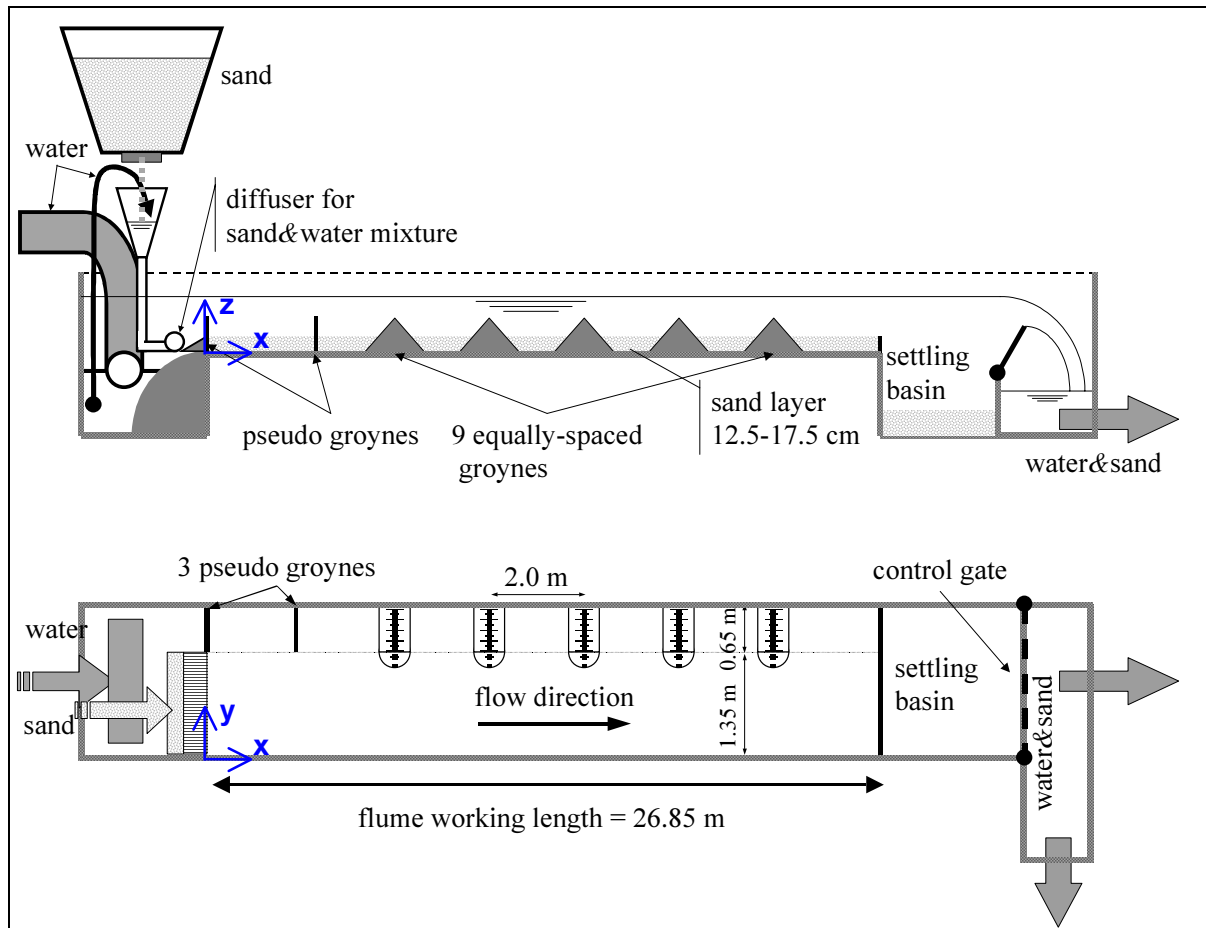


Figure 3-1 Set-up of the flume experiment (Yossef & de Vriend, 2004)

3.3 CONDITIONS FOR THE TEST CASES

Test	h_g [m]	H/h_g [-]	state of groynes		H [m]	U_{mc} [m/s]	Q [m ³ /s]	Re [-]	Fr [-]
			em.	subm					
→ G1i	0.125	1.0	<input checked="" type="checkbox"/>	<input type="checkbox"/>	0.125	0.40	0.058	11250	0.27
G1a		1.4	<input type="checkbox"/>	<input checked="" type="checkbox"/>	0.175	0.30	0.088	15626	0.23
G1b		1.7	<input type="checkbox"/>	<input checked="" type="checkbox"/>	0.213	0.30	0.111	19737	0.21
G1c		2.0	<input type="checkbox"/>	<input checked="" type="checkbox"/>	0.250	0.30	0.134	23970	0.20
G2i	0.100	1.0	<input checked="" type="checkbox"/>	<input type="checkbox"/>	0.100	0.25	0.044	7895	0.27
G2a		1.4	<input type="checkbox"/>	<input checked="" type="checkbox"/>	0.140	0.30	0.067	11924	0.24
G2b		1.7	<input type="checkbox"/>	<input checked="" type="checkbox"/>	0.170	0.30	0.085	15089	0.23
G2c		2.0	<input type="checkbox"/>	<input checked="" type="checkbox"/>	0.200	0.30	0.103	18352	0.22
G3i	0.075	1.0	<input checked="" type="checkbox"/>	<input type="checkbox"/>	0.075	0.25	0.031	5523	0.29
G3a		1.4	<input type="checkbox"/>	<input checked="" type="checkbox"/>	0.105	0.30	0.047	8385	0.26
G3b		1.7	<input type="checkbox"/>	<input checked="" type="checkbox"/>	0.128	0.30	0.060	10639	0.25
G3c		2.0	<input type="checkbox"/>	<input checked="" type="checkbox"/>	0.150	0.30	0.073	12967	0.24

Table 3-1 Hydraulic conditions for the different test cases (Yossef, 2003)

The hydraulic conditions were chosen to guarantee both bed load transport and suspended sediment transport in all cases. However, only the emerged case G1i will be discussed in this thesis.

The sand used for the experiment had the following grain characteristics: a D_{10} of $120\mu\text{m}$, a D_{50} of $160\mu\text{m}$, and a D_{90} of $232\mu\text{m}$. For the case G1i the mobility parameter θ according to Shields was calculated to be 0.097 (see equation 3.1), while the critical Shields parameter, found from the Shields curve amounts to approximately 0.05.

$$\theta = \frac{u_*^2}{(s-1)gD_{50}} \quad (3.1)$$

where

s relative density [-]

$$s = \frac{\rho_s}{\rho_w} \quad (3.2)$$

u_* bed shear velocity [m/s]

$$u_* = \frac{\sqrt{g}}{C} \bar{u} \quad (3.3)$$

where \bar{u} is the mean velocity in the main channel [m/s], and C the Chézy value, which has been estimated at $40 \text{ m}^{1/2}/\text{s}$.

3.4 MEASUREMENTS

The experiment was run for 40 hours in each test case. Bed level measurements were taken in the test section before the start of the test for reference and after 10, 20, 30, and 40 hours, respectively, velocity and suspended sediment concentration measurements were taken once in every test case after approximately 10 hours.

3.4.1 Water level measurements

The measurements of the static water level were taken at the two points US and DS (of which US is located near the inflow and DS near the outflow). Measurements were taken approximately every 10 hours. The water level measurements served to monitor the water level slope and the results will later be used to calibrate the numerical model.

3.4.2 Velocity measurements

Velocity readings were taken using two electromagnetic flow meters (manufactory: Delft Hydraulics; type: programmable EMF), which were attached to a moveable platform at a fixed distance to each other. The measuring devices recorded a signal, that is measurable. The measurements (in Volt) were taken with a frequency of 50 Hz. The EMF probes measured the a voltage in x - and y -direction simultaneously, which later had to be converted into velocities in [m/s]. An offset reading for calibration was taken at the beginning of each test case, since the measuring devices were rather sensitive to zero-offset drift.

In the emerged case G1i, the velocity readings were taken after the flume had been operated for 10 hours, that is to say after bed level changes had taken place. Measurements were taken across the width of the flume at two fixed cross-sections at approximately 60% of the water

depth, measured from the water surface. These cross-sections were located in the groyne field between groyne nr. 6 and nr. 7 and are denominated S1 and S2 (of which S2 is located at the upstream side of the groyne field near groyne nr. 6 and S1 at the downstream side near groyne nr.7, see Figure 3-2).

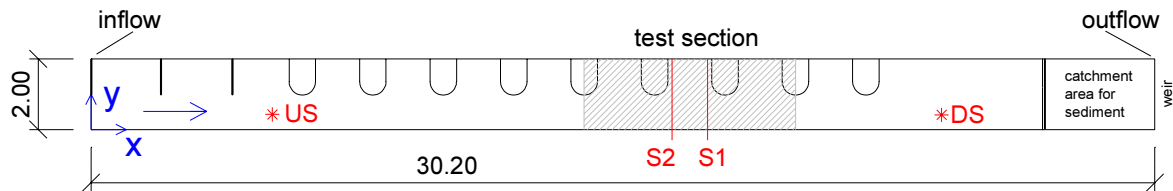


Figure 3-2 Locations of measurements

3.4.3 Bed level measurements

The measuring device used for the bed profile readings was a set of conductivity probes (manufacturer: Delft Hydraulics; type: PV-07) following the bed. These bed profilers were attached to a movable motorised carriage, which moved in x -direction at a constant velocity. The three bed profilers were attached at a fixed distance from each other. When putting the set of the three bed profilers in different positions on the carriage, bed level measurements could be taken at three different y -positions at a time. In this way the bed level readings were taken at intervals of 5cm in y -direction (between $y=0.2\text{m}$ and $y=1.8\text{m}$) and covered the test section in x -direction from groyne nr.5 to groyne nr. 8, (which corresponds to the Cartesian co-ordinates $x=14.16\text{m}$ and $x=20.84\text{m}$).

When activated, the bed profilers lowered themselves and kept a fixed distance to the sand bed, gliding just above the sand as the carriage moved lengthwise down the flume. Every 0.1 second a height measurement was recorded. The measuring devices are shown in Figure 3-3.

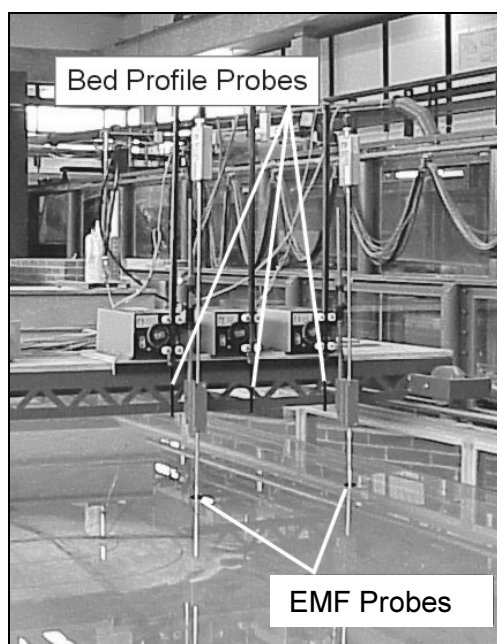


Figure 3-3 Measuring devices for the lab experiment

3.5 RESULTS

As in this thesis only the case G1i, the emerged case with a groyne height of 12.5cm, is simulated numerically only the results of this experiment are going to be presented in this chapter. Further information about the other test cases, e.g. the submerged cases, can be taken from Yossef & de Vriend (2004).

3.5.1 Flow field

The dye tests, which were made during the experiment, clearly show the presence of a primary gyre and fluctuations at the tip of the groyne. Figure 3-4 shows a picture from the dye test with an indication of the fluctuations and the circular movement of the primary gyre. The complete dye test can be viewed in Appendix C (Figure C-2).

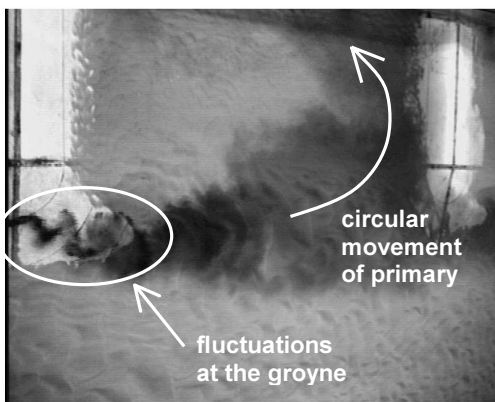


Figure 3-4

Photograph from the dye test with indication of the fluctuations at the groyne tip and the circular movement of the primary gyre.

The velocity profile in Figure 3-5 shows the velocity in x -direction at the cross-sections S1 and S2 at a depth of 60% of the water depth, plotted across the width of the flume. It is assumed that the magnitude of the downstream velocity at this depth equals the magnitude of the depth averaged velocity. The different markers stand for the two different measuring devices which were denominated 'EMF 13' and 'EMF 14'. Since the two measuring devices were attached at a fixed distance to each other and to the moveable platform, the measurements overlap at some locations. Both figures show that the magnitude of the velocity u in the main channel even exceeds a value of 0.4m/s. A possible explanation of the scatter of u in the main channel is that the time span between the velocity measurements at same locations was between 20 and 30 minutes. Furthermore, for one of the velocity measuring devices an incorrect offset reading was recorded, which had to be corrected when analysing the experimental data.

When looking at the groyne field the velocity turns negative, so the flow is directed upstream. The transition area between main channel and groyne field is the mixing layer in which the exchange of mass and momentum takes place. The mixing length is directly related to the gradient of the magnitude of u across y . As it can be seen in the figure, the gradient of the graph of the upstream cross section S2 is higher than the one in the more downstream located cross section S1, which implies that in S2 the mixing width is smaller than in S1. This conclusion also matches the picture of a wedge-shaped mixing layer shown in Figure 2-2b. The velocity profiles shown in Figure 3-5 will later be used for the calibration of the numerical model.

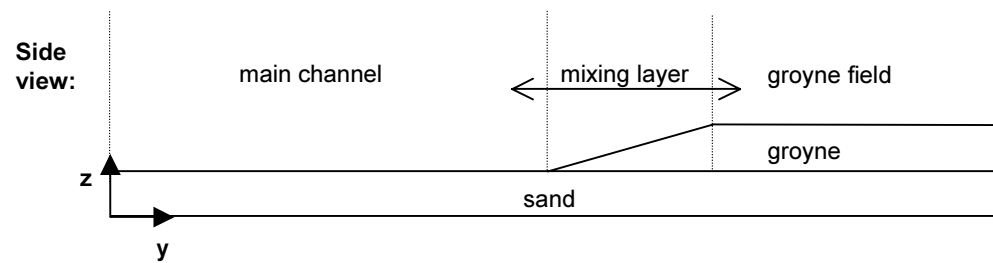
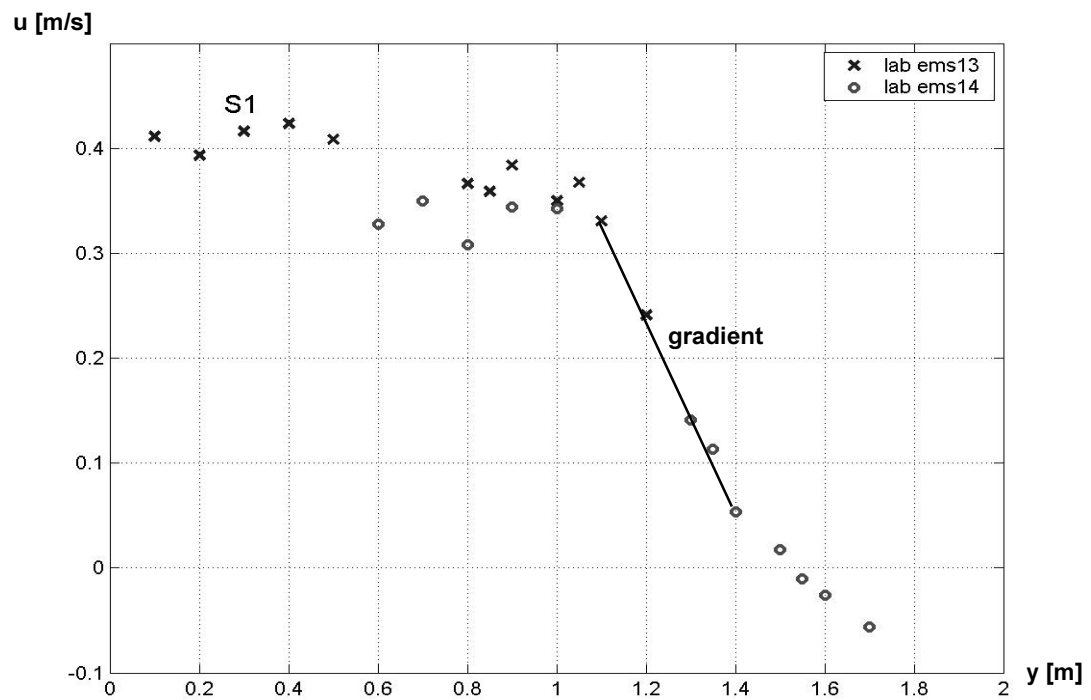
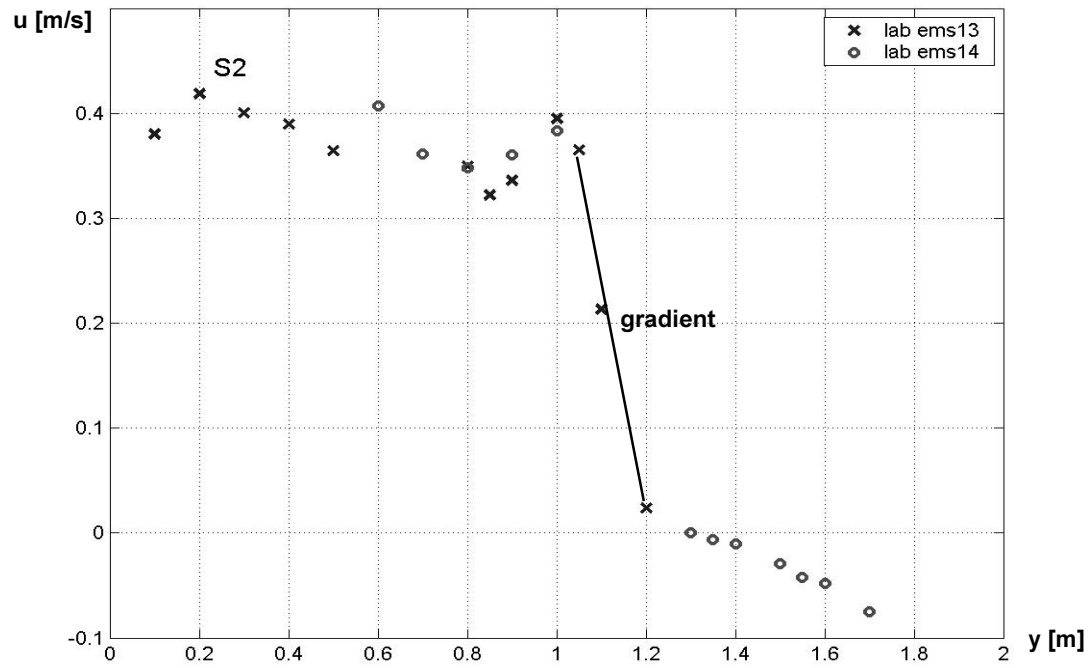


Figure 3-5 Velocity measurements along the width of the flume at the cross-sections S2 and S1

3.5.2 Bed levels

Sediment pattern in the emerged groyne field

Figure 3-6 shows a photograph taken at the end of a test with emerged groynes (case G1i). Figure 3-7 shows an example of the bed shape after 40 hours. The complete set of results of the bed level measurements (before the test, and after 10, 20, 30, and 40 hours) can be found in Appendix C (Figure C-1).

The observed sediment pattern after 40 hours shows the typical pattern of an emerged groyne field (see Figure 3-6). Following the direction of the primary gyre, the sediment enters the groyne field and settles as the flow velocity decreases. In the middle of the groyne field where the centre of the primary gyre is situated neither erosion nor sedimentation takes place and a zone free of bed-forms can be observed. The scour hole on the downstream side of each groyne tip is visible, as well. The scour hole extends at an angle with respect to the normal line (the connecting line between two adjacent groyne tips) following the path of the dynamic eddy. The scour hole varied between 7cm and 8cm in the test section. Furthermore a ridge of deposition was observed which is located at the upstream side of each groyne tip. It is wedge-shaped and its height ranged from 4cm to 5 cm (see Figure 3-7).

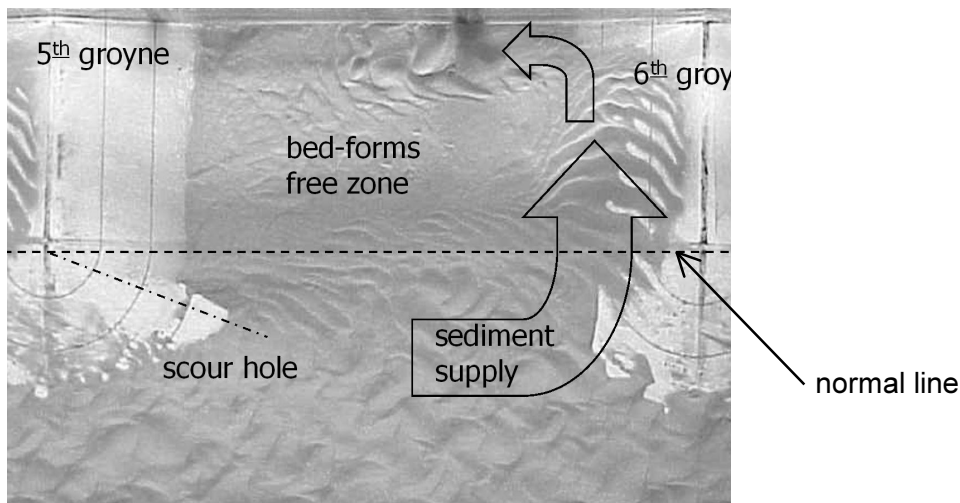


Figure 3-6 Morphological features for emerged groynes – case G1i; flow from left to right. Picture taken after the end of the test. (Yossef & de Vriend, 2004)

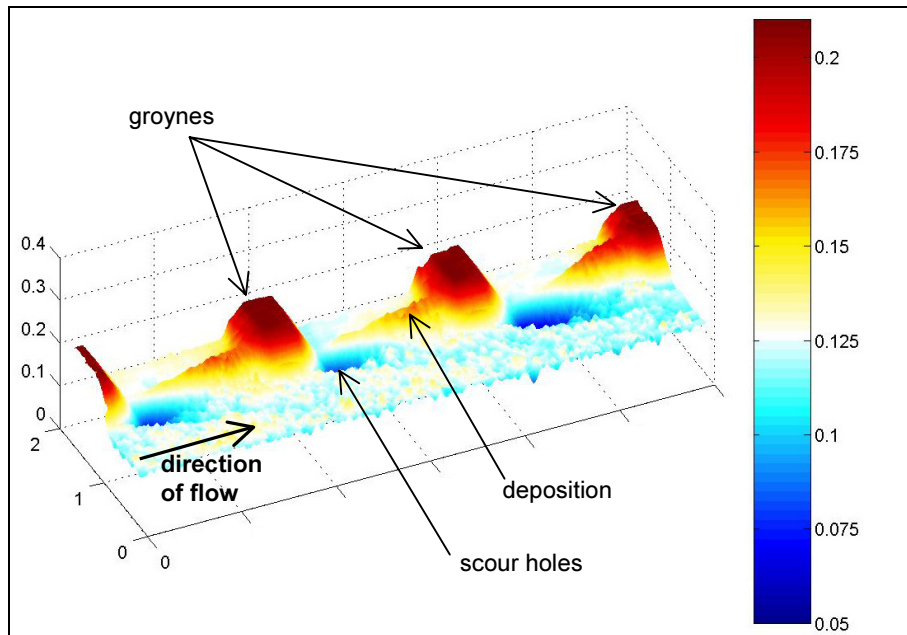


Figure 3-7 Perspective view of the results of the bed level readings after 40 hours

Overall sediment pattern

In the main channel ripples of various dimensions were observed. Their dimensions are indicated in Figure 3-8. It is remarkable that the dimensions of the ripples in the main channel, where the velocity magnitude was higher, were significantly larger than in the groyne field.

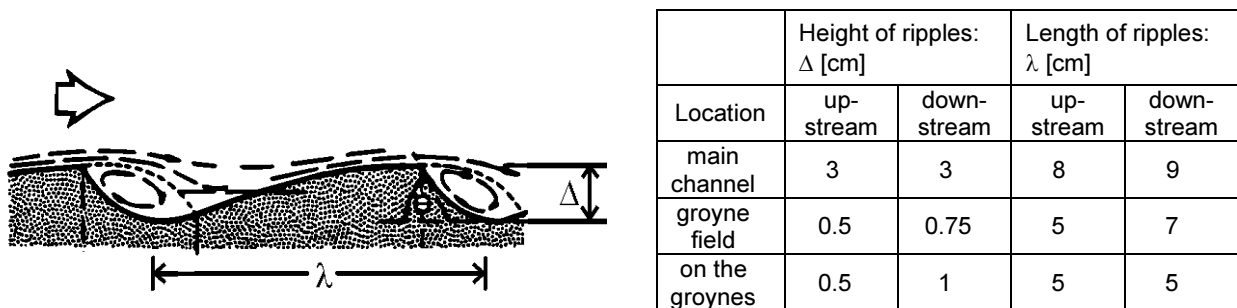


Figure 3-8 left: indication of the dimension of ripples (Van Rijn, 1993)
 right: observed dimension of ripples in the test section

Further observations outside the test section concerned the formation of an extremely deep scour hole on the first groyne and a depositional area before the outflow. The scour hole at the groyne tip of the first adjusting groyne extended far into the main channel and was significantly more pronounced than the scour holes at the other groyne tips. This can be explained from the fact, that the first groyne is exposed to the strongest current, which results in an increased erosion rate. In the region behind the last groyne, as the channel becomes wider. Consequently, deposition took place due do the decreased velocity.

4 HYDRODYNAMIC SIMULATION

In this and the following chapter one of the cases examined in the experiments is going to be simulated numerically using the Delft3D system. The emerged case Gi1, which has been discussed in chapter 3, will be set up. First, only a hydrodynamic simulation will be made and its results discussed. In the sensitivity analysis the influence of some parameters will be examined.

4.1 MODEL SET-UP

4.1.1 Computational Grid

The grid-file (extension: .grid) was created with the programme Delft-RFGRID, which is part of the Delft3D system. As the flume in the model experiment represented a straight river with groynes at a 90°-angle to the main flow, a rectangular grid could be used. Therefore the m and n -axes here correspond to the x and y -axes.

For the creation of the grid it is important that specific points, such as the crest and base of each groyne are situated at an intersection of grid lines. At these specific locations fixed points were defined. The distance between those fixed points was then divided into a number of grid cells, the size of which was chosen according to the following criteria:

- in order to resolve the high velocity gradient of the mixing layer the grid cells had to be smaller in the area where the dynamic eddy is expected, that is to say
 - in x -direction: at the downstream side of each groynes in the test section
 - in y -direction: in the groyne field and in the mixing zone.
- gradual changeover between finer and coarser grid

For these reasons the grid cell size varied at different locations on the grid. The smallest grid cell width in both x and y direction amounts to approximately 3.5cm, which is much smaller than the water depth. Figure 4-1 shows the grid with indication of the groynes in the test section. The geometry of the flume was simplified here. Instead of 11 groyne fields, only the three groyne fields of the test section and three adjacent groyne fields were modelled.

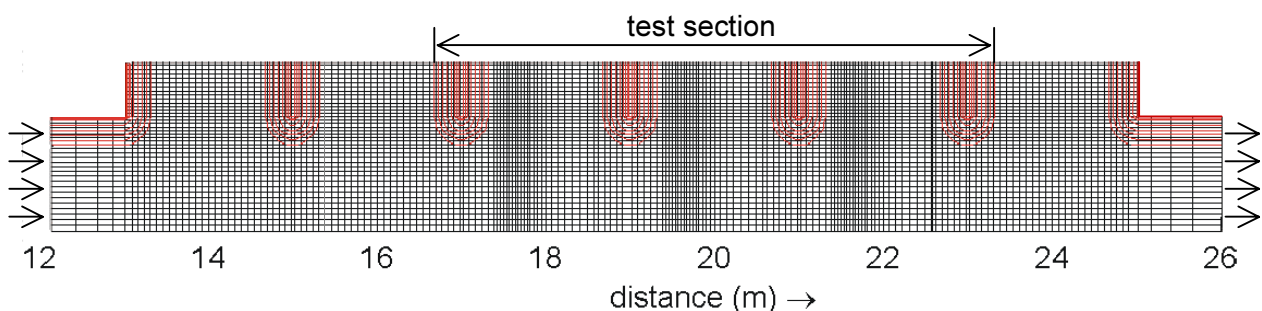


Figure 4-1 Excerpt from the grid with indication of the groynes

The complete grid, which consists of altogether 9040 grid cells $(m,n)=(226,40)$, can be viewed in Figure B-1 in Appendix B.

4.1.2 Bathymetry

The bathymetry of the numerical model is described in a depth-file (extension: .dep), which is created in the programme QUICKIN, a tool that is part of the Delft3D system. The points that define the depth at each intersection of the grid lines are called depth points. These points can be loaded from an ASCII-file. The depth file describes the water depth at each grid point. In this way the bottom surface of the flume experiment with the groynes was mapped.

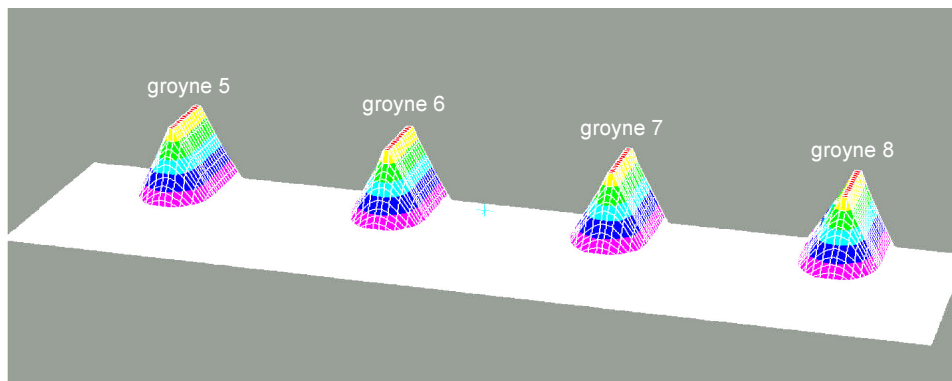


Figure 4-2 Perspective view of the initial bathymetry in QUICKIN (test section)

To assure the emergence of the groynes, the groyne tips were slightly elevated, without changing the rest of the groyne's geometry.

4.1.3 Time step

In order to assure stability and accuracy the time step should not exceed a maximum value. Time step limitations were formulated in chapter 2.1.3 when describing the HLES, (see equations 2.14 until 2.16). Especially when simulating a scenario at a lab-scale, and when using a very fine grid, the time step becomes rather small. The chosen time step of 0.024s fulfils all criteria. With $H=0.125\text{m}$, $\Delta x=0.035\text{m}$, and $g=9.81\text{m/s}^2$, the Courant number for surface waves C_{BT} , which is the most restrictive criterion, equals 2.14, which is less than 40% of the theoretically maximum allowed value. Yet, the very small time step had to be chosen for stability reasons.

4.1.4 Initial and boundary conditions

Initial conditions for the hydraulic simulation

Initial conditions have to be specified in every instationary simulation. The parameter to provide for the hydrodynamic simulation was the initial water level H_i [m]. The initial water level that was used in the hydrodynamic simulation is 25cm (which corresponds to the average water level in the flume). All initial velocities were zero.

Boundary conditions for the hydraulic simulation

There are two open boundaries that were used in the model: an inflow and an outflow boundary. The inflow boundary (upstream boundary) is located on the left-hand side of the grid. At this location a total discharge of $0.058\text{m}^3/\text{s}$ is imposed, which corresponds to the inflowing discharge for the laboratory experiment. The outflow boundary (downstream boundary) is positioned at the right-hand side of the grid. At the outflow the water level has to be specified which is in the case of G1i 24.5cm.

The discharge is specified in the as the total discharge across the cross-sectional area at the upstream boundary. Both boundary conditions are assumed to be constant in time.

As a further input constant the reflection parameter α can be specified for the open boundaries. By increasing the parameter α the reflections at the open boundaries for short wave disturbances, that propagate towards the boundary from inside the model, can be decreased. For the upstream boundary an α -value of 0 was used, which means total reflection. After several trials with different α -values at the upstream and downstream boundaries the best results were achieved when using a α -value of 12 (\rightarrow weakly dissipative) at the downstream boundary. It was observed that the water level in the entire flume rose during the initial state when using a higher α -value at the downstream boundary, while an α -value below 10 didn't dampen the occurring waves sufficiently.

4.2 CALIBRATION

The adjustment of the numerical model to match the measured values is denoted calibration. Several parameters can be used for the comparison between modelled and measured values. For the hydrodynamic simulation it is important to correctly reproduce the measured velocities and the water level.

4.2.1 Comparison points

It is necessary to choose a location where measurements in terms of time series or constant values are made available. In the flume experiment the velocity measurements were taken across the y -axis in the sections S1 and S2. The results of the velocity measurements are available in terms of time series of the velocities in the x and y - direction. For the calibration, the velocity in x -direction was of special interest. The cross-sections S2 and S1 correspond to $m=124$ (S2) and $m=143$ (S1) in the computational grid (see Table 4-1).

Measurements for the static water level were taken in two points in the flume: US and DS. The measurements were taken each morning and evening. Since the measurements yielded varying values for every day of measurement, the average water slope was taken as a reference. The values of the water level had to be in a range of a minimum and a maximum value (which was up to a tolerance of 1 cm).

The positions of the velocity and water level measurements are shown in Figure 3-2, the conversions of the co-ordinates for the computational grid are summarized in Table 4-1.

Water level measurements				
	Cartesian co-ordinates (flume experiment)		grid co-ordinates (simulation)	
	<i>x</i>	<i>y</i>	<i>m</i>	<i>n</i>
US	5.15	0.43	9	7
DS	24.15	0.42	218	7
Velocity measurements				
	Cartesian co-ordinates (flume experiment)		grid co-ordinates (simulation)	
	<i>x</i>		<i>m</i>	
S1	17.5		124	
S2	16.5		143	

Table 4-1 Co-ordinates of the location of measurements in the flume experiment and their respective grid co-ordinates

4.2.2 Calibration parameters

For the calibration procedure only the bed roughness and the slip condition / wall roughness will be used as calibration parameters.

Bed roughness

In the Master Definition FLOW file (MDF-file) the bed roughness can be expressed either in terms of the Chézy value C [$\text{m}^{1/2}/\text{s}$], or the Manning value n [m^3/s], or of the roughness height k_s [m] according to Nikuradse. As for this simulation the formulation of White-Colebrook was used, the specification of the roughness was made in terms of k_s . For a first estimation of k_s the dimensions of the measured bed forms were used. From the flume experiment it is known that the sand bed formed ripples. Nikuradse divided the roughness height in a grain-related part k'_s and a form-related part k''_s .

$$k_s = k'_s + k''_s \quad (4.3)$$

The grain-related part of the roughness and form-roughness related to ripples are according to Van Rijn (1993):

$$k'_s = 3 D_{90} \quad \text{for } \theta < 1 \quad (4.4)$$

$$k''_{s,r} = 20 \gamma_r \Delta_r \left(\frac{\Delta_r}{\lambda_r} \right) \quad (4.5)$$

where

D_{90} grain size of 90% passage [m]

γ_r Ripples presence factor [-] ($\gamma_r=1.0$ for ripples alone)

Δ_r Ripples' height [m] }
 λ_r Ripples' length [m] } for a definition of the ripple's dimensions see Figure 3-8

θ mobility (Shields) parameter.
 $\theta \approx 0,097$ (estimated, see section 3.3)

With a medium grain diameter D_{90} of $232\mu\text{m}$ and the measured ripple dimensions from the laboratory experiment (see Figure 3-8) the calculative effective bed roughness amounts to an unrealistically high value. Therefore, the actual value has to be estimated. A bed roughness of 0.01m , which was found in the calibration was used for further computations

Slip condition / wall roughness

Three different slip conditions to apply at closed boundaries (side walls) are possible:

a) free slip condition:

For this option it is assumed that there is no friction at the side walls. A free slip condition can be used for large-scale simulations where the tangential shear stress at the side walls can be safely neglected.

b) partial slip condition:

Using a partial slip condition with a specified wall roughness is reasonable for simulations of small-scale flow (as for example laboratory experiment) if the roughness at the side walls has an influence on the flow and therefore cannot be neglected.

c) no slip condition:

This condition corresponds to the case where the velocity near the side wall approaches zero.

Since an experiment at lab-scale is going to be simulated, the influence of the side walls cannot be neglected. Therefore a partial slip condition is used, and the wall roughness was to be determined by calibration. The cases 'no slip' and 'free slip' do not apply in the situation to be simulated, but nevertheless they shall be examined in the sensitivity analysis later in this chapter.

After adjusting and calibrating the numerical model the hydrodynamic simulation was run and the output examined. From further runs during the calibration it was found that the flow adapts after approximately 5 minutes (computed flow time). A total flow time of 10 min was therefore chosen for all hydrodynamic runs.

Input

In the table below all the essential input data are summarized for the hydrodynamic simulation.

Parameter	Value	Unit
Grid	specified in file	-
Bathymetry	specified in file	-
Time frame		
computational time step Δt	0.024	s
flow period	10	min
Initial conditions		
initial water level H_i	0.245	m
Boundary conditions		
upstream boundary:		
type of bound. cond.	total discharge (const.)	
Q	0.058	m^3/s
reflection parameter α	0	-
downstream boundary		
type of bound. cond.	water level boundary (const.)	
H	0.245	m
reflection parameter α	12	-
Constants		
water density ρ	1000	kg/m^3
gravitational acceleration g	9.81	m/s^2
Roughness		
bed roughness k_s	0.01	m
slip condition	partial slip condition	-
wall roughness	0.0012	m
Parameters concerning HLES		
relaxation time τ	-1	min
Prandtl-Schmidt number σ_T	0.7	-
Spatial low-pass filter coeff. f_{lp}	0.3	-
Dimensional number n_D	2	-
Slope in loglog-spectrum α	5/3	-
	} Default settings for the use of HLES	

Table 4-2 Input parameters for the hydrodynamic simulation

4.3 RESULTS

4.3.1 Adaptation of the flow

In order to determine the adaptation period of the flow to reach its equilibrium value, the specified condition at the upstream boundary was plotted against the time. In Figures 4-3a and 4-3b the temporal developments of the discharge and the water level are shown for both the locations near the upstream and downstream boundaries. It can be seen that the discharge near the upstream boundary very quickly reaches the average value of $0.058\text{m}^3/\text{s}$ as imposed with the boundary condition while near the outflow boundary the discharge doesn't react to the amount of water added until 30s later and furthermore needs a period of approximately 5 min for the adaptation. The adaptation time at the downstream boundary is due to the sudden change from a constant water level of 25cm in the entire flume and no inflow to a constant inflow discharge of $0.058\text{m}^3/\text{s}$. The water is added to the flume gradually during the first 30 seconds, which is also

shown in the rise of the water level in the initial state. The surplus of water needs to flow out of the flume before the water level and the discharge can adapt.

a) discharge in [m³/s]

b) water level in [m]

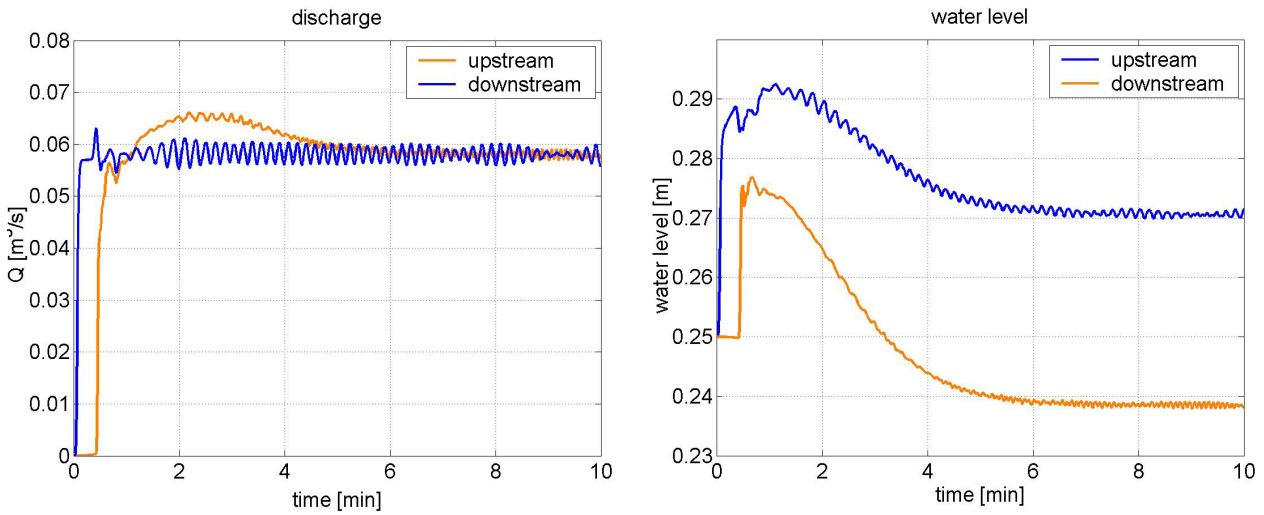


Figure 4-3 Adaptation of the flow
 a) temporal development of the discharge at cross-sections near the US and near the DS boundary
 b) temporal development of the water level at fixed points near the US and near the DS boundary

4.3.2 Instabilities

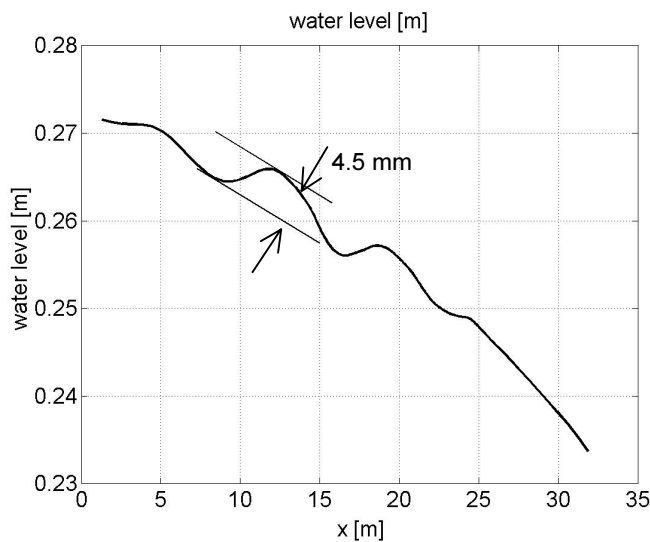


Figure 4-4 Instantaneous view of the water level progression in the main channel

From Figure 4-3 it can be seen that the water level as well as the discharge is fluctuating. These fluctuations are stronger at the upstream side than at the downstream side. When regarding Figure 4-4, which shows an instantaneous plot of the water level in the main channel across the length of the flume, it is noted that there is a wave in the main channel with an amplitude of approximately 5mm on the upstream side and with a period of 10 seconds. This wave is dissipat-

ing when travelling downstream. The reason for the appearance of the wave is possibly the reflection of the inflowing water at the first groyne. This wave could not be removed by variation of the reflection parameter α .

4.3.3 Flow field

Figure 4-5 shows the averaged velocity magnitude and the velocity components in x - and y -directions in the three groyne fields of the test section. It was averaged in the period where the flow was stable, that is to say from the 6th to the 10th minute (=end of simulation). These plots show the typical velocity distribution for a straight channel with groynes, which is also similar to the flow pattern observed by Van Schijndel & Jagers (2002). The plot of the velocity magnitude, u_m and v_m clearly show the circular motion of the water in the groyne field.

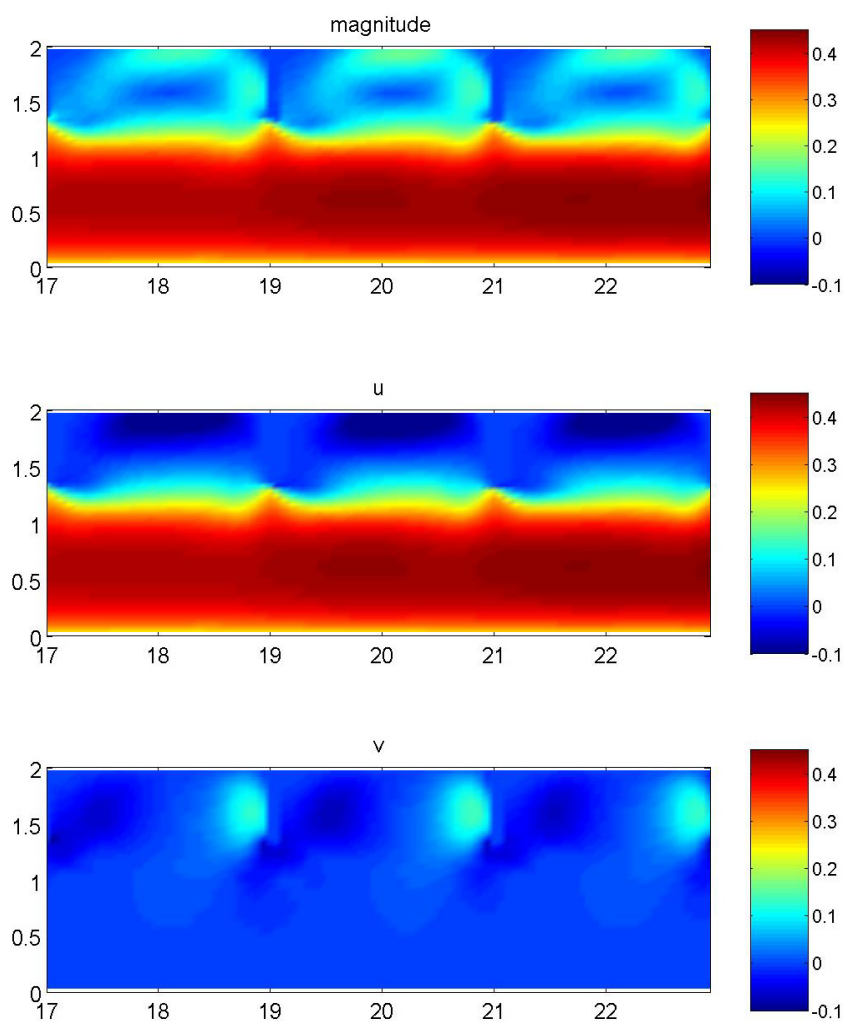


Figure 4-5 Mean velocity components in the test section: magnitude (upper plot), u -component (middle plot), and v -component (lower plot)

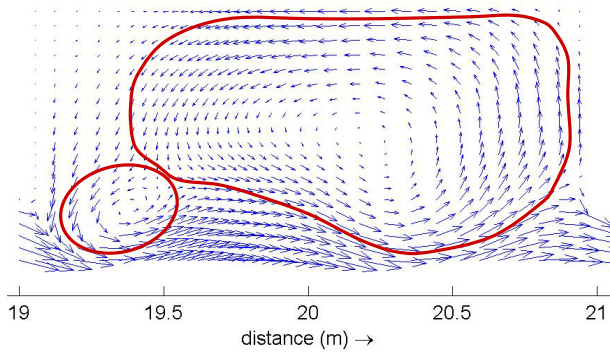


Figure 4-6:

Instantaneous picture of the velocity vectors in a groyne field with indication of the primary gyre and dynamic eddy

When examining the velocity vectors in the groyne field, the computation qualitatively reproduced the system of large turbulent gyres described in Chapter 2.1.3. As can clearly be seen in Figure 4-6 a stationary primary gyre forms, which occupies the downstream two thirds of the groyne field. However, a secondary gyre cannot be identified in the upper left corner, the velocity in this region is nearly zero. The dynamic eddy, which sheds approximately every 5 seconds from the tip of the upstream groyne into the groyne field, merging with the primary gyre is clearly visible.

Figure B-1 in Appendix B shows several momentary shots of the flow vectors in the groyne field. Every 1.2 seconds one picture was recorded. In this way the movement of the dynamic eddy is visualized over one entire period.

4.3.4 Turbulence intensity

The turbulence intensities or standard deviations for the velocity magnitude and the u - and v -components are shown in Figure 4-7 (for the definition of the turbulence intensity, see equations 2-3a and 2-3b). It can be seen that the turbulence intensity is the highest in the mixing layer. Here the v -component is fluctuating in time. The u -component is extremely high just downstream of the groyne tips, where the dynamic eddy forms and a the strongest fluctuations take place. It also has to be stated that the turbulence intensity at the in the first groyne field is higher than in the second and third groyne field.

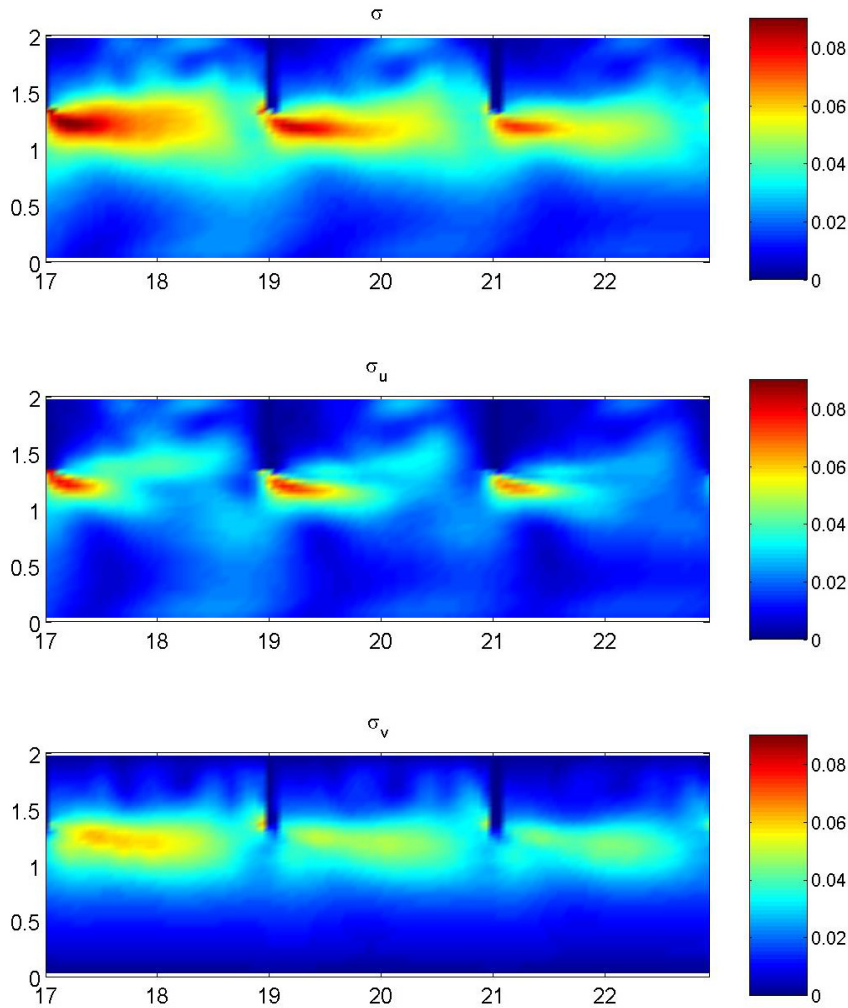


Figure 4-7 Standard deviation (Std.) of the magnitude and the velocity components in the test section: magnitude (upper plot), u -component (middle plot), v -component (lower plot)

4.3.5 Horizontal eddy viscosity

When looking at the distribution of the horizontal eddy viscosity in Figure 4-8 it can be observed that at locations where there is more turbulence the horizontal eddy viscosity ν_H is higher than in areas of steady flow, such as the main channel. The highest values of ν_H occur at the upstream and downstream sides of the groyne tips where the strongest fluctuations take place. At these locations the eddy viscosity reaches relatively high values of maximal $2 \cdot 10^{-3} \text{ m}^2/\text{s}$. In the main channel, in contrast, the eddy viscosity only reaches between $3.0 \cdot 10^{-4}$ and $5.0 \cdot 10^{-4} \text{ m}^2/\text{s}$. Near the side wall where the boundary layer is located the horizontal eddy viscosity is also higher (maximum value: $1.2 \cdot 10^{-3} \text{ m}^2/\text{s}$). The mixing layer between the main channel and the groyne field also shows an increased values of ν_H as well as a location at the upper right-hand side of each groyne field, where the flow is forced around the corner. Surprisingly, at the upstream half of each groyne field the eddy viscosity becomes extremely low. This occurs at the location where the flow is directed in the negative y -direction while the x -component of the velocity is nearly zero (see indication of the primary gyre in Figure 4-8). Another interesting fact is

that at locations where the grid is finer the computed ν_H becomes smaller. It can be therefore deduced that the mesh size influences the value of the computed horizontal eddy viscosity.

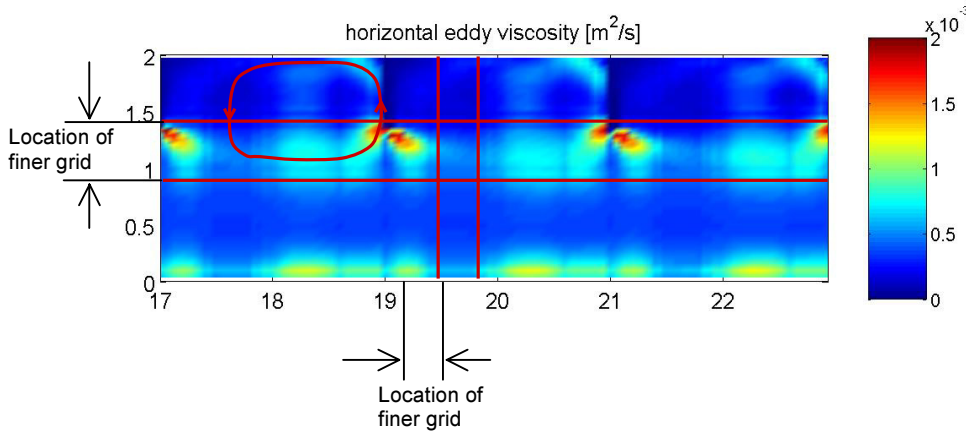


Figure 4-8 Mean horizontal eddy viscosity ν_H in the test section with indication of the primary gyre and the location of the finer grid

4.3.6 Spectral analysis

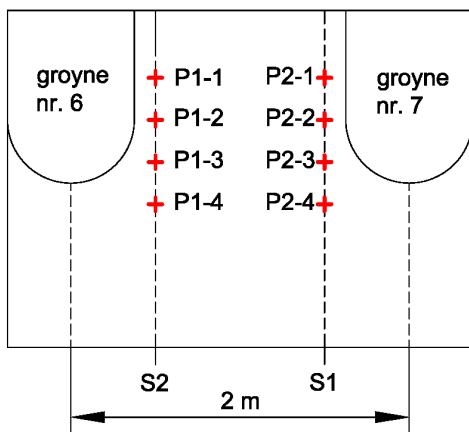


Figure 4-9 Location of the cross-sections and observation points in the middle groyne field of the test section

In order to estimate the flow periodicity a spectral analysis was made at the following points (see Figure 4-9):

- P1-2 and P2-2 (which are located on the line between the groyne tips) and
- P1-4 and P2-4 (which are located in the mixing layer).

The energy density spectra's in Figure 4-10 show the distribution of the turbulent kinetic energy of the velocity components over the frequencies. These spectra were obtained by using the time series of the velocity, and then computing the turbulent energy density using the Fast Fourier Transformation method.

All graphs show that the highest density of turbulent energy can be observed at a frequency of 0.182 Hz which corresponds to a period of 5.48 seconds. This is the period of which the dynamic eddy sheds from the groyne tip and merges with the primary gyre. The series of plots in Figure B-2 in Appendix B confirm this conclusion. A second high peak occurs at the lower fre-

quency of 0.091Hz, which is just half of the main frequency and corresponds to a period of 10.96 seconds. In the loglog-spectra it can be seen that more smaller peaks at further multiple frequencies of 0.091 Hz occur.

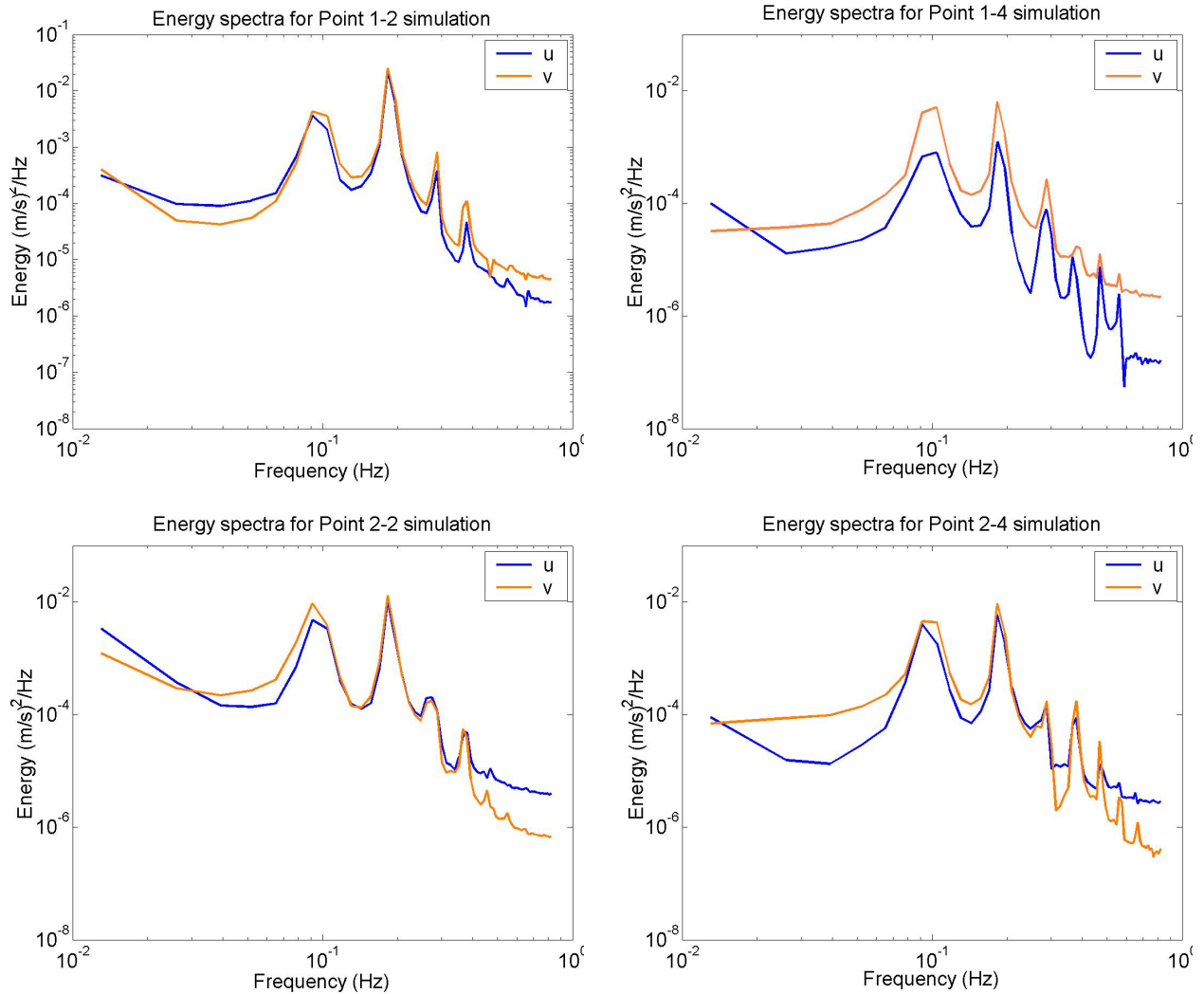


Figure 4-10 Energy density spectra for both velocity components at four monitoring points

Figure 4-11 shows a comparison between the energy density spectra at the point 1-2 from the simulation and from the experiment. The frequency range of the spectra of the experiment is much larger than for the simulation, since the high frequencies are not computed for the simulation. In order to compare the two spectra's only a section of the experimental spectra was plotted. The pictures show that the vortex shedding in the simulation is very regular while in the experiment much distortion occurs. The peak is not very pronounced for the measured velocities, the main frequency is therefore not as clear as for the simulation. The reason for that could be the fact that the measuring devices also recorded much noise. However, the main frequency of the experimental spectra lies in the same range as the main frequency of the simulation (for u : $f=0.195$ Hz and for v : $f=0.183$ Hz).

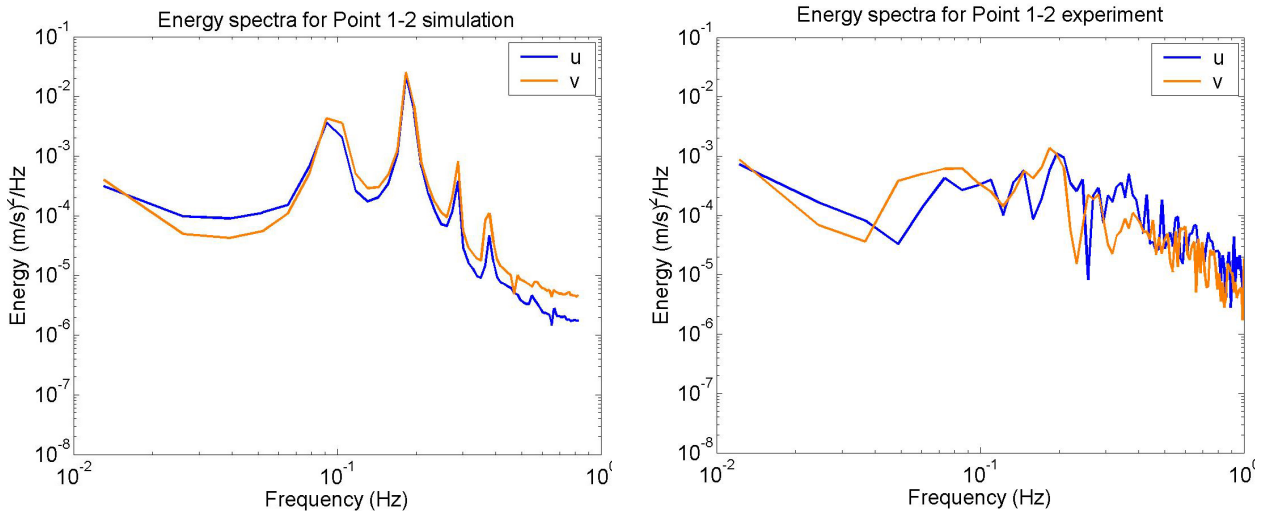


Figure 4-11 Comparison between the energy density spectra at point 1-2:
 - simulation
 - and for the experiment

4.4 SENSITIVITY ANALYSIS

In order to estimate to what extent some selected input parameters influence the result of the hydrodynamic computations, several computations with just one single modified parameter have been carried out. The influence of physical parameters such as the bed roughness and the wall roughness were observed by increasing or decreasing certain parameters by 50%. The three different slip conditions (free slip, no slip, partial slip) were tested. In the case of the partial slip condition one run with an extremely small wall roughness (0.01mm) was made in order to compare it with the case of the free slip condition.

A parameter which can also be used for adaptation is the relaxation time τ . In Chapter 2 it has been explained that for the computation of the horizontal eddy viscosity the fluctuating flow velocities u^* and v^* are defined through a high-pass-filter operator, which calculates the fluctuating component by subtracting a mean velocity, which has been averaged over the period τ (compare Eq. 2.13). The relaxation time τ is also a calibration constant. When choosing a value of $\tau \geq 0$ the high-pass filter is applied. As explained in Chapter 2.3.2 the parameter τ specifies the time span over which the velocity signals are temporally filtered. The use of a negative relaxation time (e.g. $\tau = -1$ as it is specified in the input-file, see Table 4-3) means a switching off of the filtering operation. According to the user manual of Delft3D-FLOW, when utilizing the filtering function the value of τ should preferably be twice the period of the largest eddies. This option is going to be tried out in the sensitivity analysis as well as an 50% increase and decrease of τ . Furthermore four runs were made using a constant horizontal eddy viscosity and switching off the HLES.

An overview of the runs of the sensitivity analysis is given in Table 4-4. The reference run (run1) is the numerical simulation whose input and results have been discussed earlier in this Chapter.

run	modification	Roughness parameters			parameters concerning HLES			
		bed roughness k_s [m]	slip condition [-]	wall roughness [mm]	HLES on/off	constant eddy viscosity ν_H [m ² /s]	high-pass filter on/off	relaxation time τ [min]
1	no modification (reference run)	0.01	partial	0.0018	on	-	off	-1
a) modification of roughness parameters								
2	bed roughness=0.015m (50% increase)	0.015	partial	0.0018	on	-	off	-1
3	bed roughness=0.005m (50% decrease)	0.005	partial	0.0018	on	-	off	-1
4	wall roughness=2.7 mm (50% increase)	0.01	partial	0.0027	on	-	off	-1
5	wall roughness=0.9 mm (50% decrease)	0.01	partial	0.0090	on	-	off	-1
6	wall roughness=0.01mm (extreme decrease)	0.01	partial	1 e -5	on	-	off	-1
7	slip condition: free slip	0.01	free	-	on	-	off	-1
8	slip condition: no slip	0.01	no slip	-	on	-	off	-1
b) modification of parameters concerning HLES								
9	$\tau = 0.1828$ min (2 * period of largest eddy)	0.01	partial	0.0018	on	-	on	0.1828
10	$\tau = 0.3656$ min (50% increase)	0.01	partial	0.0018	on	-	on	0.3656
11	$\tau = 0.0914$ min (50% decrease)	0.01	partial	0.0018	on	-	on	0.0914
12	no HLES, $\nu_H=0$ m ² /s	0.01	partial	0.0018	off	0	off	-
13	no HLES, $\nu_H=0.5 \cdot 10^{-3}$ m ² /s	0.01	partial	0.0018	off	0.0005	off	-
14	no HLES, $\nu_H=1.0 \cdot 10^{-3}$ m ² /s	0.01	partial	0.0018	off	0.0010	off	-
15	no HLES, $\nu_H=1.5 \cdot 10^{-3}$ m ² /s	0.01	partial	0.0018	off	0.0015	off	-

Table 4-3 Overview of the runs of the sensitivity analysis

4.4.1 Influence of the physical parameters

The influence of the roughness, the slip condition and the wall roughness on the flow field will be analysed in this section.

Influence of the bed roughness k_s :

In order to see a real difference compared to the reference run the bed roughness was increased/decreased of 50%. As can be derived by transforming the Chézy or the Manning flow formula a decreased bed roughness will implicate a decrease of the water slope i if the parame-

ters R (hydraulic radius) and the velocity are kept constant. This idea is confirmed when looking at the graph in Figure 4-12, where the average water level in the main channel across the longitudinal section is shown. It can be observed that an increasing of the bed roughness leads to a steeper water slope while a decrease of k_s causes a more flat slope. It has to be mentioned that the reference water level found from the experiments is not a single graph but a range with minimum and maximum values. However, the slope hardly changes during the experiment. Therefore each water level curve, which has the reference slope and lies between the minimum and maximum values, is acceptable.

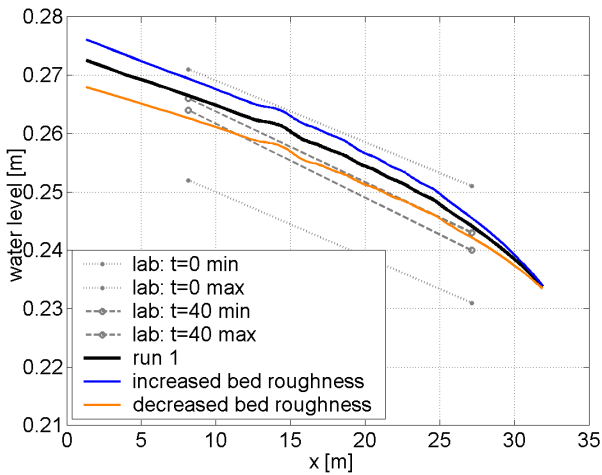


Figure 4-12:
Variation of H along x for the reference run 1 and the runs with an increased and decreased bed roughness by 50%

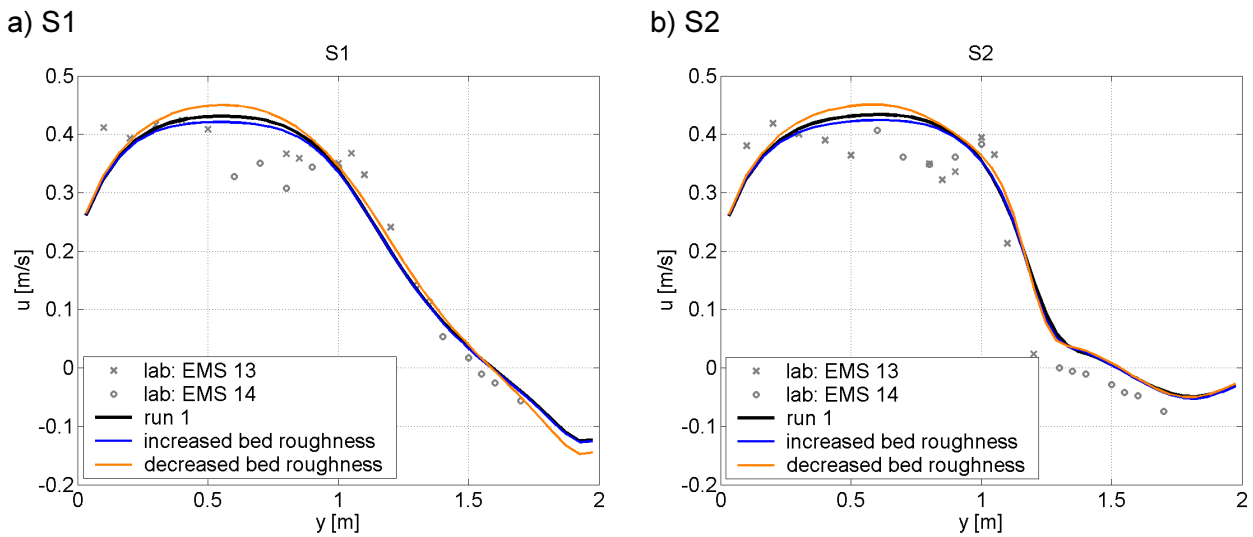


Figure 4-13 Distribution of u along S1 and S2 for the reference run 1 and the runs with a 50% increased and decreased bed roughness

In Figure 4-13 the profile of u at the cross-sections S1 and S2 can be seen for the reference run and for two runs in which only the bed roughness was modified. It can be seen that the modification of the roughness also has an influence on the magnitude of u in the main channel. In Figure 4-13 the results of the simulations are plotted against the experimental results, which are indicated in grey.

Influence of the slip condition and the side wall roughness:

Especially when simulating at a lab scale the wall roughness has a great influence on the flow field. The choice of the slip condition and the wall roughness determines the behaviour of the velocity near the closed boundaries (side walls). In order to analyse the influence of the wall roughness, this parameter was increased and decreased by 50% for the case of partial slip condition. Furthermore the case of a wall roughness of nearly zero (0.01mm) was investigated. The slip conditions 'free slip' and 'no slip' were analysed as well. The results can be seen in Figures 4-14 and 4-15.

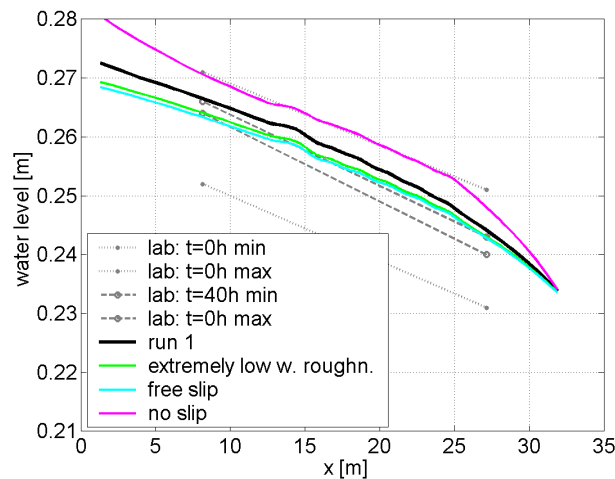


Figure 4-14:
Distribution of H across x for the following runs:
- reference run (run 1)
- run with an extremely low wall roughness (0.01mm)
- run with a free slip condition
- run with no slip condition

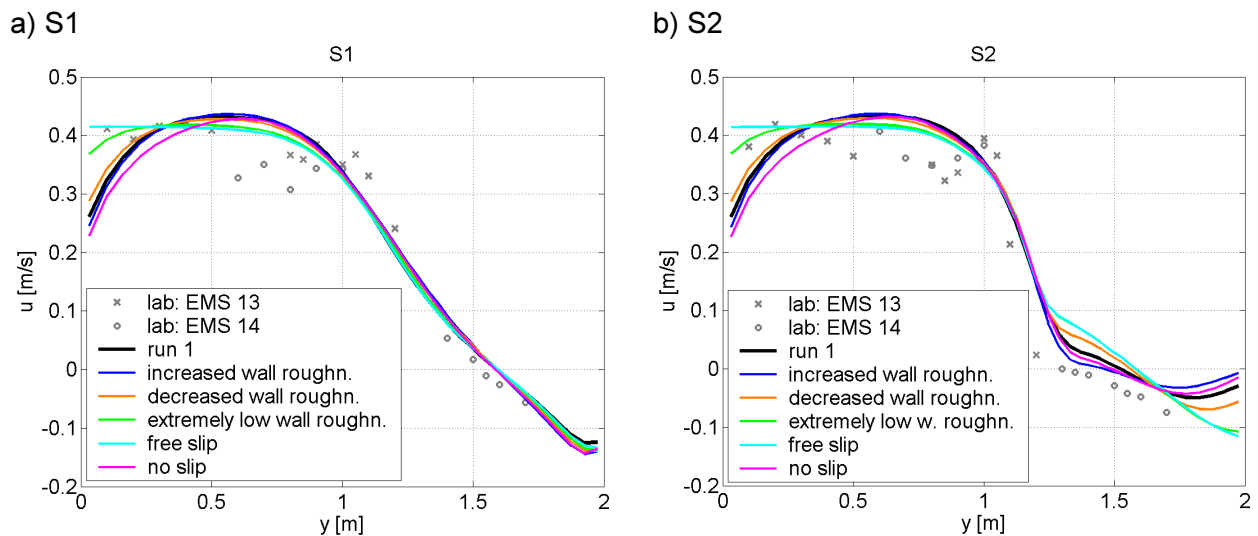


Figure 4-15 Distribution of u across S1 and S2 for the following runs
- reference run (run 1)
- run with a wall roughness increased by 50%
- run with a wall roughness decreased by 50%
- run with an extremely low wall roughness (0.01mm)
- run with a free slip condition
- run with no slip condition

If 'no slip condition' is chosen the velocity near the side walls becomes very low compared to the velocity in the main channel (see Figure 4-15). As expected a decrease of the wall roughness leads to an increase of $|u|$ at the walls and vice versa. If the wall roughness is extremely low the

velocity hardly decreases at the closed boundaries while for the case of 'free slip condition' u doesn't decrease at all. Another interesting aspect is that the water level decreases if the free slip condition or a very low wall roughness is used, while 'no slip condition' increases the water level (see Figure 4-14). A 50% increase or decrease of the wall roughness only has a minor influence on the water level and was therefore not shown in the figure.

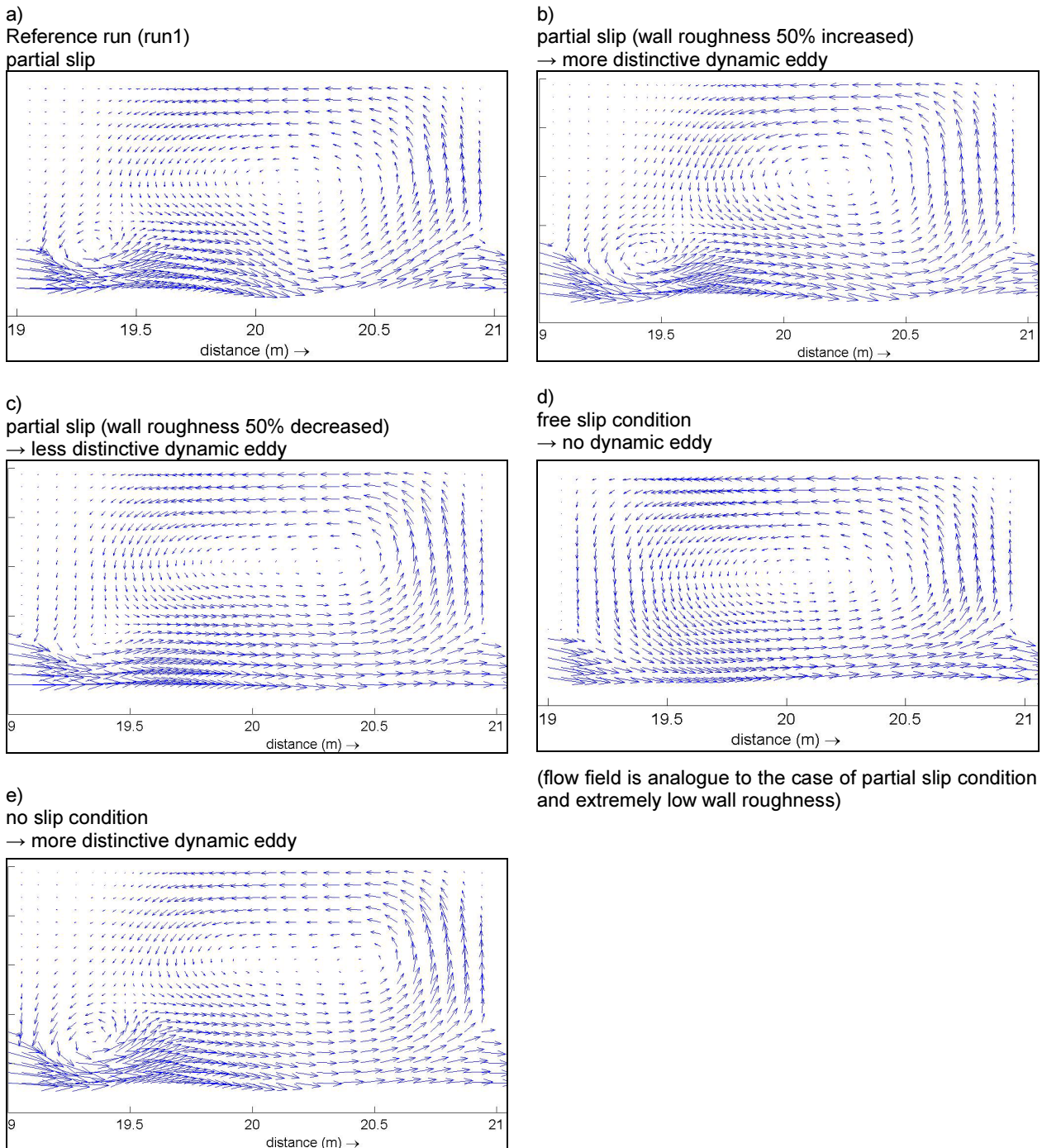


Figure 4-16 Influence of the slip condition and the wall roughness on the flow field in the groyne field

The choice of the wall roughness also has a strong effect on the eddy system in the groyne field, especially on the distinction of the dynamic eddy. Figure 4-16 shows a comparison of the flow vectors in the groyne field. It can be observed that if the free slip condition or a very low wall roughness are used there is no dynamic eddy and a large primary gyre remains, covering the entire groyne field, whereas the choice of 'no slip condition' results in a dynamic eddy which is more pronounced than the one in the reference run. The size of the primary gyre in this case is smaller than in all the other cases. In conclusion, a decrease of the wall roughness leads to a less distinct dynamic eddy while the primary gyre becomes larger whereas an increase results in a more distinct dynamic eddy and a smaller primary eddy.

4.4.2 Influence of the relaxation time

From the spectral analysis it is known that the large eddies in the groyne field have a periodical behaviour at a frequency of 0.182 Hz, which corresponds to a period of 5.48 seconds. The value of the relaxation time τ as proposed in the Delft3D-manual therefore corresponds to

$$\frac{1}{0.182\text{Hz}} \cdot 2 = 10.9655\text{s} = 0.1828\text{min}.$$

This value was chosen as relaxation time τ for a further run. As for the physical parameters an increase and a decrease of 50% was investigated. The modification of τ doesn't have any influence of the distribution of u across the width of the channel nor on the water slope i . The shape and distinction of the dynamic eddy doesn't change much when using a different value of τ (if $\tau > 0$), but the dynamic eddy was for all three modified runs more distinct than for the reference run.

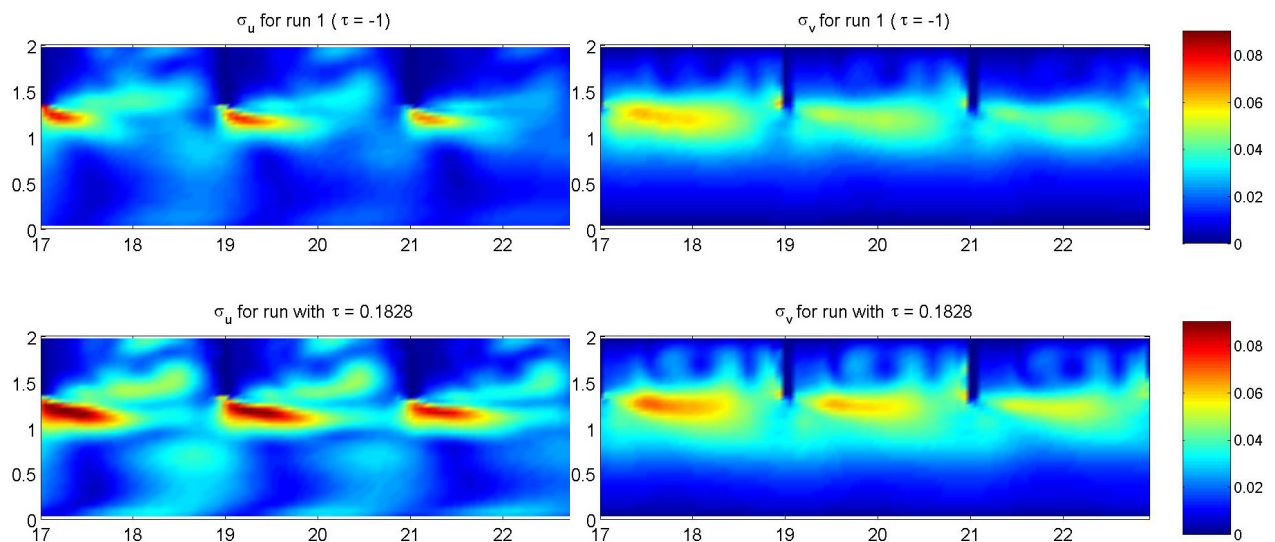


Figure 4-17 Computed turbulence intensities for the components u and v :
 - upper plots: reference run (no filtering)
 - lower plots: run with $\tau = 0.1828$

In Figure 4-17 the turbulence intensities are shown for the reference run and the run with application of the filter. As it can be seen in this figure the fluctuations are stronger when the high-pass filter is used. The computed eddy viscosity distribution for these three runs is nearly identical and is noticeably lower than the eddy viscosity, which has been calculated in the reference run, see Figure 4-18.

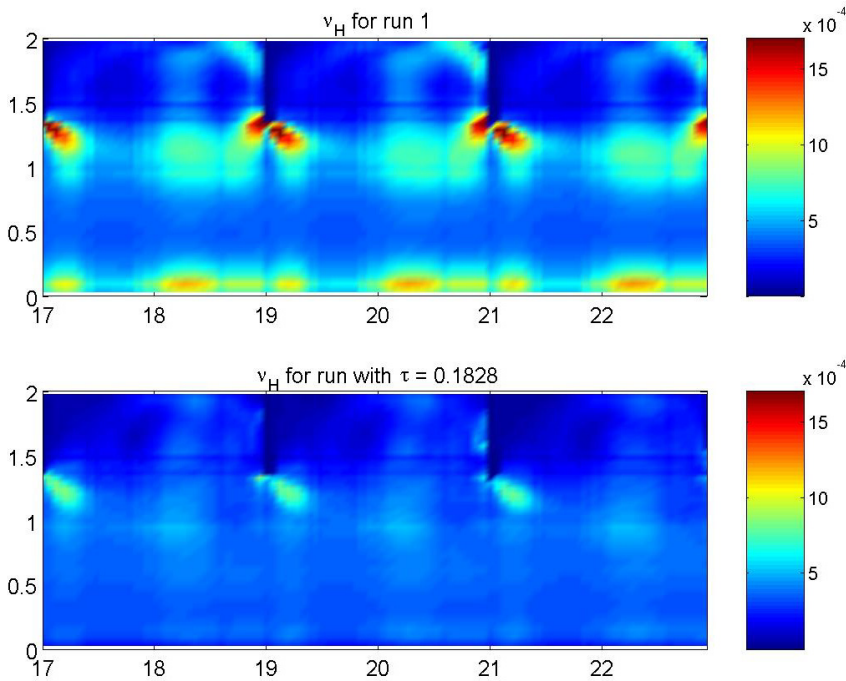


Figure 4-18 Computed horizontal eddy viscosity for the reference run (no filtering, upper plot) and for run H18 (lower plot)

4.4.3 Influence of a constant eddy viscosity

Four runs were made using a constant eddy viscosity and switching off the HLES. From the upper picture in Figure 4-18 the distribution of the horizontal eddy viscosity for the reference run is shown. The constant values of ν_H for the numerical simulation were chosen to be $0 \text{ m}^2/\text{s}$, $0.5 \cdot 10^{-3} \text{ m}^2/\text{s}$, $1.0 \cdot 10^{-3} \text{ m}^2/\text{s}$, $1.5 \cdot 10^{-3} \text{ m}^2/\text{s}$. Figure 4-19 shows the influence the constant eddy viscosity has on the slope in the distribution of u across y . With the exception of $\nu_H = 0$ (S2) it can be deduced the trend that the smaller the constant ν_H was chosen, the steeper the slope of the velocity in the groyne field (between $y=1.35$ and $y=2.0$) becomes. In contrast with the assumption that the slope of u in the mixing layer will be influenced in the same way, the graphs show no clear trend here. Generally speaking distribution of a run with a constant eddy viscosity of $1.0 \cdot 10^{-3} \text{ m}^2/\text{s}$ resembles most the distribution of the reference run.

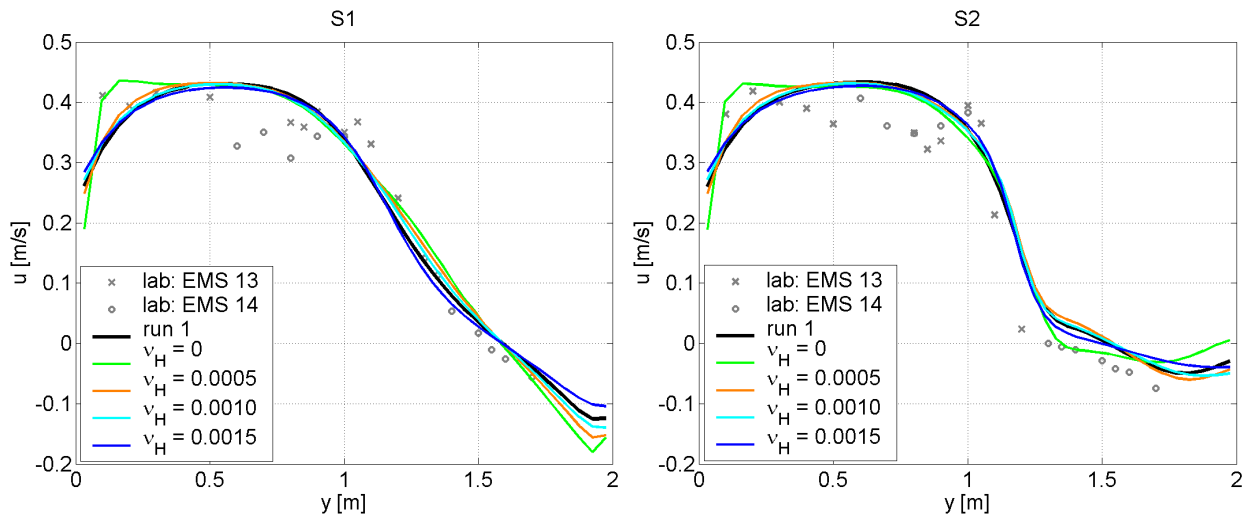


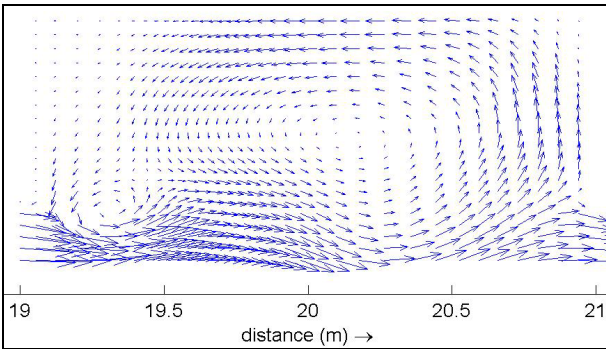
Figure 4-19 Distribution of u across S1 and S2 for the reference run (with HLES) and some runs with various constant horizontal eddy viscosities

When looking at the flow pattern in the groyne field in Figure 4-20 the dynamic eddy disappears and the fluctuations decrease when ν_H is chosen to be relatively large. However for small viscosities the flow pattern appears more fluctuating. For the extreme case of $\nu_H = 0$ the dynamic eddy is very strong and the shape of the primary gyre very unstable. Among the observed flow patterns the pattern of the computation using a constant eddy viscosity of $0.5 \cdot 10^{-3} \text{ m}^2/\text{s}$ resembles most to the reference run.

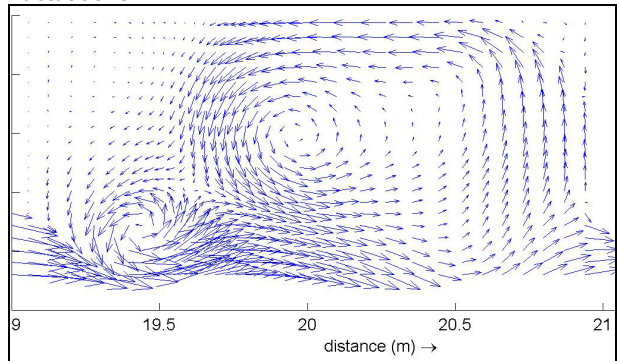
It also has to be stated that when using a large eddy viscosity the waves which occurred in the main channel (compare section 4.3.2) disappear. As a conclusion, a choice of a relatively large constant horizontal eddy viscosity results in a very stable simulation, but also dampens the fluctuations in the groyne fields, which is not desired. The use of a small constant viscosity shows a very highly fluctuating flow pattern in the groyne field, but also leads to waves in the main channel. It therefore makes sense to use HLES which calculates the horizontal eddy viscosity temporally and spatially dependent.

In order to better judge the influence of the HLES for the morphological simulation one computation shall be analysed using a constant eddy viscosity which lies between 0.5 and $1.0 \cdot 10^{-3} \text{ m}^2/\text{s}$.

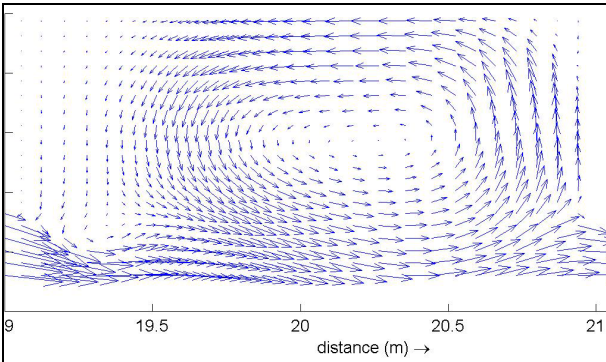
a)
Reference run (H10)
HLES used



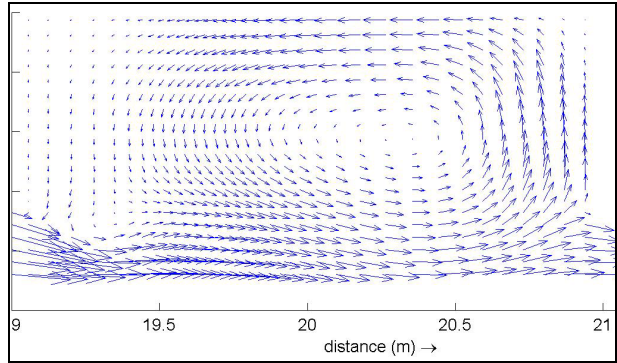
b)
eddy viscosity of $0 \text{ m}^2/\text{s}$
→ extremely distinctive dynamic eddy and very strong fluctuations



c)
eddy viscosity of $0.5 \cdot 10^{-3} \text{ m}^2/\text{s}$
→ dynamic eddy and fluctuations slightly weaker than for the reference run



d)
eddy viscosity of $1.0 \cdot 10^{-3} \text{ m}^2/\text{s}$
→ dynamic eddy and fluctuations weaker than for the reference run



e)
eddy viscosity of $1.5 \cdot 10^{-3} \text{ m}^2/\text{s}$
→ no dynamic eddy

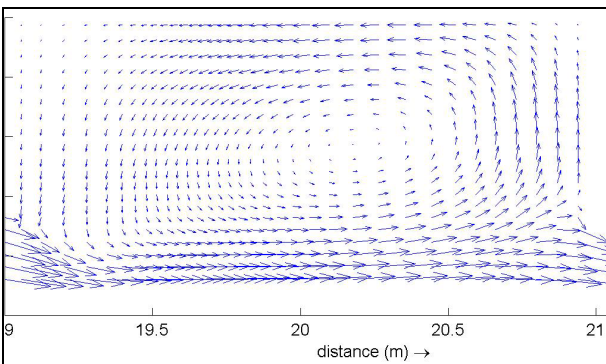


Figure 4-20 Influence of the eddy viscosity on the flow field in the groyne field when not using HLES

5 MORPHODYNAMIC SIMULATION

After the analysis of the flow field, the sediment transport can be added to the simulation. This is done using the add-on 'Online-sediment' which has been implemented in the Delft 3D system. The formulas used by this module were explained in section 2.3.2. The additional input information, which is necessary for the morphodynamic computations, concern the nature of the sediment and characteristics about the transport process itself.

5.1 MODEL SET-UP

In order to activate the Online-sediment feature in Delft3D-FLOW the presence of the sand has to be specified in the graphical user interface in the sub-data-group *Processes*. The sand is defined as a constituent, and further characterized as non-cohesive sediment. Its specific parameters have to be defined in a additional sediment input file (*.sed). The morphological input file (*.mor), which has to be loaded as well, contains specific parameters and factors which are necessary for the transport computations.

5.1.1 Sediment

The sediment, which was used in the flume experiment, was a fine grained sand of a specific density ρ_s of 2650 kg/m³ and a parameter delta (Δ), which is defined as

$$\Delta = \frac{\rho_s - \rho}{\rho} \quad (5.1)$$

and has a value of 1.65. As it can be seen in the distribution curve in Figure 5-1, the grain size is nearly uniform. Simplifying, the sediment specified in the sediment input file was therefore defined as a uniform sediment of the grain size 160 μ m, which corresponds to the D_{50} of the used sediment. Furthermore the initial thickness or the initial sediment mass at the flume bed per unit area had to be indicated. In the case of a flume with a sediment bed of 0.125m thickness but with groynes made of concrete, which are not covered by sand, the sediment mass per unit area is not constant in space. Therefore this parameter has to be defined at each point of the grid using a file (*.sdb). At the bed the sediment mass per unit area amounted to $0.125\text{m} \cdot 1650 \frac{\text{kg}}{\text{m}^3} = 206.25 \frac{\text{kg}}{\text{m}^2}$ while on the groynes the initial sediment mass was equal to zero. The critical bed shear stress according to Shields is calculated according to

$$\tau_{b,cr} = \theta_{cr} [(\rho_s - \rho)g D_{50}] \quad (5.2)$$

where $\theta_{cr} = f(\text{Re}^*)$ is the critical Shields parameter taken from to the Shields curve.

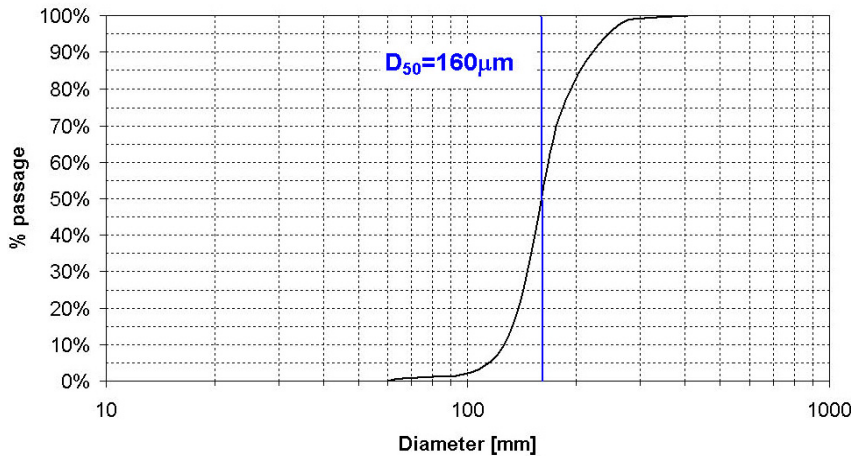


Figure 5-1 Distribution curve of the sediment with indication of the grain size used in the simulation

The sediment transport will be computed as described in Section 2.3.2. The parameters *SUS* and *BED*, which are specified in the morphological input file, are multiplication factors for the suspended sediment reference concentration and for the bed load transport vector magnitude. They serve to adjust the sediment transport rates.

5.1.2 Time management

In addition to the sediment properties further specifications concerning the time frame for the morphological computations have to be provided. Some specific parameters will be explained briefly:

- a) The *morphological scale factor* upscales the velocity of morphological changes. It is a multiplication factor, with which the morphological changes which take place during of the computed flow time, are multiplied. This method allows to compute morphological changes over a long period in moderate computing times. In this computation a t_{mor} of 100 is used which means that 6 minutes of computed flow time correspond to 10 hours of computed real time, (see Eq. 5.3 and Table 5-1)

Relation between real time and flow time:

$$t_{mor} (T_{stop} - T_{start}) = t_{real} \quad (5.3)$$

where

- t_{mor} morphological scale factor [-]
- t_{real} real period of time (morphological time) [s]
- T_{stop} stop date of morphological computation [s]
- T_{start} start date of morphological computation [s]

- b) The *spin-up interval before morphological changes*, has the purpose to prevent that initial instabilities in the sediment transport have a effect on the bed level.

5.1.3 Initial and boundary conditions

The initial and boundary conditions have to be provided with information about the sediment concentration. An initial sediment concentration has to be defined. The sediment input from the flume experiment accounted for 28.6 kg/hr. With a constant inflow discharge of $Q=0.058\text{m}^3/\text{s}$ and the assumption that all sediment spreads equally across the flume an average concentration of $c=0.137\text{kg}/\text{m}^3$ is found. As for the boundary condition, it was specified that the sediment input starts after 8min of running time, after the flow had stabilized. Ten more minutes (computed flow time) pass in which the sediment transport has time to stabilize before the bathymetry update begins at $t=14$ minutes (see Figure 5-2). It had been calculated that the suspended sediment concentration reaches the equilibrium concentration very quickly and before the sediment reaches the first groyne. As a consequence the sediment concentration at the upstream boundary condition was chosen to be the equilibrium concentration, which will be computed by Delft3D for each time step and location (for the calculation of the equilibrium concentration see Appendix A). From the experiment no data about the amount of sediment flowing out is available for the run G1i. The sediment concentration will therefore be set as the equilibrium concentration on the downstream side.

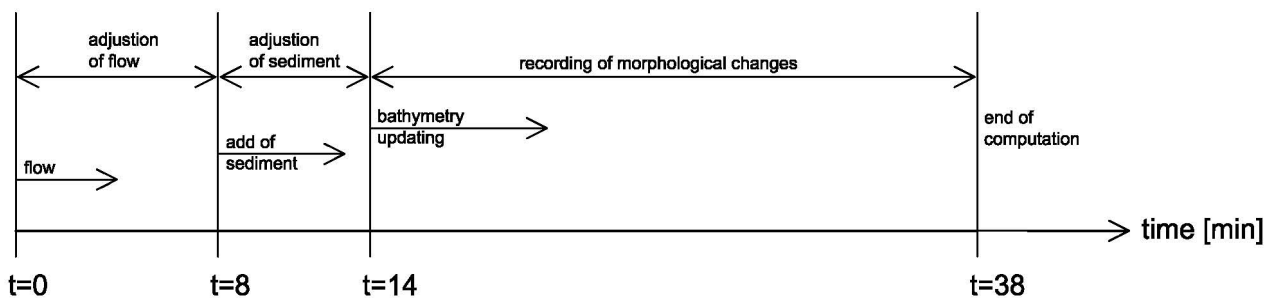


Figure 5-2 Time line for the morphological computation

Input

In Table 5-3 the input data for the morphological simulation is summarized:

Parameter	Value	Unit
Grid	specified in *.grd file	
Bathymetry	specified in *.dep file	
Time frame		
computational time step Δt	0.024	s
total time of simulation	38	min
start of sediment input after	8	min
bathymetry updating after	14	min
→ time span of morphological changes		
flow time	24	min
real time	40	h
Initial conditions		
initial water level H_i	0.245	m
initial sediment concentration c_i	0.137	kg/m ³
Boundary conditions		
upstream boundary:		
type of bound. condition	total discharge (const.)	
Q	0.058	m ³ /s
reflection parameter α	10	-
sediment concentration c_{US}	= c_e	kg/m ³
downstream boundary		
type of bound. condition	water level bound. (const.)	
H	0.245	m
reflection parameter α	12	-
sediment concentration c_{DS}	= c_e	kg/m ³
Sediment data		
sediment density ρ	2650	kg/m ³
sediment parameter Δ	1.65	-
grain size D_{50}	160	μm
critical bed shear stress for erosion θ_{cr}	0.104	N/m ²
sediment mass at bed	specified in *.sdb-file	kg/m ²
Morphological data		
morphological scale factor	100	-
spin-up interval for morph. changes	14	min
multiplication factor SUS	1	-
multiplication factor BED	1	-
Constants		
water density ρ_w	1000	kg/m ³
gravitational acceleration g	9.81	m/s ²
Roughness		
bed roughness k_s	0.01	m
slip condition	partial slip condition	-
wall roughness	0.0012	m
Parameters concerning HLES		
relaxation time τ	-1	min
Prandtl-Schmidt number σ_T	0.7	-
Spatial low-pass filter coeff. f_{lp}	0.3	-
Dimensional number n_D	2	-
Slope in loglog-spectrum α	5/3	-
	} Default settings for the use of HLES	

Table 5-1 Input parameters for the morphological simulation

5.2 RESULTS AND COMPARISON WITH THE EXPERIMENT

5.2.1 Bed levels

Generally speaking the numerical simulation yielded qualitatively the same erosion/sedimentation pattern as observed in the laboratory experiment, see Figure 5-3. However, some major differences between simulation and experiment have to be reported:

Erosion and deposition in the main channel

The erosion rate in the middle of the main channel in the numerical simulation is significantly larger than in the experiment. While only little erosion of the bed in the main channel was observed in the experiment, the computed erosion amounted to a maximum of 2.5 cm, which lies in the same range of the erosion near the groyne tip (see Figure 5-4). However, near the side wall no erosion occurred. In the early state (during the first 5 hours after bathymetry updating) even some deposition was observed in the simulation, which was not observed in the flume experiment either. This was due to the lower velocity near the wall and resulted in a reshaping of the main channel. After 10 hours (real time) the bed level in the main channel had a parabolic shape, see Figure 5-5. If a free slip condition was chosen, this shape would certainly not occur. However, the partial slip condition and the wall roughness, that was used, had been calibrated due to the flow pattern in the groyne field.

Formation and location of the scour hole

The scour hole at the groyne tip is, in contrast to the experimental results, not deeper than the main channel. After 40 hours the maximum depth of the scour hole was only 2.5 cm. This is very little compared to the measured scour holes, the depths of which reach up to 6.5 cm. In Figure 5-4, which shows the temporal development of the scour hole and the main channel, it can be seen that the scour hole develops very quickly. The erosion of the scour hole is in the same range as the erosion in the main channel, while in the experiment the erosion of the scour hole is much stronger in comparison to the erosion of the main channel. Furthermore, the location of the scour hole is not exactly the same as in the experiment. The diagonal line in Figure 5-3 indicates the direction of the movement of the dynamic eddy. It can be seen that in the simulation the scour hole is not located on this line, but closer to the main channel.

Shape and volume of the deposition ridge

The shape of the deposition ridge in the groyne field differs from the measured one. While the deposition ridge in the experiment has a large width and a small height, the simulated deposition ridge has a much larger height and a smaller width (see Figure 5-3). From this shape it can be deduced that the suspended sediment, which is expected entering the groyne field, immediately settles as soon as the velocity decreases. Figure 5-6 shows the summation of the deposition volumes per unit width over the width of the flume and the summation of the deposition volumes per unit length over the length of one groyne field. From these plots it can be also seen

that most of the computed deposition takes place in front of the groyne field, that is to say at $y \leq 1.35\text{m}$. Hardly any sediment enters the groyne field. However, the total computed volume of deposited sediment in the groyne field was $5.03 \cdot 10^{-3} \text{ m}^3$, which is approximately 81% of the measured volume of deposition. Even though the computed deposition ridge is higher than in the experiment, the total volume of deposition is less than the volume from the experiment.

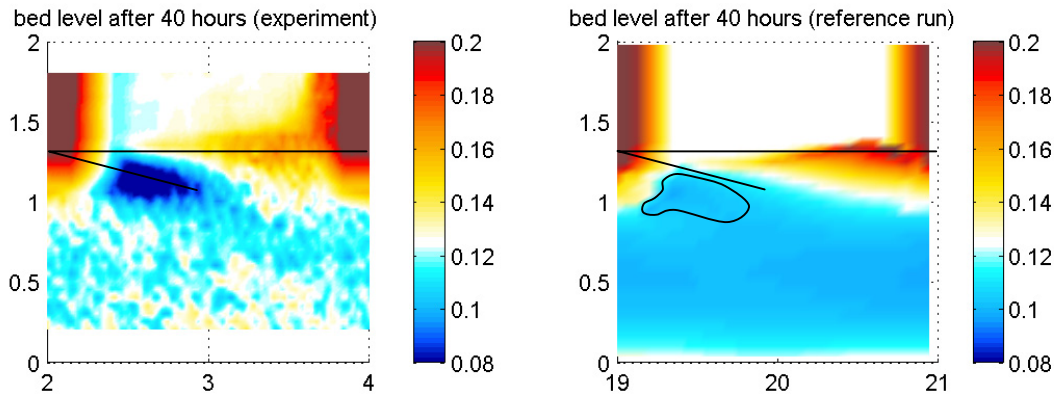


Figure 5-3 Comparison of simulation and experiment: bed levels after 40 hours

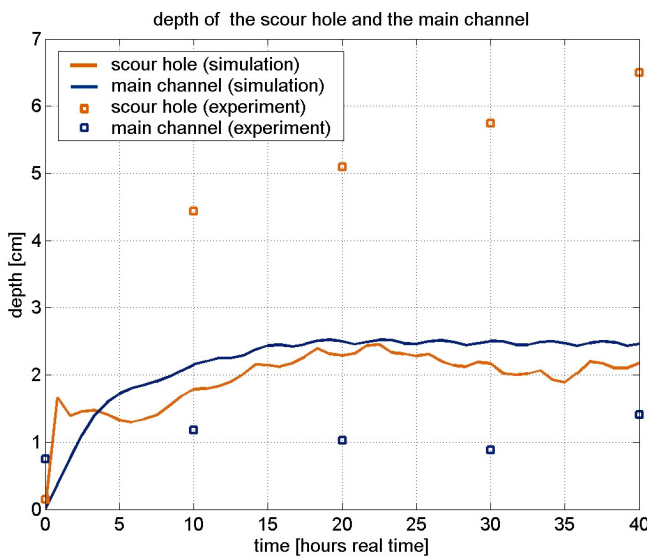


Figure 5-4: Comparison of simulation and experiment: temporal development of the erosion at the deepest point of the scour hole and the middle of the main channel

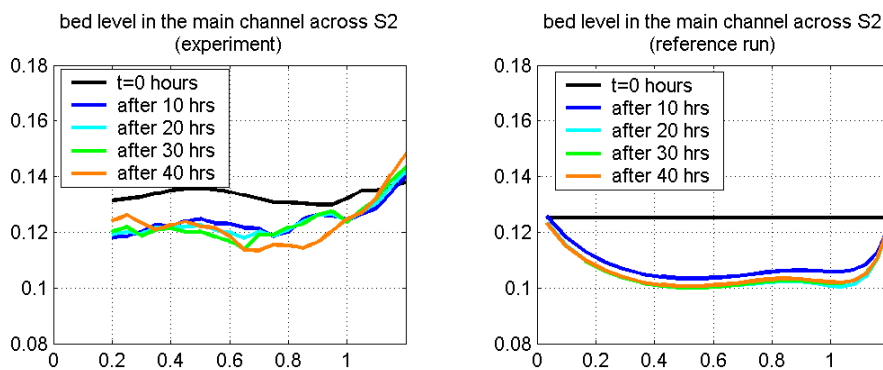


Figure 5-5 Comparison of simulation and experiment: bed levels in the main channel

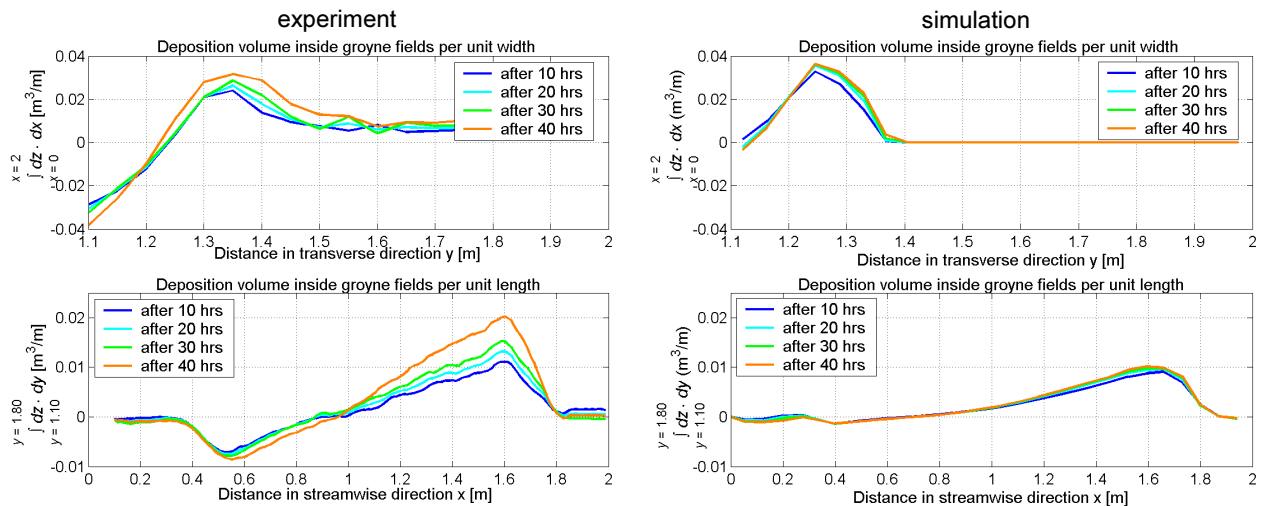


Figure 5-6 Deposition volumes inside the groyne fields (upper plots are the summations over the length of one groyne field, lower plots are the summations over the width of one groyne field)
 - left picture: experiment
 - right picture: simulation

Ripples

The ripples observed in the flume experiment were not observed in the simulation. This was expected because the grid is too coarse to resolve the small ripples. Yet, the influence of the ripples on the flow is taken into account in the bed roughness.

5.2.2 Sediment transport rate

As it can be seen in Figure 5-7 on the next page, both the suspended sediment transport and the bed load transport mainly take place in the main channel. The y -component of both bed load transport and suspended sediment transport is much lower in both cases, which explains that hardly any sediment enters the groyne field. The fact that no sediment enters the groyne field, is a major difference from the experiment.

Figure 5-8 shows the mean velocity in y -direction (upper plot), the mean suspended sediment transport in y -direction (middle plot), and the mean concentration along the normal line (lower plot). The normal line is located along $y=1.35$ m. At the section where the v is positive, some suspended sediment is transported into the groyne field and the concentration is higher. The rate of suspended sediment transport is extremely low, though (order of magnitude: 10^{-10} kg/sm²). The bed load transport in v -direction, (which has not been plotted here) amounted to zero along the normal line. When comparing the mean concentration with that in the experiment at one specific point, the computed value is only approximately 7% of the measured one.

A possible explanation for the suspended sediment transport being so extremely low is that the flow component in the y -direction in this region is not correctly represented. The upper plot in Figure 5-8 also shows, that the measured velocity component in v is twice as high as the computed v -component of the velocity at this point.

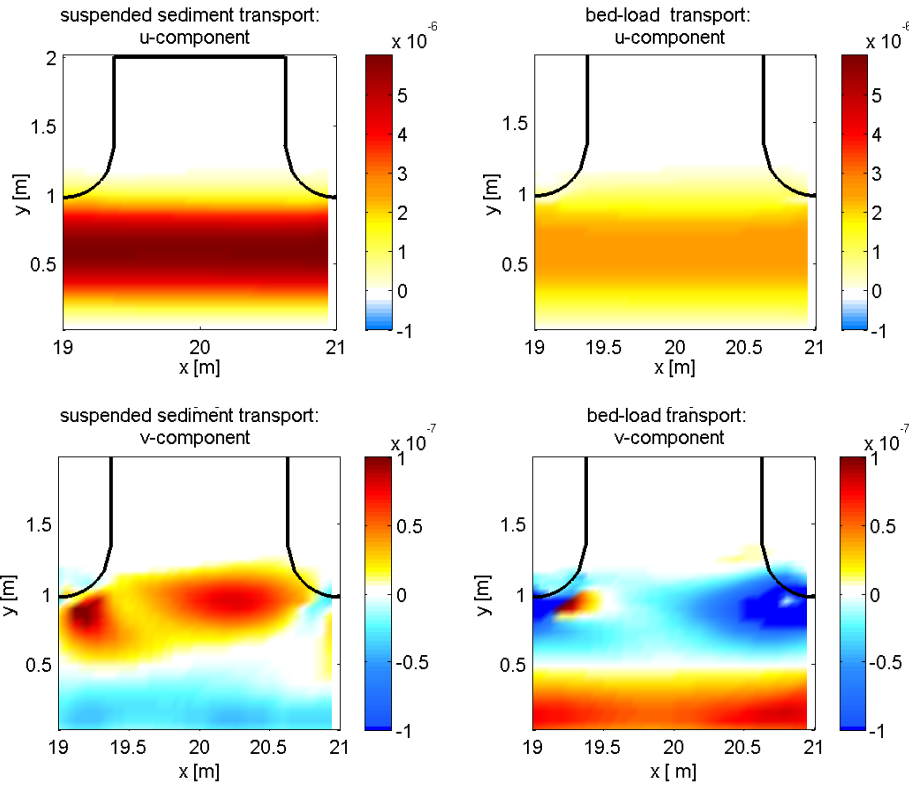


Figure 5-7 Components of the mean depth averaged suspended sediment and bed-load transport [kg/sm^2] in one groyne field

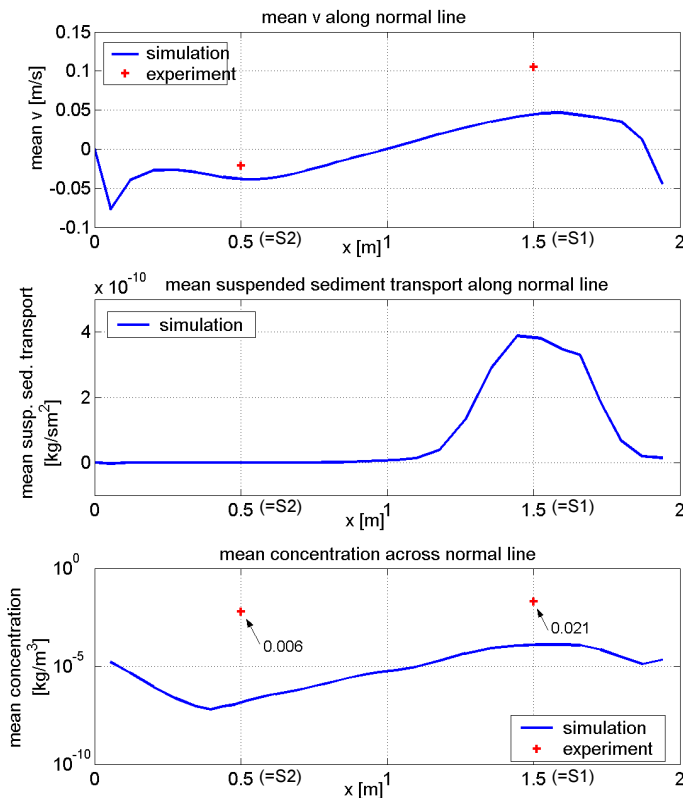


Figure 5-8:

upper plot: mean velocity (y -component) for the simulation along the normal line and for the experiment at two points ($x=S2, y=1.35$ and $x=S1, y=1.35$)

middle plot: mean suspended sediment transport (y -component) along the normal line

lower plot: mean concentration for the simulation along the normal line and for the experiment at two points ($x=S2, y=1.35$ and $x=S1, y=1.35$)

5.2.3 Suspended sediment concentration

The left picture in Figure 5-9 shows the temporal development of the equilibrium concentration near the upstream and downstream boundaries. As in the morphological input file it had been specified that the equilibrium concentrations are defined at the upstream and downstream boundaries, c_e corresponds to the concentration of the sediment at these locations.

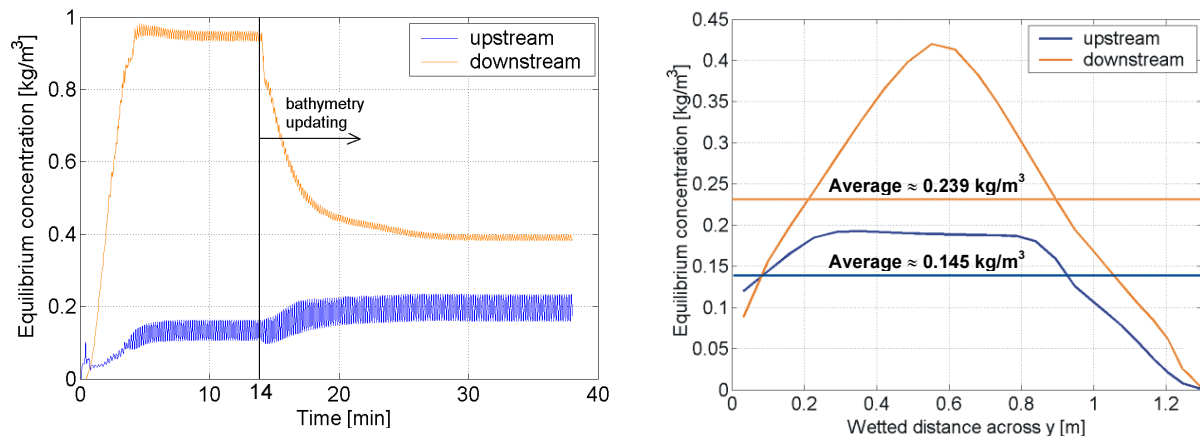


Figure 5-9 Equilibrium concentration at two monitoring points upstream and downstream
left: c_e as a function of time
right: c_e at the last time step ($t=38$ min computed flow time) across y (wetted distance) with average values of c_e

In the initial state the concentration downstream is much higher than the concentration at the upstream end. As soon as the bathymetry updating begins ($t=14$ min computed flow time) the erosion in the main channel takes place and the water level decreases slightly. As a consequence the wetted area decreases at the upstream end and increases at the downstream end. Consequently the upstream concentration increases while the downstream concentration decreases. At approximately $t=24$ min (computed flow time), which corresponds to 16.7 hours (computed real time after bathymetry updating) the erosion in the main channel stops and both concentrations reach a steady state. In the second picture in Figure 5-9 the distribution of these concentrations and their average values are plotted across the wetted width of the channel. The average concentration c_e at the downstream end is now approximately 65% higher than the upstream concentration.

Figure 5-10 shows the transverse sediment concentration profile across the cross-sections S1 and S2. It can be seen that at the location between the main channel and the groyne field the concentration gradient is very high, which goes along with the quick settling of the sediment in front of the groyne field. When comparing the distribution of the computed concentrations with the concentration measurements, it can be seen that the gradient of the measured concentrations is much lower. Theoretically, the suspended sediment concentration needs a certain adaptation time and length to reach the low equilibrium concentration in the groyne field. It is possible, that the transport module assumes a too low adaptation length, which results in this high gradient.

In addition, the concentration in the main channel near the side wall strongly decreases, which is not realistic either. This is due to the velocity profile in the main channel, which is a result of the partial slip condition and the chosen wall roughness. Therefore, a different slip condition will be investigated in the sensitivity analysis.

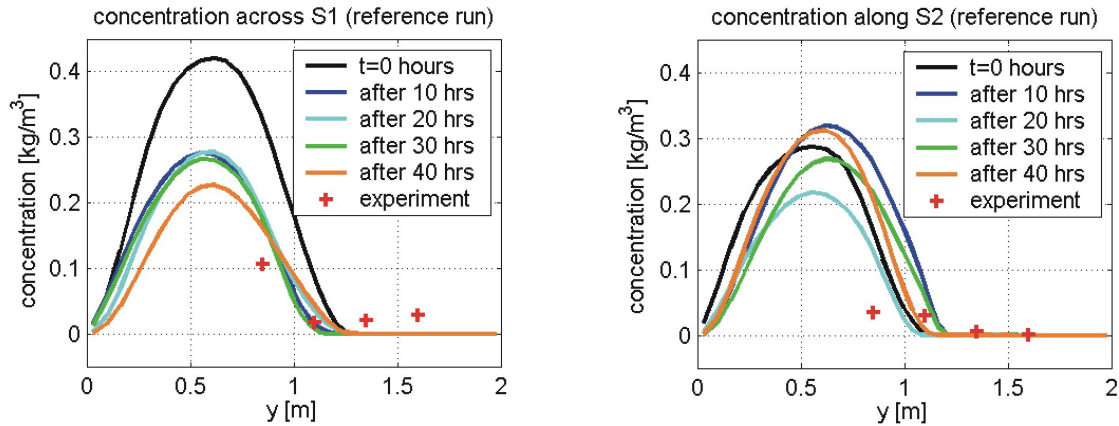


Figure 5-10 Transverse sediment concentration profile across S1 and S2

Several attempts will be made in order to improve the erosion/deposition pattern. The modifications and their influence will be discussed in the sensitivity analysis.

5.3 SENSITIVITY ANALYSIS FOR THE MORPHODYNAMIC COMPUTATIONS

In the following chapter the influence of several modifications will be investigated. Several attempts will be made in order to improve the erosion/deposition pattern in the main channel and the groyne field. Some runs in the sensitivity analysis have different conditions than those in the laboratory experiment. However, the goal of this sensitivity analysis is to achieve a better accordance with the measured bed levels and to evaluate, which modification leads to a better result.

At first the sediment will be represented by several grain size fractions instead of only one. As a second modification, the actual bed shear stress will be multiplied by factors, which will vary spatially. In this way the actual bed shear stress will be modified at locations of higher turbulence, which is expected to result in an intensified erosion rate at these locations. It is assumed that in this way the scour holes, which are of too weak distinction, will be better reproduced. The influence of a modification of the relaxation time τ , the transport boundary conditions, and the slip condition will be analysed, in further runs. An overview of the modifications is given in Table 5-2:

run	modified parameter	description of modification
M1	no modification (reference run)	-
M2	segmenting of the sediment 3 grain sizes	initial conditions } sediment data } see Table 5-3
M4	enhancement of the bed shear stress	use of add-on, which loads a file that specifies locations and factors for the enhancement of the bed shear stress
M5	modification of the relaxation time	$\tau = 0,1828$ min instead of -1 min (compare section 4.4.2)
M6a	modification of the transport boundary conditions	transport boundary conditions: no equilibrium concentration at boundaries, instead: upstream: sediment concentration $C_{us} = 0,137 \text{ kg/m}^3$ downstream: sediment concentration $C_{ds} = 0,069 \text{ kg/m}^3$
M6b	modification of the transport boundary conditions	transport boundary conditions: no equilibrium concentration at boundaries, instead: upstream: sediment concentration $C_{us} = 0,478 \text{ kg/m}^3$ downstream: sediment concentration $C_{ds} = 0,239 \text{ kg/m}^3$
M7	modification of the slip condition	free slip condition instead of partial slip

Table 5-2 Overview over the sensitivity analysis for the morphological runs

5.3.1 Influence of the sediment gradation

Use of three sediment fractions

The sediment, which has been simplified to a uniform sediment for the input of the original run, is now represented more realistically. A fine and a coarse fraction are added, that is to say, the fractions with the diameter D_{90} and the D_{10} each cover 25% of the total amount while the fraction with the mean diameter D_{50} accounts for 50% of the total amount (see Figure 5-11). It is expected, that the fine particles will get in suspension more easily. They are furthermore expected to enter the groyne field and not to settle so quickly, which will change the shape of the depositional pattern on the upstream side of each groyne. A detailed description of the modified sediment data is given in Table 5-3.

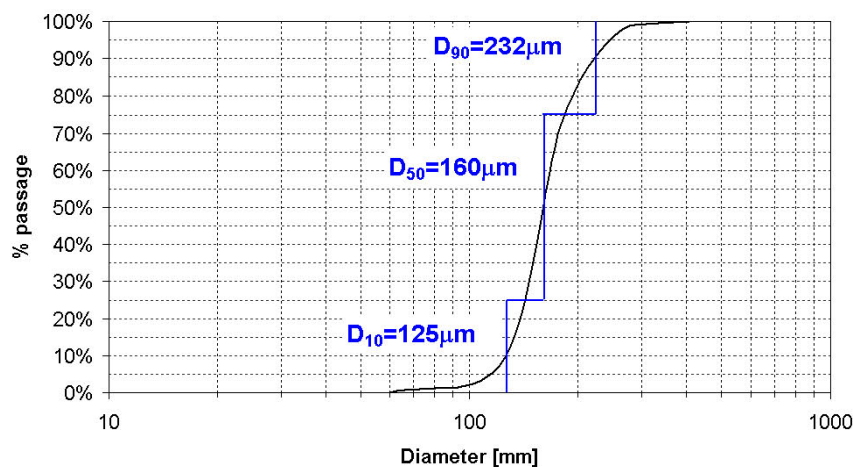


Figure 5-11 Distribution curve of the sediment used in the flume experiment with indication of the grain sizes used in the simulation (run M2)

Parameter	Value	Unit
Initial conditions		
initial water level H_i	0.245	m
initial sediment concentration c_i		
fraction D_{10}	0.0342	kg/m ³
fraction D_{50}	0.0685	kg/m ³
fraction D_{90}	0.0342	kg/m ³
Sediment data		
grain diameter		
fraction D_{10}	125	μm
fraction D_{50}	160	μm
fraction D_{90}	232	μm
initial mass of sediment at bed		
fraction D_{10}	25%	} specified in *.sdb-files
fraction D_{50}	50%	
fraction D_{90}	25%	

Table 5-3 Modifications for the input when using three grain size fractions (run M2)

The result of this run is shown in Figure 5-12. The plot of the bed level after 40 hours shows a decrease of the deposition height and a deeper scour hole (depth of scour hole: 4cm). Consequently, the better representation of the sediment fractions improves the erosion/deposition pattern. Figure 5-13 shows the bed level height after 0, 10, 20, 30, and 40 hours of simulation (real time) along the cross section, where the scour hole forms ($y=1.0$ m). When using three grain fractions instead of only one, the scour hole becomes noticeably deeper. When investigating the sediment transport, no changes are observed compared to the reference run. The shape of the deposition ridge does not differ from the one in the reference run, which means that the suspended sediment doesn't enter the groyne field, even though a finer graded fraction was added for this simulation.

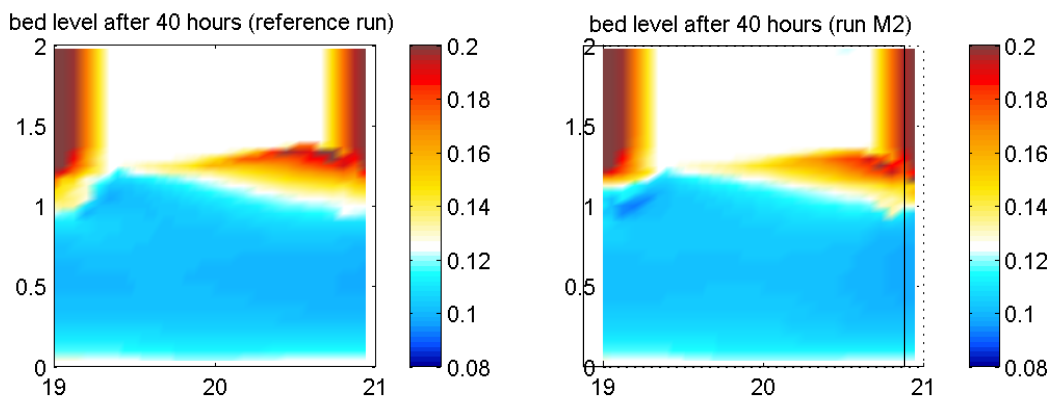


Figure 5-12 Comparison of simulations: bed levels after 40 hours for the reference run and for run M2 (3 grain sizes)

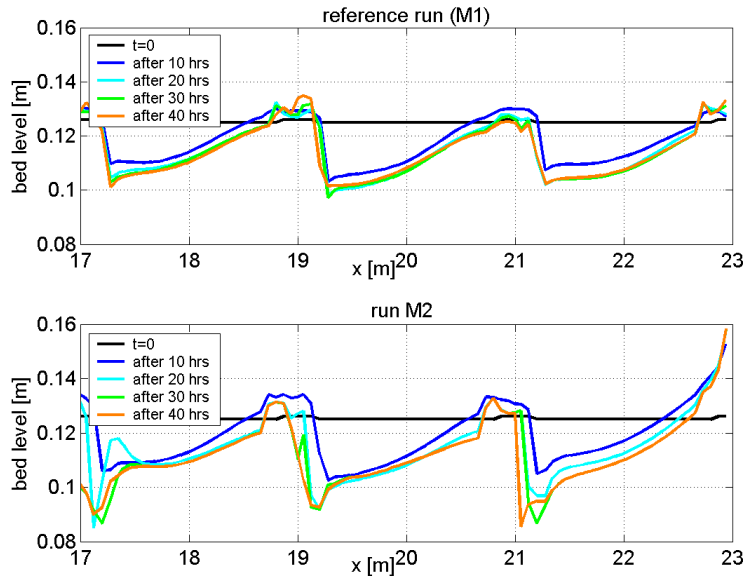


Figure 5-13 Comparison of simulations: bed level at $y=1\text{m}$ in the reference run (M1) and in run M2 (3 grain fractions)

Instabilities

The run with more than one sediment fraction shows instabilities. At some single locations near the groyne tip, where the water is shallow, the computed deposition is extremely high. This always concerns one single grid cell or a few adjacent grid cells and has no influence on the adjacent locations or the overall result (see Figure 5-14). Therefore the results of this computation could be used and analysed anyhow.

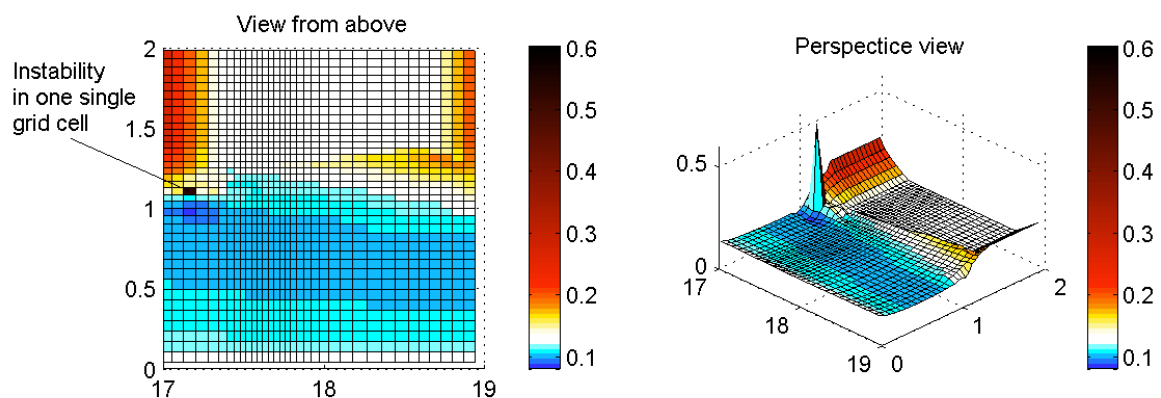


Figure 5-14 Example of an instability for one run with several grain size fractions

5.3.2 Influence of spatially varying enhancement of the actual bed shear stress

In order to improve the morphological pattern, and especially to increase the depth of the scour holes, the bed shear stress at locations of higher turbulence can be enhanced. Another version of Delft3D-FLOW was used for this computation, which has the appropriate feature. The enhancement is achieved as follows:

$$\tau_{b,new,m,n} = \sqrt{\tau_{b,m,n}^2 + (\alpha \tau_{b,ref})^2} \quad (5.3)$$

where

α multiplication factor [-]

$\tau_{b,new,m,n}$ enhanced bed shear stress at grid point m, n [N/m^2]

$\tau_{b,m,n}$ actual bed shear stress at grid point m, n [N/m^2]

$\tau_{b,ref}$ actual bed shear stress at reference point [N/m^2]

Thus, for each grid point a reference point and an α -value can be defined in a file. In this case each point was chosen to be its own reference point, so equation (5.3) simplifies to:

$$\tau_{b,new,m,n} = |\tau_{b,m,n}| \sqrt{(1 + \alpha^2)} \quad (5.4)$$

To find out at which locations the factor is going to be applied, it is referred to Figure 4-7, which shows the turbulence intensity in the test section. It is expected, that a higher turbulence causes an increased erosion. Therefore the factor α was defined in dependence of the turbulence intensity. Since only in the region of a high turbulence intensity an enhancement of the bed shear stress should take place, a minimum value for the turbulence intensity was defined. Referring to Figure 4-7 a minimum value of 0.05 was defined. In this way only the regions behind the groyne tip and the mixing layer were included.

$$\alpha = \frac{\sigma_{uv}}{\sigma_{uv,max}} \quad \text{for all } \sigma_{uv} > 0.05 \quad (5.4)$$

This approach predominantly resulted in a different shape of the scour holes. The long shape of the scour holes was analogous to the shape of the increased turbulence intensity. The scour hole itself was in this case only little deeper than in the reference run. By increasing the factor α the scour hole can be deepened. Furthermore, the shape of the deposition ridge and the amount of deposited sediment is influenced by this measure. After several hours, however, the erosion of the main channel makes the scour hole disappear, as it did in the reference run. In order to see the difference of the shape of the scour hole, Figure 5-15 shows the bed level in the early state of 2.5 hours after the bed level updating. It can be concluded, that this method doesn't improve the results of the simulation. Instead, the erosion/deposition pattern looks artificial, furthermore it leads to an extremely high deposition rate.

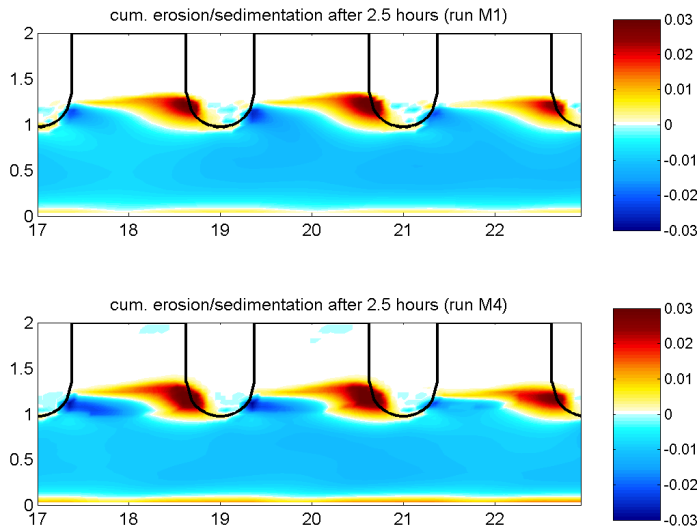


Figure 5-15 Comparison of the erosion/deposition pattern after 2.5 hours for the reference run and for run M4

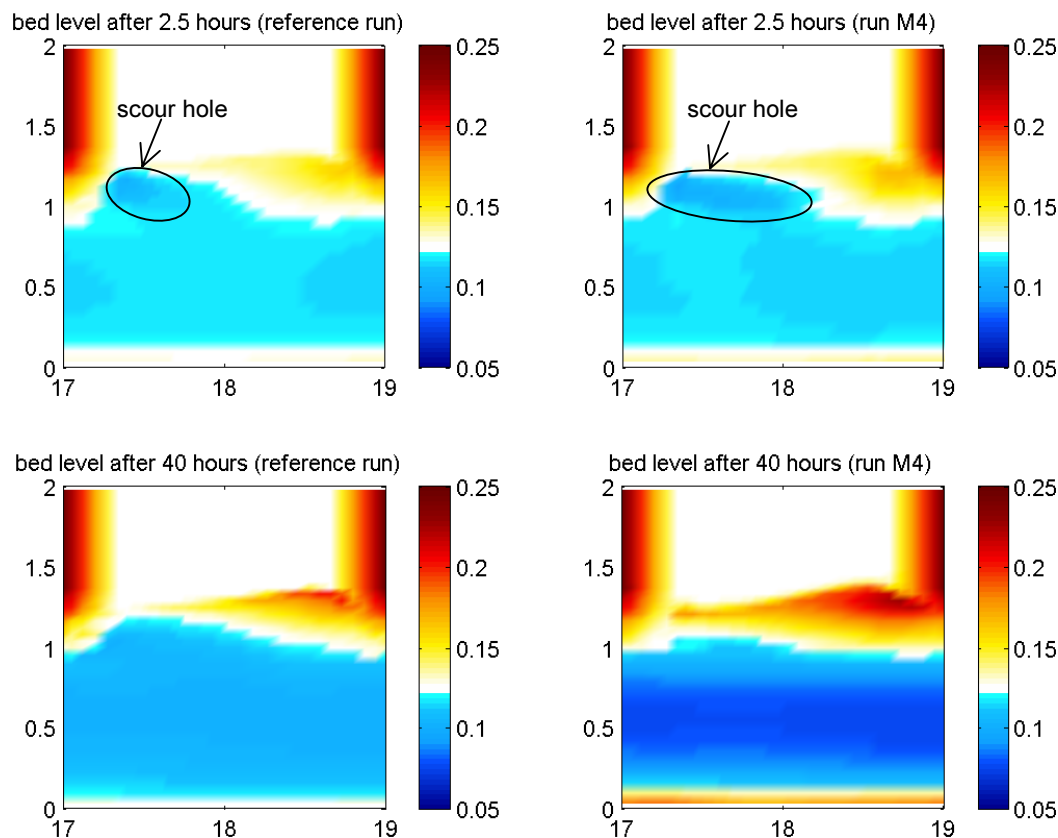


Figure 5-16 Comparison of simulations: bed level after 2.5 hours (upper plots) and after 40 hours (lower plots) for the reference run and for run M4 (enhanced bed shear stress) with indication of the scour holes

5.3.3 Influence of the relaxation time τ

In the sensitivity analysis for the hydrodynamic simulation the influence of the use of a relaxation time of 0.1828 min was investigated. It was observed, that the velocity fluctuations are stronger, the primary and dynamic eddy are more distinct, and that the horizontal eddy viscosity is lower than in the reference run (compare Section 4.4.2). The influence of a modified τ on the morphological changes will be analysed in this section.

The modification of τ had no clear influence on the erosion. However, the deposition volume has strongly increased (see Figure 5-17). When using a τ of 0.1828 min, the velocity of the primary gyre is greater than in the reference run. Consequently, a greater amount of sediment is carried near the groyne field. The sediment is also carried a little further into the groyne field before it settles, which can be seen from the shape of the depositional ridge. This can be explained with the increased velocity of the primary gyre, when a τ of 0.1828 min is used. However, the amount of deposition is much too high compared to the experiment.

Another interesting aspect is the small scour and the small deposition near the side wall are represented in this run (see Figure 5-17) and are located at the correct place. As the bed level readings of the experiment only covered the section from $y = 0,2$ m until $y = 1,8$ m, this feature cannot be seen in the picture of the experimental results (see left picture in Figure 5-3). The photograph of the bed levels taken at the end of the experiment shows this erosion/deposition pattern near the wall, though (see Figure 3-6). The appearance of this erosion/deposition pattern lead to the conclusion, that Delft3D qualitatively computes the flow and the locations of erosion and the deposition in the groyne field correctly. Hence, it must be the sediment transport model that causes the discrepancies between the computed and the measured morphological development.

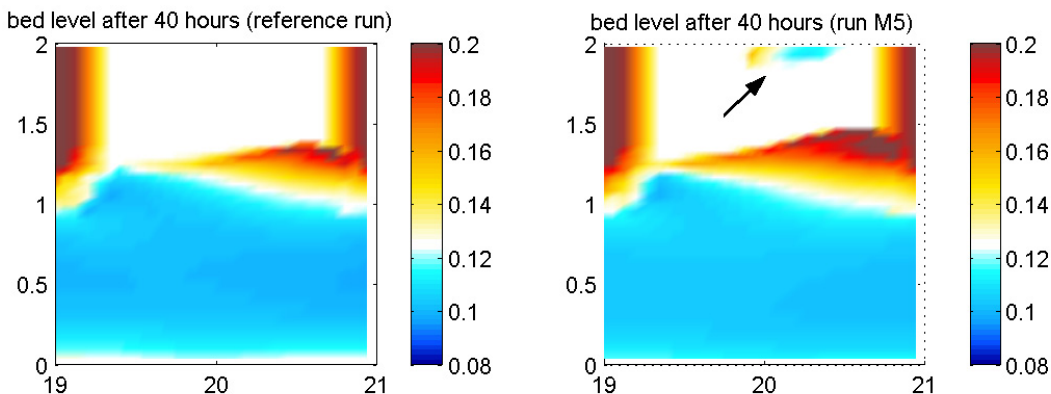


Figure 5-17 Comparison of simulations: bed level after 40 hours for the reference run and for run M5 (modified relaxation time) with indication of the erosion/deposition pattern near the side wall

5.3.4 Influence of the transport boundary conditions

From Section 5.2.3 (Figure 5-9) it is known, that the erosion in the main channel occurs in combination with a decrease of the ratio $C_{e,ds}/C_{e,us}$. In the reference run the concentrations at the boundaries were set to the computed equilibrium concentrations. Here the erosion of the main channel started at a very high ratio ($C_{e,ds}/C_{e,us} > 8$) and stopped at $C_{e,ds}/C_{e,us} \approx 1.65$. In order to decrease the erosion in the main channel, the sediment concentrations at the boundaries will not be set equal to the computed equilibrium concentrations in these two runs. Instead the concentrations at the boundaries will be set to fixed values. It is expected, that the erosion in the main channel will decrease if the ratio C_{ds}/C_{us} is decreased. For these two runs the ratio C_{ds}/C_{us}

was chosen to be very low ($c_{ds}/c_{us} = 0.5$), to make sure that more sediment flows into the flume than flows out of it. For the first attempt (run M6a) the downstream concentration will be set to a very low value by decreasing it to $0,5 * c_{us}$. The upstream concentration will be set to $0,137 \text{ kg/m}^3$, which corresponds to the sediment input of the laboratory experiment and is also in the same range as the computed upstream equilibrium concentration in the reference run. In the second attempt (run M6b) the upstream concentration will be increased to $2 * c_{ds}$. The computed value from the reference run ($c_{ds} = 0.239 \text{ kg/m}^3$) will be used for the downstream concentration.

Parameter	Value	Unit
<i>run M6a</i>		
Transport boundary conditions		
upstream boundary:		
sediment concentration c_{us}	=0,137	kg/m^3
downstream boundary:		
sediment concentration c_{ds}	=0,069	kg/m^3
<i>run M6b</i>		
Transport boundary conditions		
upstream boundary:		
sediment concentration c_{us}	=0,478	kg/m^3
downstream boundary:		
sediment concentration c_{ds}	=0,239	kg/m^3

Table 5-4 Modifications of the transport boundary conditions for the run M6

The first attempt (run M6a) didn't show any changes of the erosion/deposition pattern at all. When analysing the computed concentrations of the sediment near the downstream boundary, they hardly differed from the equilibrium concentrations. The setting of the low value for the concentration at the downstream boundary therefore doesn't influence the concentrations and therefore the bed level changes in the rest of the flume.

In the second run (run M6b) the erosion of the main channel didn't occur. Both the concentrations and the sediment transport strongly increased in the entire flume. The scour holes, that developed very quickly after the bathymetry updating, were filled by the increased bed load transport and the deposition near the groyne tips strongly increased due to the surplus of sediment. These results are clear consequences of the elevated concentration specified at the upstream boundary. This situation cannot be compared with the experiment, since it simulates a complete different situation.

In conclusion, it is stated that only modifying the downstream boundary condition doesn't have an influence on the morphology of the flume, while the modification of the upstream transport condition leads to results, that cannot be compared with the laboratory experiment.

5.3.5 Influence of the slip condition

As it was stated in Section 5.2.1 the erosion in the middle of the main channel was strong while near the walls no erosion occurred, which resulted in a reshaping of the main channel. This was

not observed in the experiment and is due to the decreased velocity in x-direction near the wall. Even though the use of a partial slip condition with a specified wall roughness was the result of the calibration (Section 4.2), the use of a free slip condition will be investigated in this section.

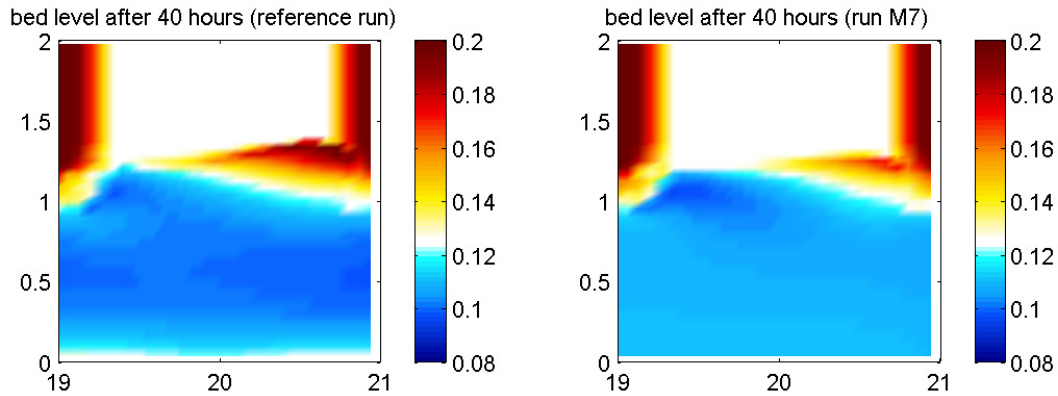


Figure 5-18 Comparison of simulations: bed level after 40 hours for the reference run and for run M7 (free slip condition)

Figure 5-18 shows the bed level after 40 hours (real time) for both the reference run and run M7. The erosion in the main channel was less than in the reference run, which is due to the slightly decreased velocity in the middle of the main channel. Near the side wall erosion takes place, since the velocity does not decrease, when a free slip condition is chosen. (The influence of the slip condition/wall roughness on the velocity profile was shown Figure 4-15.) Consequently, the shape of the main channel differs from the reference run (see Figure 5-19) and resembles more to the experiment. As the erosion rate in the main channel was less than in the reference run, the scour hole near the groyne tip is now clearly visible in Figure 5-18. However, the amount of deposited sediment is much too low.

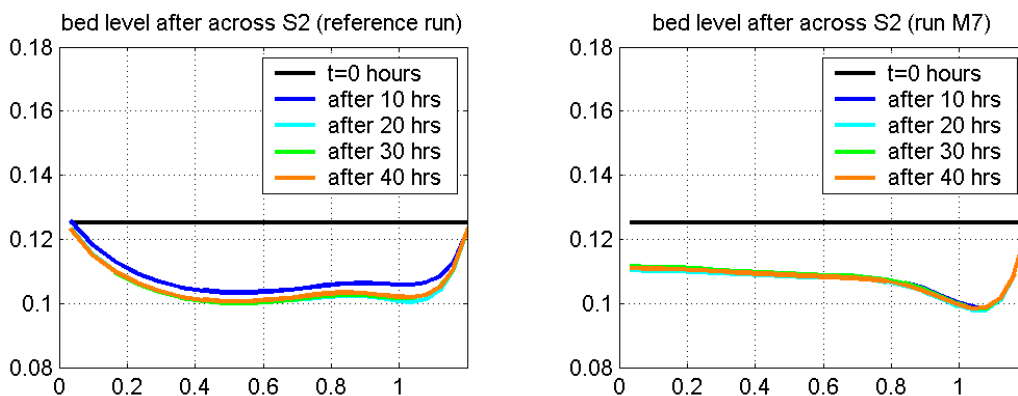


Figure 5-19 Comparison of simulations: bed level in the main channel across S2 for the reference run and for run M7 (free slip condition)

Figure 5-20 shows a comparison between the transverse sediment concentration profile across S1 and S2. The concentration near the side wall is in the same range as the concentration in the main channel. This results from the velocity profile, which is computed, when a free slip condition is defined at the walls. This distribution of the concentration is more realistic compared

to the concentration profile in the reference run. Hence, the concentration gradient before the groyne field is still very steep and the concentration of sediment in the groyne field is nearly zero.

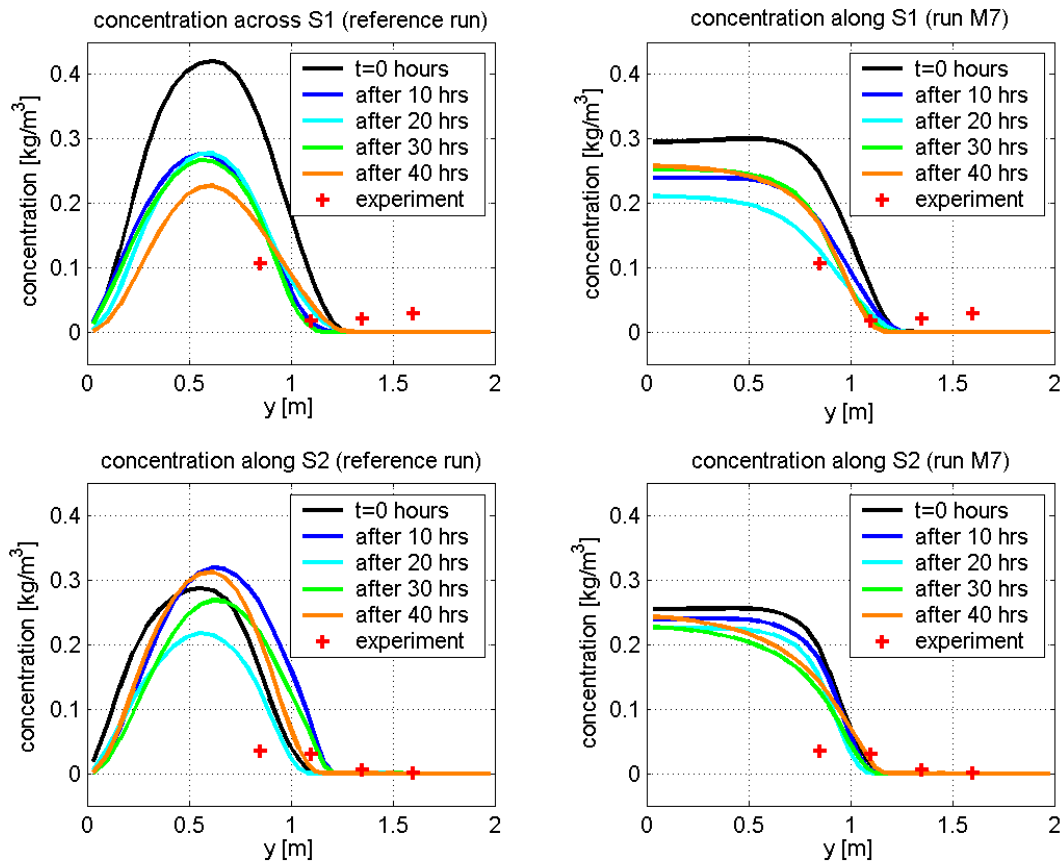


Figure 5-20 Comparison of simulations: concentration across S1 and S2 for the reference run (left plots) and the run M7 (free slip condition, right plots)

Some of the above mentioned modifications of the reference run showed no improvement of the erosion/deposition pattern in the main channel and the groyne field. Hence, an improvement concerning the depth of the scour hole can be achieved by the use of 3 grain sizes instead of only one. However, instabilities occurred in this simulation. The morphology in the main channel is better represented when using a free slip condition instead of a partial slip condition with a rough side wall. Yet, it is known from the sensitivity analysis of the hydrodynamic simulation, that the flow pattern in the groyne field didn't show a dynamic eddy. The use of a free slip condition therefore only improves the flow conditions and morphological changes in the main channel.

The sediment transport into the groyne field is not reproduced in an acceptable way in any of the above mentioned simulations. One cause for this might be, that the velocity, with which the water entered the groyne field, was computed to be too low. It is furthermore possible, that the adaptation time and length for the concentration to reach the equilibrium concentration in the

groyne field are underestimated by the transport module, which results in a very steep gradient of the transverse concentration profile, and a quick settling of the sediment.

6 DISCUSSION, REMARKS, AND CONCLUSIONS

6.1 DISCUSSION

In this section a general comparison of the results of the simulation with the experiment will be made and the model's abilities to simulate the situation in the experiment will be evaluated.

Hydrodynamic computations

When comparing the results of the hydrodynamic simulations with the computed flow pattern, we can conclude, that the numerical model represents the overall flow pattern observed in the experiment (e.g. discharge, water level and velocities) well. The full shape and distinction of the turbulent eddies and gyres in the groyne field cannot be compared with the experiment, since the velocities in the groyne field were only measured at certain points along two cross-sections (see 6.2). Evidence of the presence of a dynamic eddy could be inferred from Energy spectra of the points in the mixing layer. Furthermore, both the primary gyre and an indication of the dynamic eddy were observed in the dye test. In order to calibrate the model, the input parameters (e.g. the slip condition/wall roughness) were set, so that the appearance of the turbulent structures in the groyne field qualitatively matched the appearance of the turbulent structures in literature and in results from previous experiments, where these structures have been recorded. This resulted in the modelling of a primary eddy, which covers about two thirds of the groyne field, and a clearly visible dynamic eddy, the frequency of which is in the range of the main frequency that was found from the measurements. These turbulent flow patterns, which contribute much to the mixing processed between the main channel and the groyne fields, were represented well in the hydrodynamic computation. Nevertheless, the transverse velocity of the water entering the groyne field was underpredicted, which, in the morphodynamic computations had an influence on the shape of the depositional ridge, forming at the upstream side of each groyne.

Morphodynamic computations

The morphodynamic computations gave good results concerning the general erosion/deposition pattern near the groyne tips and in the groyne fields. Even the effect of the side wall in the groyne field (small scour and deposition) is reproduced in one computation (M5), which leads to the conclusion that the morphodynamic patterns are generally well reproduced. Yet, the model poorly reproduced the sediment transport into the groyne fields. Furthermore, the depth of the scour hole was underestimated in all simulations.

- Scour hole:

In all morphodynamic computations the scour hole was too shallow compared to the measured scour hole. It also appears that the slip condition/wall roughness and thus the presence of the dynamic eddy does not have an influence on the depth of the scour hole in all simulations. This

was found by comparing the results from a case with a free slip condition with a case with a partial slip condition. The case with free slip conditions yielded a large primary gyre and hardly any fluctuations near the groyne tip, instead of a smaller primary gyre and a clear dynamic eddy. Yet the scour hole depth did not differ much from the reference case. An explanation for this is the location of the scour hole, which is not situated, where the dynamic eddy sheds from the groyne tip, but closer to the main channel. The distinction of the eddy therefore doesn't affect the scour hole. Apparently the scour hole forms as a result of the narrowing of the flow, instead of the velocity fluctuations near the groyne tip. The depth of the scour hole was only influenced by using three grain sizes instead of only one, which means a more realistic representation of the used sediment. The use of graded instead of uniform sediment improves the erosion/deposition pattern, but also leads to instabilities in the computation.

- *Deposition:*

The volume of sediment, which deposited on the upstream side near the groyne tip was computed to be 81% of the volume computed from the measurements, and is therefore roughly in accordance with the experiment. However, the shape of the deposition ridge did not match with the observations from the experiment. The sediment didn't enter the groyne field before settling, but instead settled in front of the groyne field, as soon as the velocity decreased. This was a major problem with all simulations.

A similar observation was made near the wall of the main channel. At this location the velocity was lower than in the middle of the main channel, which leads to deposition in the early state of the simulation. This has not been observed in the experiment. The differences between the deposition patterns of experiment and simulation lead to the conclusion, that the sediment is not kept in suspension long enough. On the other hand a decrease of the grain size or the settling velocity would result in a stronger erosion in the main channel, which is not desired either. Apparently the morphological model doesn't include the relevant processes sufficiently well.

6.2 RESTRICTIONS

Data of the laboratory experiment

Velocity measurements were taken only at two sections across the width of the flume. For the study of the turbulent flow in the entire groyne field and the system of gyres no comparison could be made with the laboratory experiment. The only visualizations of the flow pattern in the entire groyne field were made by means of the dye test, which only gives a qualitative view on the turbulent structures in the groyne field.

As the two devices for the velocity measurements were sensitive to zero-offset drift, offset readings had to be taken before the velocity test. Since the offset reading of one of the measurements was incorrect, the measured velocities had to be corrected when analysing the experimental data. This is a source of inaccuracy of the measured velocities.

As the velocity readings did not cover the locations close to the wall, it was not possible to compare the computed velocities near the wall with the ones from the experiment. This information could have been helpful for the calibration of the slip condition/wall roughness, which has a great influence on both the flow pattern in the groyne field and the bed level changes in the main channel and the groyne field.

Simplifications of the set-up of the numerical model

At first a model of the actual geometry of the flume was used, which included all 12 groynes, that were used in the experiment. The number of grid cells became very high, and consequently the time for the morphological computations was long as well, since a small time step had to be used. In order to reduce the computing time, the grid was simplified as described in Section 4.1. No significant changes of the flow pattern occurred in the test section in comparison with the simulation using the extended geometry.

Assumptions and simplifications in the flow module

Delft3D-Flow comprises many assumptions and simplifications. One important assumption to mention is the hydrostatic pressure assumption, which has been explained in Section 2.1.2. Even though the grid was chosen to be very fine, not all turbulence scales could be resolved. For the modelling of the small-scale 2D-turbulence the sub-grid model also uses assumptions and simplifications. Three dimensional turbulence motion can only be accounted for when using several horizontal layers. When simulating two dimensional, the vertical velocity profile is not accounted for.

The online sediment module uses some empirical formulae and approximations when computing the sediment transport and the bed level changes. Another simplification is, that the morphological changes are computed using instantaneous results from the flow at a certain time, and are upscaled using the morphological factor. This may give rise to some instabilities, or exaggerated changes in a single time step.

The sediment transport formula is suited for uniform steady flow, which is not the case in an emerged groyne field.

The adaptation time-scale and length-scale calculated based on the assumptions that the velocity gradient is rather mild, whereas in such a case it is very steep.

6.3 RECOMMENDATIONS

- To find out, how the model could be improved hydrodynamically and morphodynamically, a more simple laboratory experiment could be carried out and modelled numerically, in which the flow pattern is not as complex as in groyne fields. Possible proposals are e.g. a model of a mixing layer forming between two parallel flows with different velocities, or the model of a flow, which is disturbed by only one single groyne.

- In order to evaluate the model for a larger domain in the parameter space, an investigation of the other emerged cases of the laboratory experiments can be made and compared to the case G1i. Furthermore, the submerged cases should be simulated numerically as well, since both the flow conditions and the morphological patterns are much different in these cases.
- In this thesis only one three-dimensional simulation (with 10 layers and a hydrostatic pressure assumption) was performed. Since the morphological pattern didn't differ significantly from the results of the reference run, this simulation has not been discussed in Section 5.3. It would be interesting though, to investigate the effect of the different turbulence models, which can be specified in the 3D-simulations, on the results of the computations. Furthermore, the influence of some input parameters could be studied in three-dimensional computations as well.
- Large-scale morphological simulations using Delft3D-FLOW (with HLES and Online-sediment) delivered more realistic results of the morphological patterns in groyne fields, compared to the results of the simulations in the thesis on hand. For this reason, a comparison between a large-scale and a lab-scale simulation could be done.

6.4 CONCLUSIONS

It is stated, that Delft3D-FLOW with the add-ons HLES and Online-sediment generally represents the situation in the experiment well. The turbulent flow pattern in the entire groyne field can only qualitatively be compared with the laboratory experiment, but the computed turbulence structures are in good accordance with those observed in former experiments and in literature. Delft3D also represents the morphological features of erosion and deposition with some drawbacks: the sediment, which is in suspension, settles too quickly, as soon as the velocity decreases. The scour hole was not located at the exact same place, as it is observed in the experiment and where the dynamic eddy forms. This results into the scour hole not being influenced by these turbulent fluctuations near the groyne tip. Here the formulation in the sediment transport equation in the 'Online-sediment' module should be inspected.

7 REFERENCES

Bijlsma, A.C., Uittenbogaard, R.E., Blokland, T. (2003):

"Horizontal large eddy simulation applied to stratified tidal flows"
Int. Shallow-Flows Symp., Balkema.

Lesser, Roelvink, Van Kester, Stelling (2004):

"Development and validation of a three-dimensional morphological model"
to be published in Coastal engineering in 2004
WL | Delft Hydraulics / Delft University of Technology, faculty of Civil Engineering.

Liek, G.A. (2002):

"Horizontal Large Eddy Simulation using Delft2D-MOR - the influence of large horizontal eddies on the shape, depth and extent of scour holes"
M Sc. Thesis, Delft University of Technology, faculty of Civil Engineering.

Liek, G.A., Roelvink, J.A., Uittenbogaard, R.E. (2002):

"The influence of large horizontal eddies on the shape, depth and extent of scour holes"

Nestmann, F., Lehmann, B. (2002):

"Morphodynamik von Fliessgewässern", Lecture notes
Universität Karlsruhe (TH), faculty of Civil Engineering, IWK (Institute for water management and rural engineering)

Van Rijn, L.C. (1993):

"Principles of sediment transport in rivers, estuaries coastal seas and oceans"
Aqua publications, Amsterdam.

Van Schijndel, S.A.H., Jagers, H.R.A. (2002):

"Anticiperend onderzoek kribben"
WL | Delft Hydraulics, Delft.

Van Schijndel, S.A.H., Jagers, H.R.A. (2003):

"Complex flow around groynes"
Proc. Shallow Flows, Delft, 16-18 June 2003. Rotterdam: Balkema.

Thiemann, K.E. (2003):

Research report laboratory experiment
Delft University of Technology, faculty of Civil Engineering.

Uijtewaal, W.S.J., Lehmann, D.C., Van Mazijk, A., Weitbrecht, V. (1999):

"Auswirkungen von Bühnenfeldern auf den Transport gelöster Stoffe in Flüssen"
Delft University of Technology, faculty of Civil Engineering, section of Fluid Mechanics

Uijtewaal, W.S.J., Lehmann, D.C., Van Mazijk, A. (2001):

"Exchange processes between a river and its groyne fields: model experiments"
Journal of Hydraulic Engineering, ASCE, vol. 127, no. 11, pp. 928-936.

Uijtewaal (2003):

"Turbulence in Hydraulics", Lecture notes.
Delft University of Technology, faculty of Civil Engineering, section of Fluid Mechanics.

Uittenbogaard, R.E., Van Vossen, B. (2003):

"Subgrid-scale model for Quasi-2D turbulence in shallow water"
Int. Shallow-Flows Symp., Balkema.

WL | Delft Hydraulics (2003):

"Delft3D-FLOW User Manual release 3.10"
WL | Delft Hydraulics, Delft.

Yossef, M.F.M., Klaasen, G.J. (2002):

"Reproduction of groynes-induced river bed morphology using LES in 2-D morphological model"
River Flow 2002, Proc. of the Int. Conf. on Fluvial Hydraulics, Louvain-la-Neuve, Belgium, 1099-1108.

Yossef, M.F.M (2003):

"Sediment exchange between the main channel and the groyne fields of a river - Design of a mobile-bed experiment"
Delft University of Technology, faculty of Civil Engineering.

Yossef, M.F.M., Uijtewaal, W.S.J. (2003):

"On the dynamics of the flow near groynes in the context of morphological modelling"
XXX IAHR Congress, Thessaloniki, Greece, 361-368.

Yossef M.F.M., de Vriend H.J., (2004):

"Mobile-bed experiments on the exchange of sediment between main channel and groyne fields"
River Flow 2004, Naples, Italy.

A DELFT3D-FLOW - MODEL DESCRIPTION

Files in Delft3D-FLOW

Input files

The master definition FLOW (MDF-file) file is the main input file for the hydrodynamic and morphodynamic simulation programme. In this file all the necessary data for running the simulation is specified. It may though contain attribute files, such as the grid- and the depth file, which contain detailed and specific data about the input. In the table below the different types of attribute files that were used for the numerical simulation and their extensions are given.

data described in attribute file	extension
grid	*.grd
grid enclosure	*.enc
bathymetry	*.dep
boundary locations	*.bct
boundary flow conditions	*.bnd
boundary transport conditions	*.bcc
sediment input data	*.sed
mass of sediment at bed	*.sdb
morphological input data	*.mor
enhancing of bed shear stress	*.inp
monitoring points (cross sections)	*.crs
monitoring points (observation points)	*.obs

Table A-1 Used attribute files for the simulation

Output files

file	contained data
map file	all computed data for each recorded map-time step, grid point and layer
history file	all computed data for each recorded history-time step, but only for the defined monitoring points/cross sections

Table A-2 Used output files for the simulation

Assumptions

In the Delft3D-FLOW system, the flow model is based on the depth averaged shallow water equations, which are resolved on a curvilinear grid. The vertical momentum equation is reduced to the hydrostatic pressure relation since vertical accelerations are assumed to be small in comparison to the gravitational acceleration, and can therefore be neglected. It is furthermore as-

sumed that the fluid is incompressible and has a constant density, and that the flow is a free surface flow.

For 3D computations it is assumed that the velocity has a vertical logarithmic profile. In order to model the vertical momentum exchange a vertical eddy viscosity and diffusivity coefficient are used which are in this case computed by the $k-\varepsilon$ turbulence model.

Formulas for the flow computations

σ -co-ordinate-system

The flow -module calculates the non-steady flow in two or three dimensions. When simulating 3-dimensional the σ -co-ordinate-system is used, which means that the vertical is divided into several layers of variable thickness. At the bottom $\sigma = -1$ and at the surface $\sigma = 0$.

The vertical σ -co-ordinate is scaled as:

$$\sigma = \frac{z - \xi}{H} \quad (\text{A.1})$$

where ξ is the free-surface elevation above the reference plane (at $z=0$) and H the total water depth [m],

Momentum equations for a curvilinear grid

Delft3D-FLOW solves the Navier-Stokes-equations in two horizontal depth-averaged dimensions on a curvilinear grid. For the general case of curvilinear co-ordinates ξ and η the momentum equations in ξ - and η -direction are given:

$$\begin{aligned} \frac{\partial u}{\partial t} + \frac{u}{\sqrt{G_{\xi\xi}}} \frac{\partial u}{\partial \xi} + \frac{v}{\sqrt{G_{\eta\eta}}} \frac{\partial u}{\partial \eta} + \frac{\omega}{d + \zeta} \frac{\partial u}{\partial \sigma} + \frac{uv}{\sqrt{G_{\xi\xi}} \sqrt{G_{\eta\eta}}} \frac{\partial \sqrt{G_{\xi\xi}}}{\partial \eta} - \frac{v^2}{\sqrt{G_{\xi\xi}} \sqrt{G_{\eta\eta}}} \frac{\partial \sqrt{G_{\eta\eta}}}{\partial \xi} - fv \\ = -\frac{1}{\rho_w \sqrt{G_{\xi\xi}}} P_\xi + F_\xi + \left(\frac{1}{(d + \zeta)^2} \frac{\partial}{\partial \sigma} \left(\nu_v \frac{\partial u}{\partial \sigma} \right) \right) + M_\xi \end{aligned} \quad (\text{A.2})$$

$$\begin{aligned} \frac{\partial v}{\partial t} + \frac{u}{\sqrt{G_{\xi\xi}}} \frac{\partial v}{\partial \xi} + \frac{v}{\sqrt{G_{\eta\eta}}} \frac{\partial v}{\partial \eta} + \frac{\omega}{d + \zeta} \frac{\partial v}{\partial \sigma} + \frac{uv}{\sqrt{G_{\xi\xi}} \sqrt{G_{\eta\eta}}} \frac{\partial \sqrt{G_{\eta\eta}}}{\partial \xi} - \frac{u^2}{\sqrt{G_{\xi\xi}} \sqrt{G_{\eta\eta}}} \frac{\partial \sqrt{G_{\xi\xi}}}{\partial \eta} - fu \\ = -\frac{1}{\rho_w \sqrt{G_{\eta\eta}}} P_\eta + F_\eta + \left(\frac{1}{(d + \zeta)^2} \frac{\partial}{\partial \sigma} \left(\nu_v \frac{\partial v}{\partial \sigma} \right) \right) + M_\eta \end{aligned} \quad (\text{A.3})$$

where

u , v , and w flow velocities [m/s]

$\sqrt{G_{\xi\xi}}$, $\sqrt{G_{\eta\eta}}$ coefficients used to transform curvilinear into rectangular co-ordinates [m]

- ξ, η co-ordinates of the curvilinear grid [-]
 ω vertical velocity in the σ -co-ordinate system (computed from the Continuity equation)
 σ velocity in the σ -direction in the σ -co-ordinate system [m/s]

$$\sigma = \frac{z - \zeta}{d + \zeta} = \frac{z - \zeta}{H} \quad (\text{A.4})$$

where

- H total water depth [m]
 d water depth below the reference plane [m]
 ζ free-surface elevation above the reference plane [m]
 z vertical co-ordinate [-]

P_ξ, P_η represent the pressure gradients [$\text{kg}/(\text{m}^2\text{s}^2)$]

M_ξ, M_η represent the contributions due to external sources of momentum [m/s^2]

F_ξ, F_η represent the Reynolds stresses [m/s^2]

$$F_\xi = \nu_H \left(\frac{1}{\sqrt{G_{\xi\xi}} \sqrt{G_{\xi\xi}}} \frac{\partial^2 u}{\partial \xi^2} + \frac{1}{\sqrt{G_{\eta\eta}} \sqrt{G_{\eta\eta}}} \frac{\partial^2 u}{\partial \eta^2} \right) \quad (\text{A.5})$$

$$F_\eta = \nu_H \left(\frac{1}{\sqrt{G_{\xi\xi}} \sqrt{G_{\xi\xi}}} \frac{\partial^2 v}{\partial \xi^2} + \frac{1}{\sqrt{G_{\eta\eta}} \sqrt{G_{\eta\eta}}} \frac{\partial^2 v}{\partial \eta^2} \right) \quad (\text{A.6})$$

where ν_H is the horizontal eddy viscosity [m^2/s]

Continuity equation in notation adapted to a curvilinear grid:

$$\frac{\partial \zeta}{\partial t} + \frac{1}{\sqrt{G_{\xi\xi}} \sqrt{G_{\eta\eta}}} \frac{\partial \left[(d + \zeta) U \sqrt{G_{\eta\eta}} \right]}{\partial \xi} + \frac{1}{\sqrt{G_{\xi\xi}} \sqrt{G_{\eta\eta}}} \frac{\partial \left[(d + \zeta) V \sqrt{G_{\xi\xi}} \right]}{\partial \eta} = Q \quad (\text{A.7})$$

where

Q contributions per unit area due to discharge or withdrawal of water

$$Q = H \int_{-1}^0 (q_{in} - q_{out}) d\sigma \quad (\text{A.8})$$

where q_{in} and q_{out} are local sources and sinks of water per unit of volume [$1/\text{s}$]

Formulas used in the Online-sediment add-on

In this section the formulas, which are referred to in the description of the Online-sediment are listed.

Settling velocity of the sediment

w_s sediment settling velocity of the non-cohesive sediment [m/s]

$$w_s = \frac{10\nu}{D_s} \left[\left(1 + \frac{0.01(s-1)gD_s^3}{\nu^2} \right)^{0.5} - 1 \right] \quad \text{for } 100\mu\text{m} < D_s < 1000\mu\text{m} \quad (\text{A.9})$$

where

D_s representative diameter of sediment [m]

s relative density of the sediment fraction [-]

$$s = \frac{\rho_s}{\rho_w} \quad (\text{A.10})$$

ν kinematic viscosity of water [m²/s]

Calculation of the sediment mixing coefficient

(for the case of non-cohesive sediment dispersion and application of the k - ε turbulence model)

Vertical sediment mixing coefficient

$$D_V = \beta_{\text{eff}} \frac{\nu_V}{\sigma_c} \quad (\text{A.11})$$

where

β_{eff} effective Van Rijn's 'beta' factor [-]

$$\beta_{\text{eff}} = 1 + (\beta - 1) \frac{\tau_c}{\tau_w + \tau_c} \quad (\text{A.12})$$

β Van Rijn's 'beta' factor [-]

$$\beta = 1 + 2 \left[\frac{w_s}{u_*} \right]^2 \quad (\text{A.13})$$

u_* local bed shear velocity [m/s]

ν_V vertical eddy viscosity [m²/s] calculated by the k - ε turbulence closure model (Eq. A.15)

τ_c bed shear stress due to currents [N/m²]

τ_w bed shear stress due to waves [N/m²]

Calculation of the vertical eddy viscosity (k - ε turbulence closure model)

$$\nu_H = c'_\mu L \sqrt{k} \quad (\text{A.14})$$

where

c'_μ constant [-] determined by calibration

k turbulent kinetic energy [m^2/s^2]

L mixing length [-]

$$L = c_D \frac{k\sqrt{k}}{\varepsilon} \quad (\text{A.15})$$

where c_D is another constant [-] determined by calibration and ε is the dissipation.

The k - ε turbulence closure model produces both the turbulent energy k and the dissipation ε by production terms representing shear stresses at bed, surface, and in the flow. The 'concentrations' of k and ε in every grid cell are then calculated by the transport equations.

Calculation of Van Rijn's reference concentration $c_a^{(l)}$

The sediment concentration at the reference height is needed for the calculation of the sink and source terms. These terms will be necessary for the calculation of the erosion and deposition and shall not be explained further in this thesis. For more information it is referred to the Delft3D-FLOW user manual.

Van Rijn's reference height concentration c_a :

$$c_a = SUS \eta 0.015 \rho_s \frac{D_{50} (T_a)^{1.5}}{a (D_*)^{0.3}} \quad (\text{A.16})$$

where

c_a mass concentration at the reference height a

SUS user-specified multiplication factor [-]

η relative availability of sediment of the fraction (l) in the mixing layer [-]

$$\eta = \frac{\text{mass of sediment in mixing layer}}{\text{total mass of sediment in mixing layer}} \quad (\text{A.17})$$

ρ_s specific density of the sediment [kg/m^3]

T_a non-dimensional bed shear stress [-]

$$T_a = \frac{\mu_c \tau_{b,c} - \tau_{cr}}{\tau_{cr}} \quad (\text{A-26})$$

μ_c efficiency factor current [-]

$$\mu_c = \left(\frac{f'_c}{f_c} \right) \quad (\text{A.18})$$

f'_c grain-related friction factor [-]

$$f'_c = 0.24 \left[\log_{10} \left(\frac{12H}{3D_{90}} \right) \right]^{-2} \quad (\text{A.19})$$

f_c total current-related friction factor [-]

$$f_c = 0.24 \left[\log_{10} \left(\frac{12H}{k_s} \right) \right]^{-2} \quad (\text{A.20})$$

μ_w efficiency factor waves [-] ($\mu_w = 0$ if waves are not included)

$\tau_{b,c}$ bed shear stress due to currents [N/m^2]

τ_{cr} critical bed-shear stress [N/m^2]

a reference height according to Van Rijn, specifying the thickness of the bed load layer [m]

Calculation of the equilibrium concentration c_e

Delft3D computes the equilibrium concentration c_e at e.g. the upstream boundary using the actual mixing values, which have been calculated by the flow, and an upwind method of numerical integration to solve the stationary advection-diffusion equation.

B NUMERICAL SIMULATIONS

Grid and bathymetry

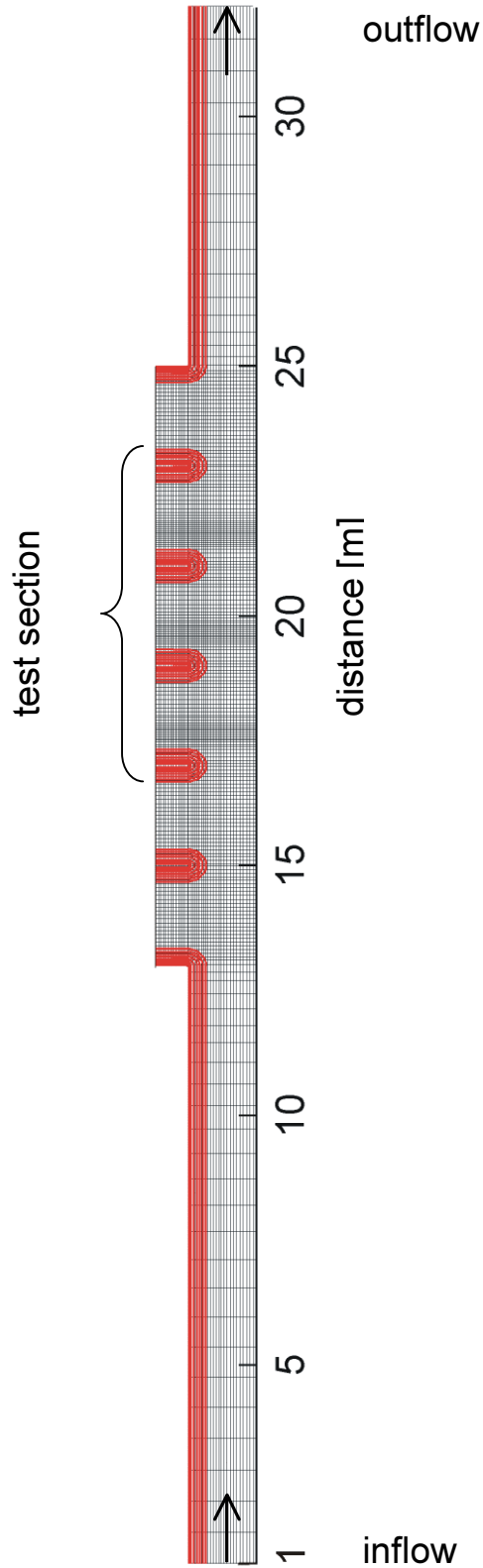
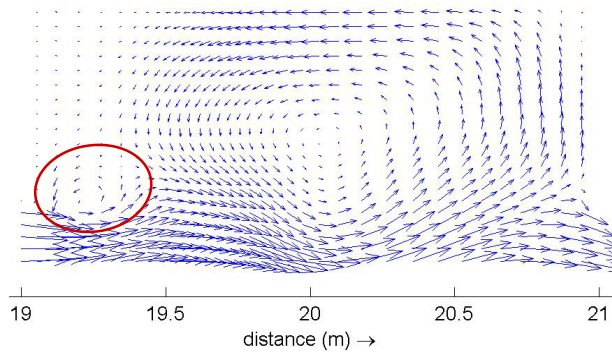


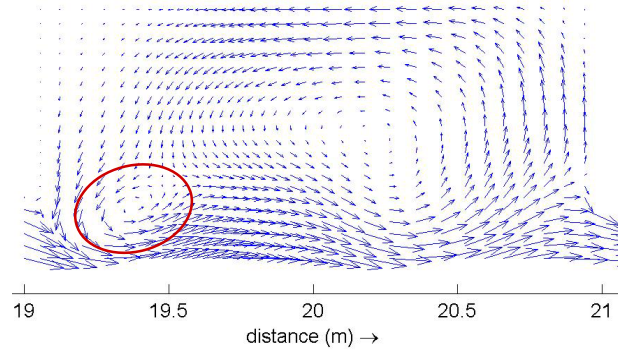
Figure B-1 Grid with contour lines of the bathymetry

Flow pattern in the groyne field

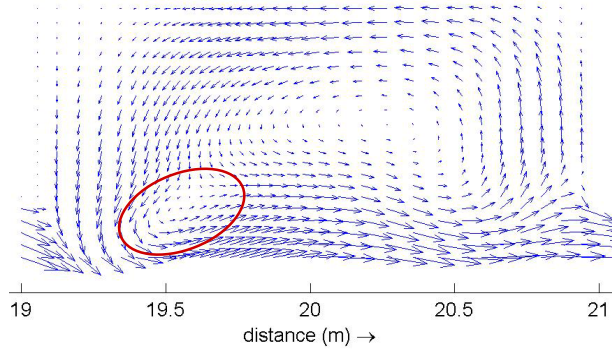
a) $t=0$



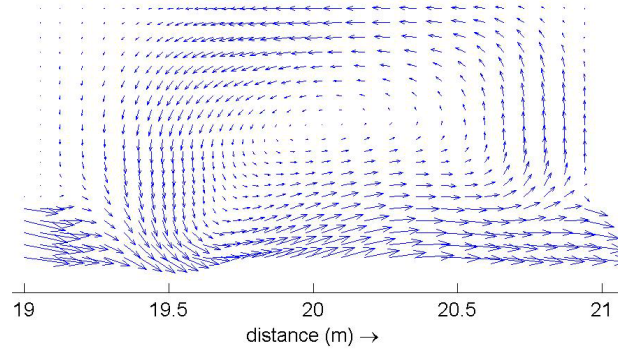
b) $t=1.2s$



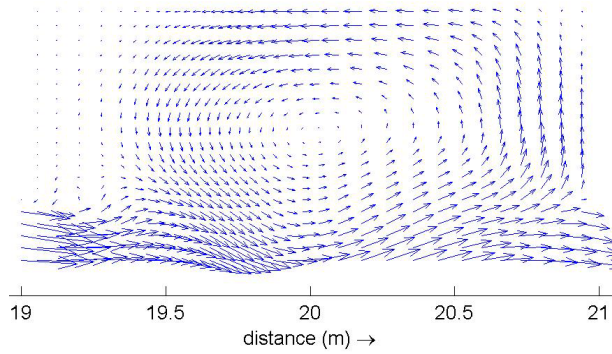
c) $t=2.4s$



d) $t=3.6s$



e) $t=4.8s$



f) $t=6.0s$

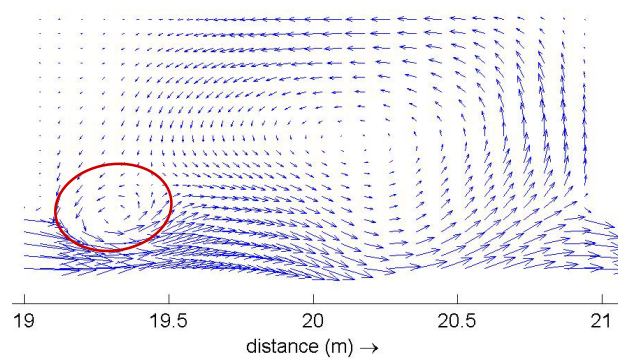


Figure B-2: Velocity vectors in the groyne field for run H10 with indication of the dynamic eddy

C RESULTS OF THE EXPERIMENTS

Bed levels before the test, after 10, 20, 30, and 40 hours

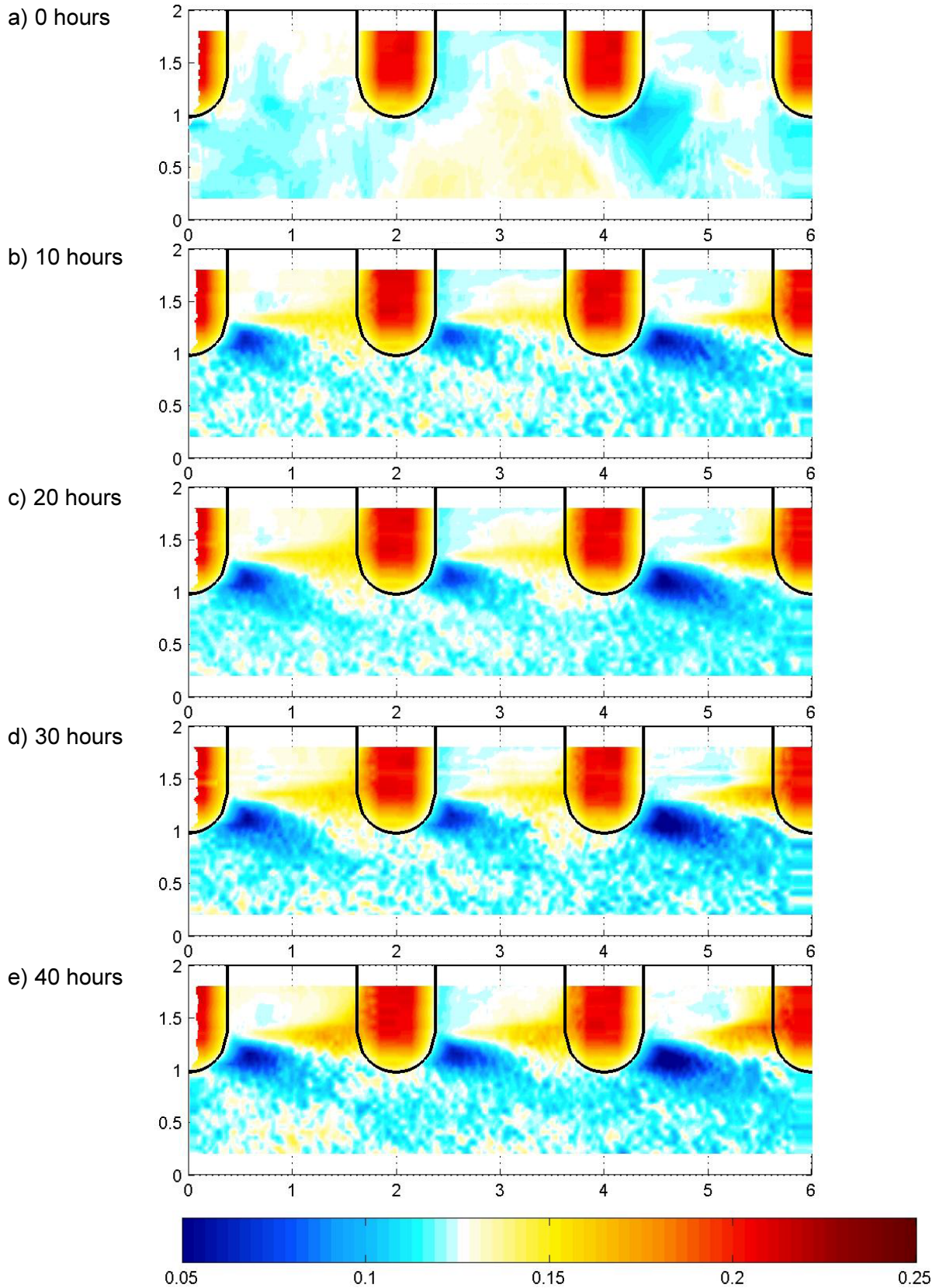


Figure C-1 Results of the bed level measurements: bed levels

Dye test in the emerged groyne field

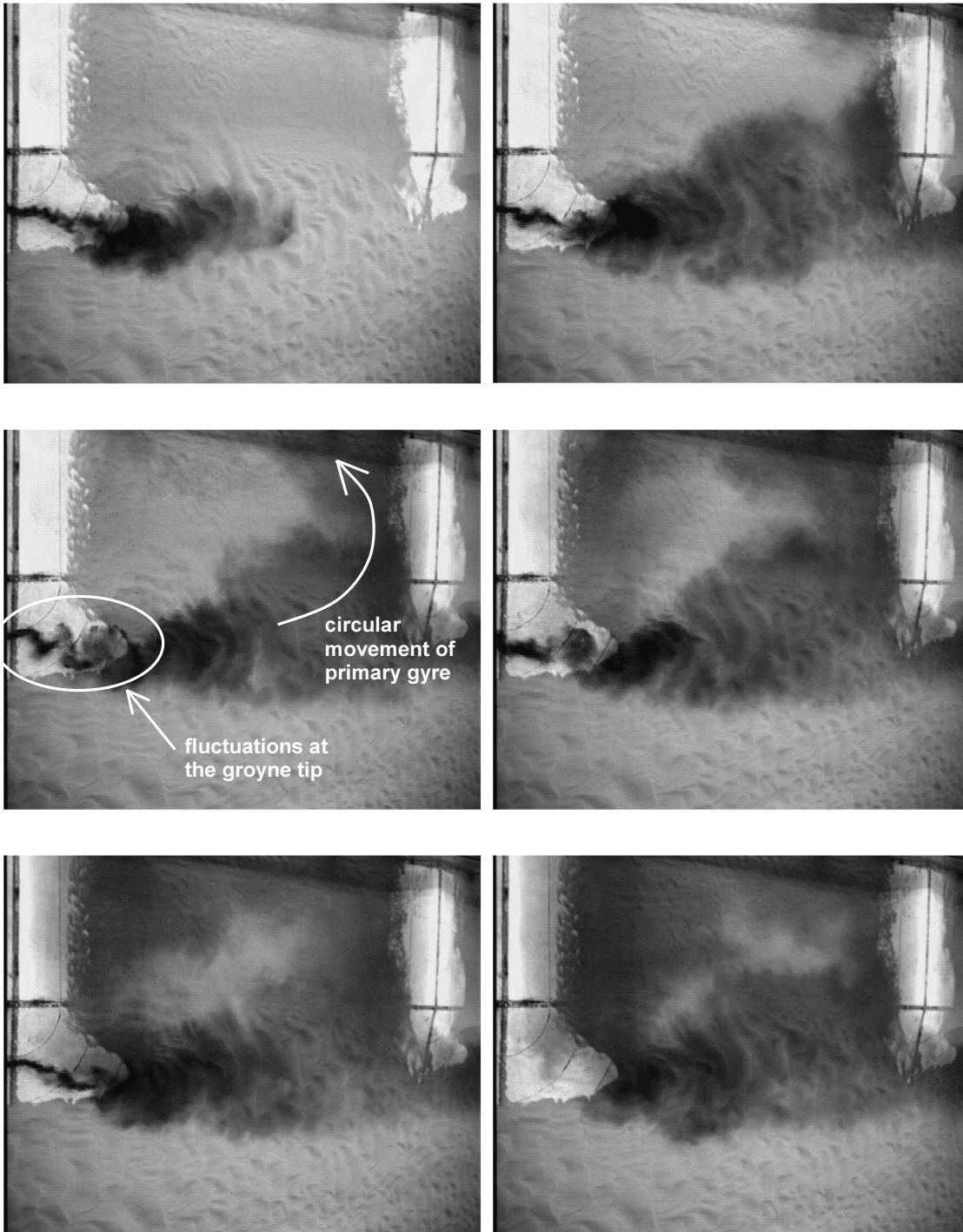


Figure C-2 Photographs from the dye test with indication of the fluctuations at the groyne tip and the circular movement of the primary gyre.

D CONTENTS OF THE DATA MEDIUM

The attached CD-ROM contains the following folders:

- **THESIS:**
contains a copy of this diploma thesis (both as a word-file and a pdf-file)
'DiplomaThesis.doc'
'DiplomaThesis.pdf'

- **FIGURES:**
contains all figures in this diploma thesis.

- **DATA:**
contains the most important input files.